EVALUATION OF MICROWAVE ANECHOIC CHAMBER ABSORBING MATERIALS

by

Stephen A. Brumley

A Thesis Presented in Partial Fulfillment
of the Requirements for the Degree
Master of Science

ARIZONA STATE UNIVERSITY

May 1988

EVALUATION OF MICROWAVE ANECHOIC CHAMBER

ABSORBING MATERIALS

by

Stephen A. Brumley

has been approved

April 1988

APPROVED:

Thomas E. Tice, Chairperson

Constantine A. Balanis

Russell W. Taylor

Supervisory Committee

ACCEPTED:

Joseph Palais

Department Chairperson

Brian E. Mitchell

Dean, Graduate College

ABSTRACT

This thesis discusses an anechoic chamber absorber evaluation which was conducted for the purpose of improving anechoic chamber and compact range performance through better absorber characterization. The need for a better understanding of anechoic absorbers is first illustrated by a review of past work in this area and a discussion of present chamber requirements. The approach taken to obtain this improved characterization of absorbers was to experimentally investigate the scattering nature of various types and sizes of materials. This study shows that performance of conventional absorber materials is dependent on selection of the material's shape, size and orientation with respect to the incident energy direction, and that performance is also altered by the use of fire retarding chemicals used in the absorber. Nonhomogeneities in the material composition and physical structure were also found to significantly modify performance, in some cases even improving it. Also shown is the need for improved evaluation techniques and procedures over conventionally used methods. Improved techniques using modern imaging and wideband radar approaches are presented. Several measured performance results for various absorber types and sizes are presented which show the usefulness of these evaluation techniques and demonstrate relative performance characteristics for these materials. Applications of the results of this study are addressed and recommendations for future work in this area are also presented.

ACKNOWLEDGMENTS

Several individuals and organizations have contributed in numerous ways to this thesis. Without their help and assistance the research and basis for this thesis would not have happened. In particular, the author wishes to extend his appreciation to the following: to the absorber vendors, namely Rayproof (Keene), Emerson & Cuming, and Rantec for their donations of the generous amount of absorber materials used to conduct this study; to Hughes Aircraft Company (Radar Systems Group) and to Motorola Inc. (Government Electronics Group) for their support and assistance; to the dedicated and skillful technicians who performed many of the actual absorber measurements; to my advisor, Dr. Tom Tice for his assistance and guidance; to Ray Immell and Dr. Russ Taylor of Motorola who contributed to the evaluation hardware design and construction; and finally to my wife, Rita, and new daughter, Kristin, for their many hours of patience and support.

TABLE OF CONTENTS

LIST OF FIGURES

1.0 INTRODUCTION

Electromagnetic radiation and scattering measurements are ideally conducted in a perfect reflection-free environment where there exist no interactions between the object being tested and the test surroundings. Such a testing environment would represent a true 'free-space' condition. However, in practice an ideal environment of this type is not possible. Practical methods for conducting such tests are in using either long outdoor test ranges or enclosed test chambers making use of absorbing materials to cover their inside surfaces to simulate a reflection-free environment. Enclosed test chambers of this type are referred to as 'anechoic chambers' and are very widely used for both radar cross-section (RCS) and antenna radiation measurements. The accuracy of measurements conducted in such enclosures is strongly determined by how well the application of absorbing materials simulates a free-space environment. Therefore, the performance and implementation of such anechoic absorbing materials are important parameters associated with anechoic chamber performance.

The history of anechoic absorbers dates back prior to the 1950's when the first chambers were developed. A detailed review of this early work is presented by Emerson [1]. Narrow-band absorber designs had already been developed and used during the second world war, but broad-band designs, more suitable for anechoic chambers, were

not developed until the late 1940's. Early commercial absorbers were constructed using carbon loaded animal hair to achieve broad-band performance. These initial absorbers were suitable over the UHF and low microwave bands. Soon after, shaped foam materials were developed which offered superior performance over the early animal hair designs. In the 1960's most of the materials still considered today as the state-of-the-art in anechoic absorbers were developed. Such commonly used material designs as the urethane foam pyramidal absorber became commercially available during this time. These materials offered greatly improved performance over a wider range of incidence angles and frequencies.

Since the 1960's, the only real advancement in absorber technology has been the addition of fire retarding chemicals to improve the safety aspects of the material. The reasons for this relatively long inactive period are many, but are strongly related to the fact that the majority of the chamber designers and users were content with the current materials; and absorber vendors found difficulty in obtaining funds for further research and development [2]. However, since the mid 1980's, recent demands for improved anechoic chamber performance and new standards in measurement accuracy and instrumentation, especially for low-level RCS measurements, have placed new requirements on the application and understanding of

anechoic absorber materials. The increased application of compact range test facilities has also shown the need for an improved understanding and characterization of current materials in order to address these chamber design requirements.

The research behind this thesis was conducted in order to obtain a better characterization and understanding of these absorbing materials. The results of an improved characterization directly benefit both the chamber designer and the general user who are faced with these increased requirements. One application of such results is in the development of complete and accurate chamber performance prediction models to aid in chamber design and performance optimization. The lack of characterization of the absorbing materials makes the development of such models difficult. In addition to a better absorber knowledge, the results of this thesis have also led to new and modified absorber designs and shapes and in much improved absorber evaluation techniques.

The approach taken to characterize anechoic absorbers was to obtain and evaluate several sample pieces from the various vendors who manufacture these materials. Numerous shapes and sizes of material were obtained. Performance evaluations were conducted on these samples. Experimental techniques were used, instead of an analytical modeling approach, because of the problems encountered by past

researchers in modeling the nonhomogeneities associated with the absorbers. Chapter 2 presents a description of the evaluation approach used as well as a review of the past work conducted in this area.

Chapter 3 presents a detailed discussion of the absorber evaluation techniques and tests which were conducted on the absorber samples. Both conventional absorber testing techniques and the improved techniques developed during this study, based on modern wideband radar instrumentation, are presented. The improved techniques offer both increased measurement sensitivity and accuracy and an added diagnostic evaluation capability to the area of absorber testing. Appendix A reviews the theory of inverse synthetic aperture imaging which is one of the techniques used. Additional information about the absorber imaging technique is also found in [3].

Many of the actual absorber evaluation results are illustrated and discussed in Chapter 4. Because of the large amount of data obtained, only the most significant results are presented. Data is given which describe some of the scattering behaviors of typical pyramidal, wedge and convoluted absorbers as well as show the performance levels obtained for various sizes and orientations of the materials. The effects on performance of fire retarding salts, painted surfaces, and metal backings are also given. From the results of these tests, new material designs were

developed and provided by some of the vendors. The performance of these materials is also given. Additional results of some of the evaluations not presented in Chapter 4 are published in [4],[5].

A brief description of some of the applications and uses of the absorber performance results and evaluation techniques is given in Chapter 5. Topics relating to improved absorber and chamber performance are presented. Measured and predicted RCS background performance levels are also presented for a chamber which was designed using the results of this study and which demonstrate a good understanding of the absorbers.

This thesis concludes with Chapter 6 which summarizes the results of this study and gives recommendations to help direct future research activities in anechoic absorber and chamber development.

2.0 BACKGROUND AND EVALUATION APPROACH

2.1 REVIEW OF PAST WORK

Anechoic absorbers are presently available from at least four major vendors. All of these commercially produced materials are similar in design and shape and are available in various sizes and thicknesses. The initial design of these materials dates back to before the 1960's as noted in Chapter 1 and in [1]. From the late 1960's to the mid 1980's very little anechoic absorber research and development was conducted. As a result, the amount of published or available data on such materials has been limited. The lack of published absorber research in the area of anechoic materials may be somewhat explained by the enormous attention which was being given to classified absorber work in the area of radar absorbing materials (RAM) [6] and by the fact that most anechoic chamber designers and users were content with the existing materials.

Within the last few years, a renewed interest in improved chamber performance and absorbers has led to an increase in research activities. As a result, more information and knowledge about these materials should start to appear in the near future. The research associated with this thesis is part of this recent activity. Other recent studies in this area [7]-[9] have shown the need for additional absorber research and characterization; however,

very little additional absorber performance data has been provided. Such studies have shown that better absorber evaluation techniques are required in order to fully evaluate the performance of these materials and that inconsistencies in the absorber's composition and performance are also present. Analytical modeling approaches have also been attempted [9]-[11] which show that techniques and procedures do exist which provide some basis for continuing the research. The final application of these techniques is rather complex because of the lack of the material's electrical characteristics and the rough, lossy (absorbing), and inhomogeneous nature of the material. Thus, the effectiveness of purely analytical approaches is limited.

Development of improved absorber evaluation techniques has also been somewhat limited. The technique used for most free-space testing of absorbers, since before 1960, has been the NRL arch method [12]-[14]. This method is described in Chapter 3 of this thesis and is shown to have some limitations. Only slight variations of the arch have been attempted over the years, mostly involving time-gated or Doppler-filtered instrumentation [15],[16]. The improved techniques, used for this thesis, made use of modern wideband RCS measurement methods. The first reference to the use of standard RCS measurement techniques as opposed to arch methods was from Buckley [17]. Other recent studies

making use of time-domain RCS measurements [4],[9] have shown that such techniques offer significant advantages in absorber diagnostic evaluations. Free-space testing of absorbers at the UHF and lower frequencies was also found to be inaccurate and provided limited results if too small a sample was employed. For this reason, waveguide and transmission line testing techniques were developed [18]. These techniques are still commonly used today for absorber evaluations below 1 GHz.

Present anechoic absorbers are available in three distinct shapes - pyramidal, wedge, and convoluted. The thickness or length of these materials and shapes range from 1 inch to 12 feet. As stated earlier, only a very limited amount of data is available on these materials even though they have been fabricated and used for many years. One example of this lack of available data is in the relative performance differences and advantages between the various shapes which are available. In the past, recommendations or guidelines for the applications of the various shapes were solely based on general rules-of-thumb, past experience, or intuition. Comparative performance results had not been demonstrated until recently [4],[9]. Measured data shown in Chapter 4 of this thesis clearly shows some the advantages and performance results for the various types of materials.

Another example is in characterizing the performance

of the material as a function of its length or size. Generally, the longer or thicker the material, the lower in frequency the material is expected to provide adequate performance. A rule-of-thumb used is that the material should be 2 to 3 wavelengths thick in order to achieve better than 40 dB reflectivity at normal incidence [14]. Figures 2.1 and 2.2 illustrate the typical extent of data from which such decisions are made. The figures show the expected reflectivity performance for given absorber thicknesses for both normal and specular off-normal incidences. The exact origin of such data is unclear, but plots similar to Figures 2.1 and 2.2 commonly are shown in most absorber articles or vendor catalogs. The actual absorber performance is highly dependent on the material's shape, its orientation with respect to the angle of incidence, and the polarization and phase nature of the illuminating wave which impinges on the absorber. The presence or lack of a metal backplane can also modify the absorber's performance. These factors have not been adequately considered in the past. This current study was intended to better characterize the performance of these absorber materials.

The general design methodology of anechoic absorbers is another parameter which has only intuitively been explained in the past. The best discussions of the fundamental effects of absorbers are found in [9],[19]-[23]. Both the absorbing and scattering behaviors of the materials are

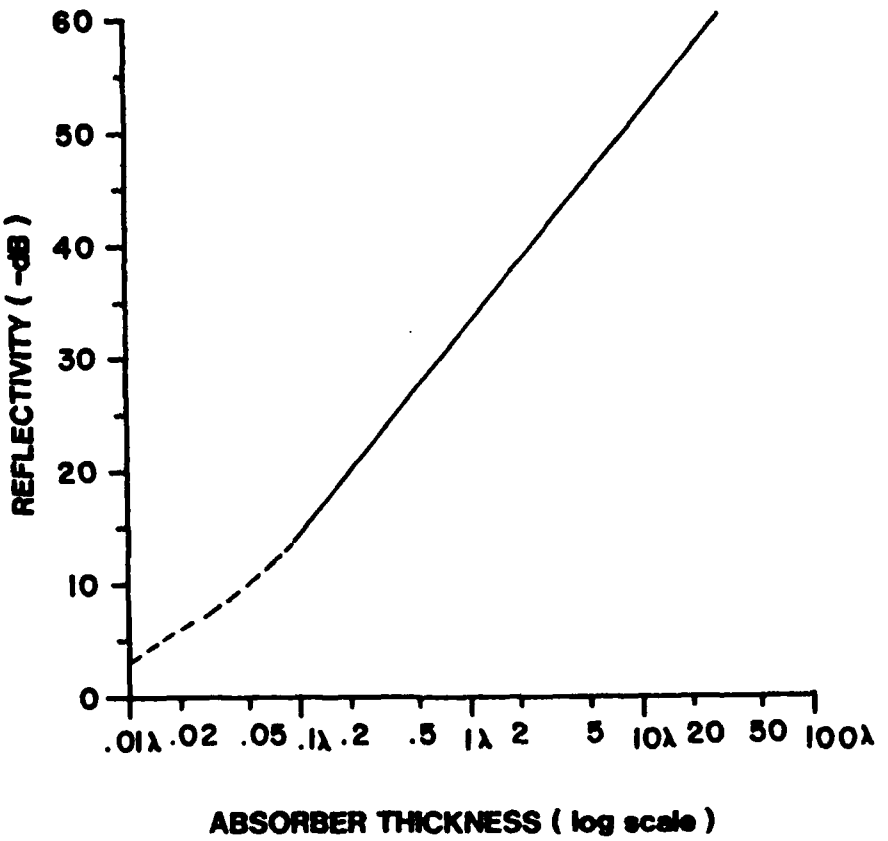

Fig. 2.1. Typical reported performance of anechoic absorbers versus material thickness at normal incidence (from [36]).

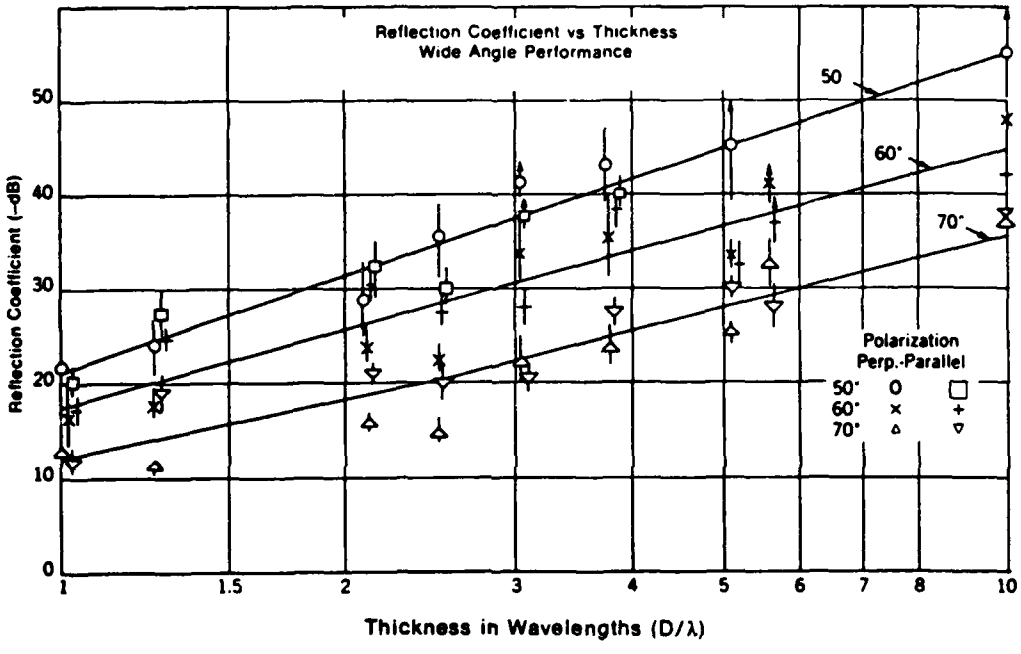

Fig. 2.2. Typical reported off-normal specular performance of anechoic absorbers versus material thickness (from [1]).

required in order to determine the absorber's performance. The shape of the material is partially intended to provide a gradual impedance change from free-space into the lossy carbon material that is embedded in the absorber. This impedance matching concept is expected to be best exhibited at the lower frequencies and at near-normal incidence; however, not enough data is found to adequately evaluate the effectiveness of the impedance matching versus absorber size and frequency.

For higher frequency operation, because of the relatively large absorber sizes compared to the wavelength, the shapes are expected to be more effective in scattering or redirecting the incident energy than at providing an impedance match into the material. Edge and tip diffraction also contributes to the absorber's scattering direction and level. The level of the absorber's performance degradation due to these scattering contributions or the dependency on the exact absorber's shape or orientation also has not been adequately determined in the past. Chapter 4 of this thesis better discusses the scattering mechanisms associated with typical absorber shapes and sizes and presents measured data which illustrate these mechanisms. Comparative performance results for numerous absorber shapes and sizes are also presented.

2.2 PRESENT ABSORBER EVALUATION APPROACH

As stated in Chapter 1, the approach used for this absorber study was to obtain numerous samples of absorbers and perform various experimental evaluations on each sample. Each test configuration generally consisted of at least sixteen individual pieces of absorber on an 8 by 8 foot sample area. Plane-wave illumination on the large sample area was achieved by the use of a free-space compact range in an existing anechoic chamber. These evaluations also made use of modern imaging and wideband radar instrumentation and technology. The use of such non-conventional absorber testing techniques provided improved measurement accuracy and sensitivity as well as a diagnostic measurement capability. Chapter 3 discusses the test configurations and various performance evaluations which were conducted and defines the techniques used. This section summarizes the different performance parameters which were evaluated and Chapters 4 and 5 illustrate many of the results and conclusions which were obtained.

The materials which were evaluated during this study included 8, 12, and 18 inch thick pyramidal and wedge shaped absorbers as well as 3 and 6 inch convoluted materials. Three different vendors supplied the sample pieces of absorber. In all, 176 pieces of absorber were donated to the Arizona State University for the purpose of

this study. Various materials were evaluated both with and without fire retarding chemicals and paints to determine the effects of these parameters on performance. Tests were also conducted on various materials both with and without a metal backplane to determine the importance of a metal absorber backing.

Other studies included the effects of gaps and spaces between absorber pieces and the effects of discontinuities between material types. Various absorber orientations and installation procedures were also considered. Backscattering measurements were conducted for various orientations with incident-field excitations being from normal to near-grazing (90 degrees from normal) incidence.

The frequencies where the absorber evaluations were conducted included as a minimum the 2.9 to 6.9 GHz and the 13.8 to 17.8 GHZ bands. Other tests were conducted as low as 1.5 GHz and up to 18 GHz. The various sizes of materials and the frequencies selected enabled absorber evaluations to be conducted on materials from one to more than thirty wavelengths in thickness. The frequencies used for the various tests are provided with each of the specific results presented in Chapter 4.

The polarizations which were evaluated included both VV (transmit vertical, receive vertical) and HH (transmit horizontal, receive horizontal) with respect to the chamber floor. No cross-polarized results were obtained. In all

cases, both the amplitude and phase of the backscattered fields were recorded.

As a result of the measurement techniques used, the absorber's reflectivity or backscattering could also be calibrated directly in units of cross-sectional area, typically dBsm (dB with respect to a square meter). In some cases the use of calibrated data in this way enables the absorber results to be more easily applied in RCS chamber models and design applications.

In addition to the experimental evaluations, other absorber parameters were also considered. These parameters mostly involved the fabrication processes used in the construction of the various materials. Tours were made at many of the plants where the materials are fabricated and tested to obtain a better understanding of the methods used in construction and to attempt to correlate these processes with the performance levels achieved. Incoming inspections were also conducted on the materials supplied by the vendors to determine differences in the material's weight, size and consistency. Areas where modified fabrication techniques could improve absorber performance were then considered. Some of the conclusions from these parameter studies are presented in Chapters 4 and 5; however, individual references to the vendors, and/or their performance levels, are not presented in fairness to the vendors. The vendors are randomly referred to as vendor A,B or C.

3.0 ABSORBER MEASUREMENT TECHNIQUES

3.1 INTRODUCTION

There exist many microwave anechoic chambers throughout the world and almost all of these chambers use some form of absorbing material to simulate a reflection-free environment as discussed in Chapter 1. The quality of these chambers is very much dependent on the performance of the absorbing materials used. It has also been shown that an improved characterization and understanding of anechoic absorbing materials is important to both the chamber designer and the chamber user in order to address the present requirements being placed on the performance of these chambers.

In many ways, the preferred approach to obtaining such absorber performance data is by direct measurement or evaluation of the absorber itself. Analytical techniques for predicting the performance of such materials are very difficult to employ and in many cases do not lead to the correct result as reviewed in Section 2.1. This is because of the inconsistencies and unpredictable parameters involved with the absorbers themselves. As a result, statistical and probabilistic techniques are often used in most analytical approaches.

This chapter addresses the conventional methods used for absorber evaluations and also describes improved

techniques, developed during this study, which allow for more diagnostic and accurate characterizations to be conducted. Details of the absorber evaluations which were performed during this study are also presented.

The absorber measurement technique used during the past 25 years, and still used today by nearly all vendors, for free-space absorber testing is that known as the NRL (Naval Research Lab) arch. Section 3.2 discusses the NRL arch method and presents some of its limitations and capabilities.

Some of the very same RCS measurement techniques which are placing new and more difficult requirements on chamber performance levels, and thus on the absorber, are also very applicable for the evaluation and measurement of the absorber itself used in these facilities. One of the significant contributions of this study was in applying these advanced techniques to absorber evaluations. Such techniques have been used during this study to obtain some of the required but missing performance data on materials needed by today's chamber designers and users. The advantages associated with these techniques are mainly realized though the use of compact range technology, coherent wideband radar instrumentation and synthetic aperture imaging. These techniques are illustrated and described along with some significant example measurements in Section 3.3.

Results of applying inverse synthetic aperture

imaging techniques had not been available in the past for absorber materials. These techniques allow for two-dimensional time or range information to be obtained about the test sample which can be used to separate or discriminate against unwanted or error signals in the measurement and to provide diagnostic type information about the scattering characteristics of the material. Enough resolution can be obtained in these images to actually look at the scattering performance of a single cone or section of absorber. Increased sensitivity levels and accuracy can also be obtained which are required for adequate absorber evaluations of low scattering level absorber materials.

Other uses and applications of absorber evaluation techniques are in new material design and development and in quality assurance or incoming inspection testing. The new techniques described in this chapter are directly suitable for these applications and again have several advantages for these types of tests as well. The diagnostic and range-resolution capabilities being of the most benefit in these applications.

3.2 CONVENTIONAL NRL ARCH

The NRL arch was one of the first tools used by absorber researchers and vendors to conduct free-space absorber evaluations, especially at microwave frequencies.

After over 25 years, it is still commonly used today. It has become somewhat of a "standard" technique and most absorber users are familiar with its use. Some reasons for its popularity are its ease of operation, its minimal test equipment requirements, and its initial effectiveness in evaluating general absorber performance. But, with demands for better absorber performance and characterization, the traditional NRL arch technique has some limiting disadvantages. The technique itself as well as some of these weaknesses will be further addressed.

The typical NRL arch measurement setup is illustrated in Figure 3.1. The measurement technique consists of mounting two antennas, usually horn antennas, around the inner circumference of a constant radius arch. One of the antennas is used to transmit energy at a desired frequency and polarization and the other antenna is used to receive the energy radiated back from the test sample which is placed over a flat metal surface at the center of the arch. The reflected energy, measured from the sample, is then compared to the level of the flat metal surface alone (usually at near normal or specular incidence) and a reflectivity number is obtained. Typical reflectivity values reported by most absorber vendors are -50 dB for materials with thicknesses of six wavelengths or greater [24]-[27].

The antennas can be positioned so that either bistatic or quasi-monostatic performance at desired angles is

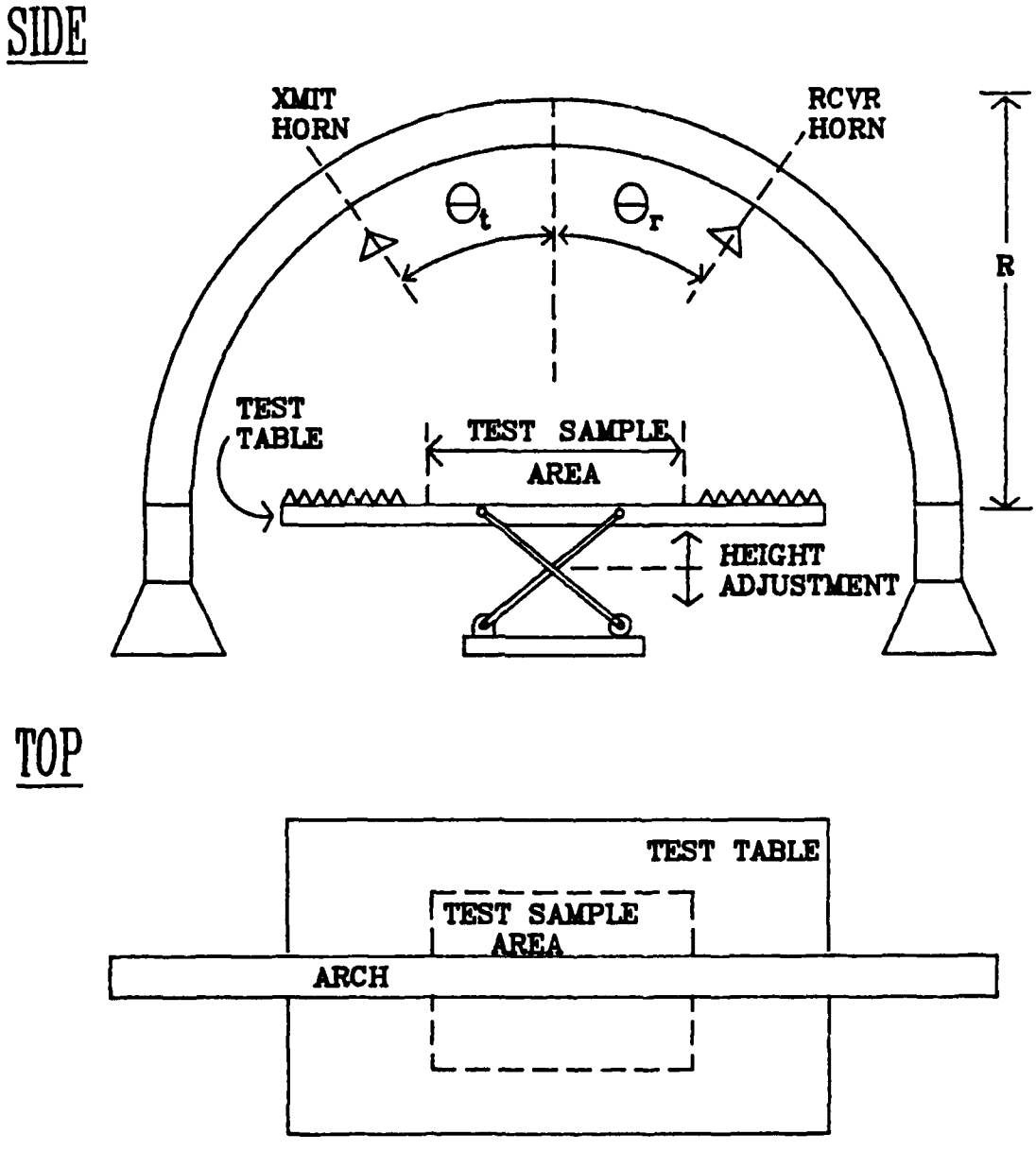

Fig. 3.1. Typical NRL arch measurement setup.

observed. For quasi-monostatic testing, the antennas are located at the same angular position and usually form a small bistatic angle. The radius of the arch, measured from the test sample, is typically from 4 to 16 feet for most common setups. The table on which the test samples are placed is usually covered with additional absorbers resulting in a larger absorber covered area than which is actually measured. This is done to help reduce edge effects as well as unwanted reflections from the floor and other scattering sources. The only other instrumentation required for a basic setup is a source generator operating at the desired frequency with appropriate power output and a general reflection-test-set or power meter.

The problems and deficiencies of this technique are as follows:

a) The radiating and receiving antennas used in the arch produce spherical wave illumination over the test sample area such that the illuminating field has a very high degree of phase and amplitude taper. This is especially true since the evaluations are almost never conducted under far-field conditions. The effects of such an illuminating field condition are not necessarily serious if the amplitude and phase tapers are minor or if they represent the environment in which the absorber being tested is to be applied. However, the illumination on the sample area can be quite distorted and the actual far-field or plane

wave incidence performance of the absorber may not be measurable. It should also be realized that most usable anechoic absorbers do not scatter specularly like the metal calibration surface. As a result, the absorber scatters the incident illuminating fields differently than the flat calibration surface and the performance results become dependent on the incident fields and the size of the test sample. In many cases it is also desired to evaluate the absorber's rough surfaces, nonhomogeneities and random scatterer effects on performance. For these evaluations, it is desirable to produce plane wave (or far-field) conditions.

A typical test sample illumination pattern is shown in Figure 3.2. A conical corrugated source horn having a gain of 15 dB is assumed. The radiation pattern of the source antenna and the size of the arch determines the size of the test sample. For a four-foot radius arch (R=4 foot), using the half-power beamwidth of the source antenna, a sample size of 2.2 feet is obtained. For this case, the phase errors at the edge of the test sample are 117 degrees at 2 GHz and 590 degrees at 10 GHz. The total amplitude taper, including space attenuation, for this case are 3.35 dB. For a 12 foot arch, the same analysis results in a 6.8 foot sample size with 350 degree phase error at 2 GHz and a 1770 degree error at 10 GHz. The phase deviations across the test sample for these cases can be very significant and can

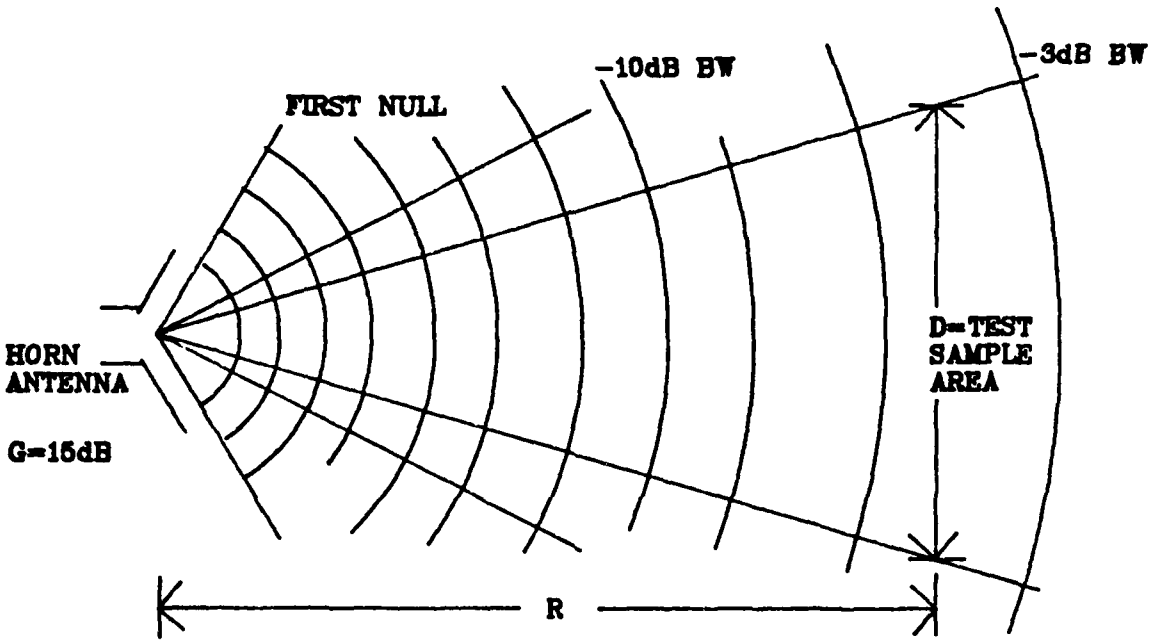

Fig. 3.2. Test sample illumination pattern from a spherical wave source.

lead to errors in the absorber evaluations.

b) Another problem with the NRL arch is that the test sample size is often too small and inadequate to represent the performance of an entire wall or section of absorber. This is generally caused by the size of the arch and the source antenna pattern as described in a). When a reasonably directive antenna is used and a far-field condition is closely established, the sample size becomes generally smaller than a 2 by 2 foot section, even for a 16 foot arch. For absorber designs which have only 1 or 2 shaped structures per square foot, the entire sample may only represent 4 or 8 structures (shapes). Such a sample size is not adequate and repeatability of the data between tests and different samples is usually not possible since the result is very dependent on the vector summation of only a few scatterers (shapes). The fact that non-homogeneities and inconsistencies are also found with the material further results in measurement anomalies when too small a sample is tested. It is preferred to have a sample size which includes as many individual shapes or absorber pieces as possible. This is difficult to achieve with the arch technique.

c) With some arch setups, an inadequate test sample smaller than the illuminating pattern of the source is sometimes used, especially for low frequency applications. In this case, edge scattering from the sample can corrupt

the results. Earlier work in this area [18] suggests that a sample size of at least 10 wavelengths be used to reduce these edge effects. This is generally not a limitation at microwave frequencies.

d) Probably the most limiting problem found with the arch measurement technique is the presence of unwanted and interfering error signals and its inability to separate or discriminate against these signals. Some of these error signals are illustrated in Figure 3.3. One of the most significant error signals is that caused by the horn-to-horn coupling. Application of an absorber material between the horns and proper feed design and alignment can help reduce this problem but coupling levels below -50 to -60 dB are difficult to achieve, especially for cases where the horns are separated to evaluate bistatic absorber results. Other problems are caused by scattering from the arch structure itself or from scatterers in the surrounding environment. Standing waves can also exist between the antennas and the sample which cause time delayed error responses.

In some cases, time-gated or coherent wideband radar instrumentation can be used to separate and isolate these error signals. However, it is usually found that for many arch geometries, the path lengths between the absorber sample itself and the error signals are so similar that practical gate lengths cannot be used without significantly effecting the measurement of the absorber. This is

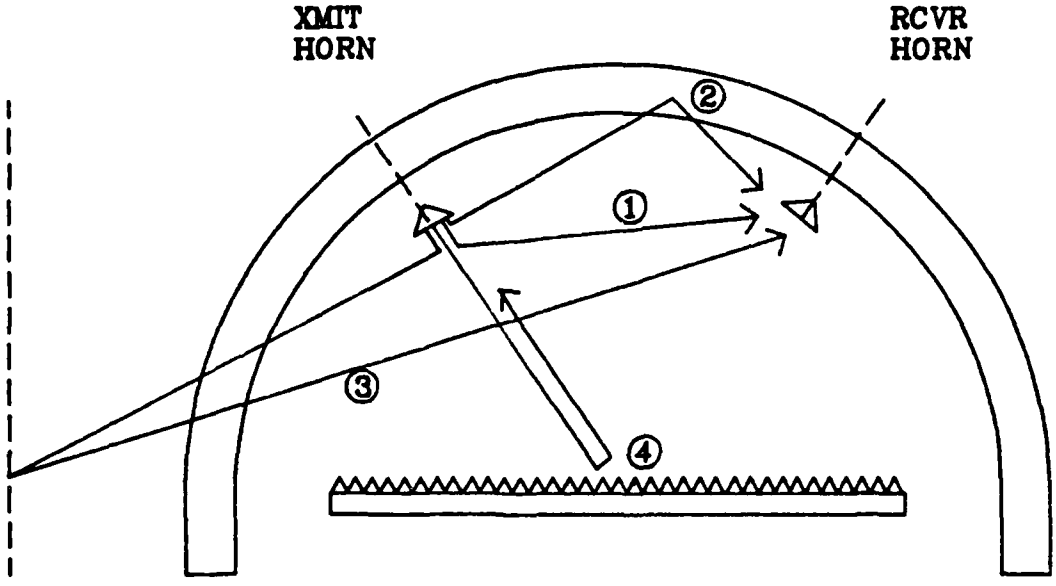

① DIRECT HORN-TO-HORN COUPLING

② ARCH STRUCTURE SCATTERING

③ SURROUNDING ENVIRONMENT SCATTERING

④ STANDING WAVE GENERATION

Fig. 3.3. The sources of error signals usually found with the NRL arch.

especially true for bistatic cases where the antennas are significantly away from normal incidence.

The effect of these error signals on the absorber measurement is that the total signal being received is a vector summation of all signals, both desired and undesired. The relative magnitude of the desired signal to the sum of the undesired ones determines how much error may be introduced. Figure 3.4 shows the possible error associated with various ratios of undesired to desired signals. The limits are determined for the cases where the two fields add both in-phase and out-of-phase according to

$$\underline{E}_t = E_1 + E_2 e^{j\phi} \qquad (1)$$

where E_1 is the magnitude of the total undesired signal, E_2 is the magnitude of the desired scattered signal, $\underline{E}_t$ is the total signal and ϕ is the relative phase between $\underline{E}_1$ and $\underline{E}_2$ and is either 0 or π for the worse cases.

The results show that if E_1 is 20 dB below E_2 then the accuracy of the measurement of E_2 is better than +/- 1 dB. This suggest that in order to measure a -50 dB reflectivity level within this accuracy, the undesired signal levels would have to be below -70 dB. This is a very difficult goal to achieve with the arch and is one reason why

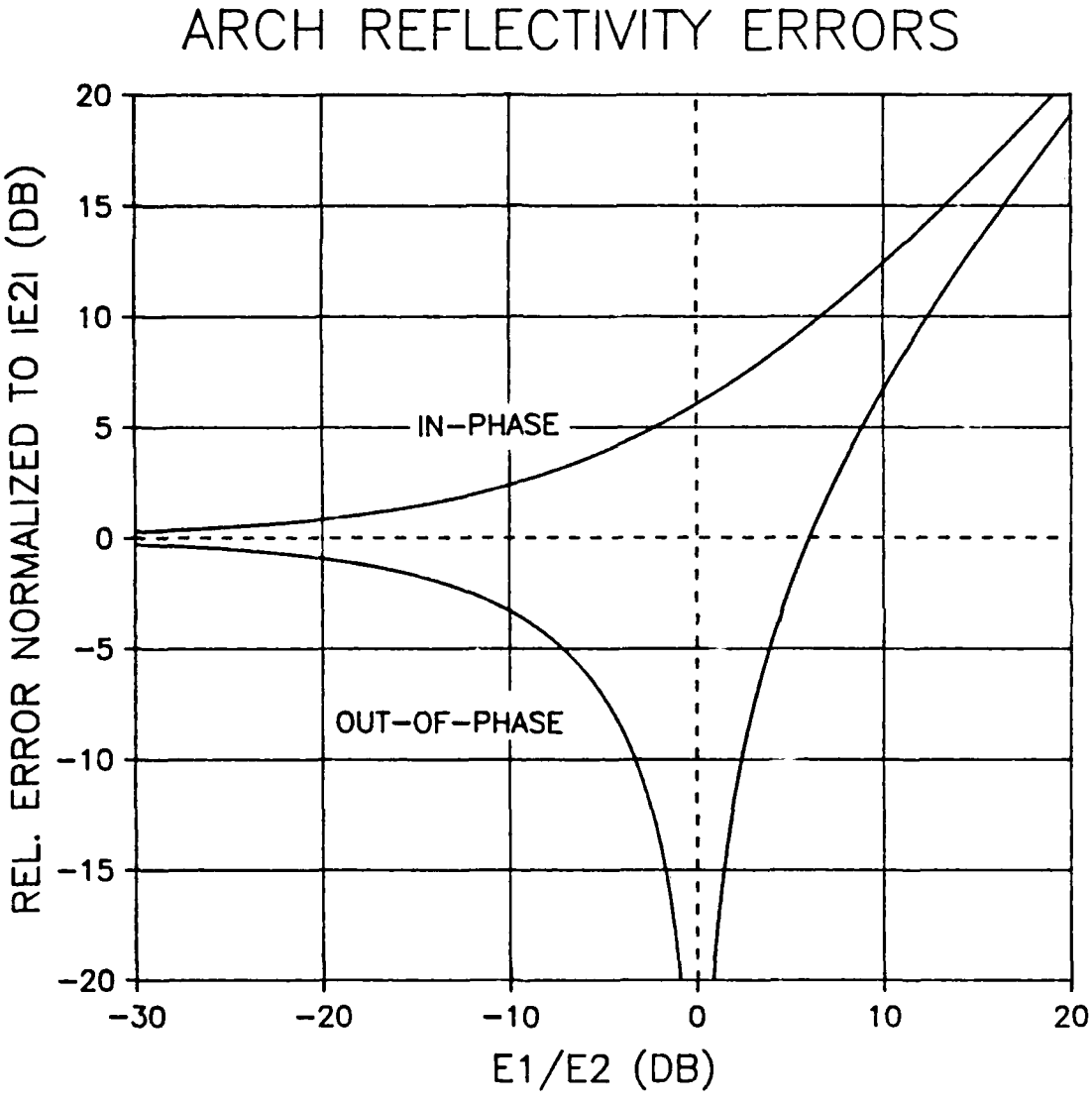

Fig. 3.4. Possible error in NRL arch measurement as a function of the undesired to the desired signal strengths.

performance levels below -50 dB are seldom quoted from an arch measurement. However, if E_2 is approximately equal to E_1 or even larger than E_1 then the error can become increasingly large. Another interesting case is where the ratio is +20 dB, ie., the undesired signal is 20 dB stronger than the desired signal. For example, if E_1 is at a value of -50 dB and E_2 is then -70 dB then the total received signal would be -50 dB with less than +/- 1 dB signal variation. These results could very easily be interpreted to suggest that the absorber performed at a -50 dB level when in fact it was 20 dB better. Also the performance of the absorber could vary quite a bit, even +/-10 dB, without significantly changing the apparent result of the measurement.

One method used to determine the level of error in the arch measurement caused by an undesired signal, as long as E_1 is less than E_2 is to move the entire test sample table in a vertical position a distance greater than a quarter wavelength and record the maximum and minimum levels during this movement. This setup is shown in Figure 3.1. The total deviation of the received signal then determines the ratio of E_1/E_2 as in Figure 3.4. The method commonly used is to then subtract a value from the maximum value measured which would place the net result back on the 0 dB error line for that given ratio. Another technique used [12],[13] is to take the average of the two values measured. Figure 3.5

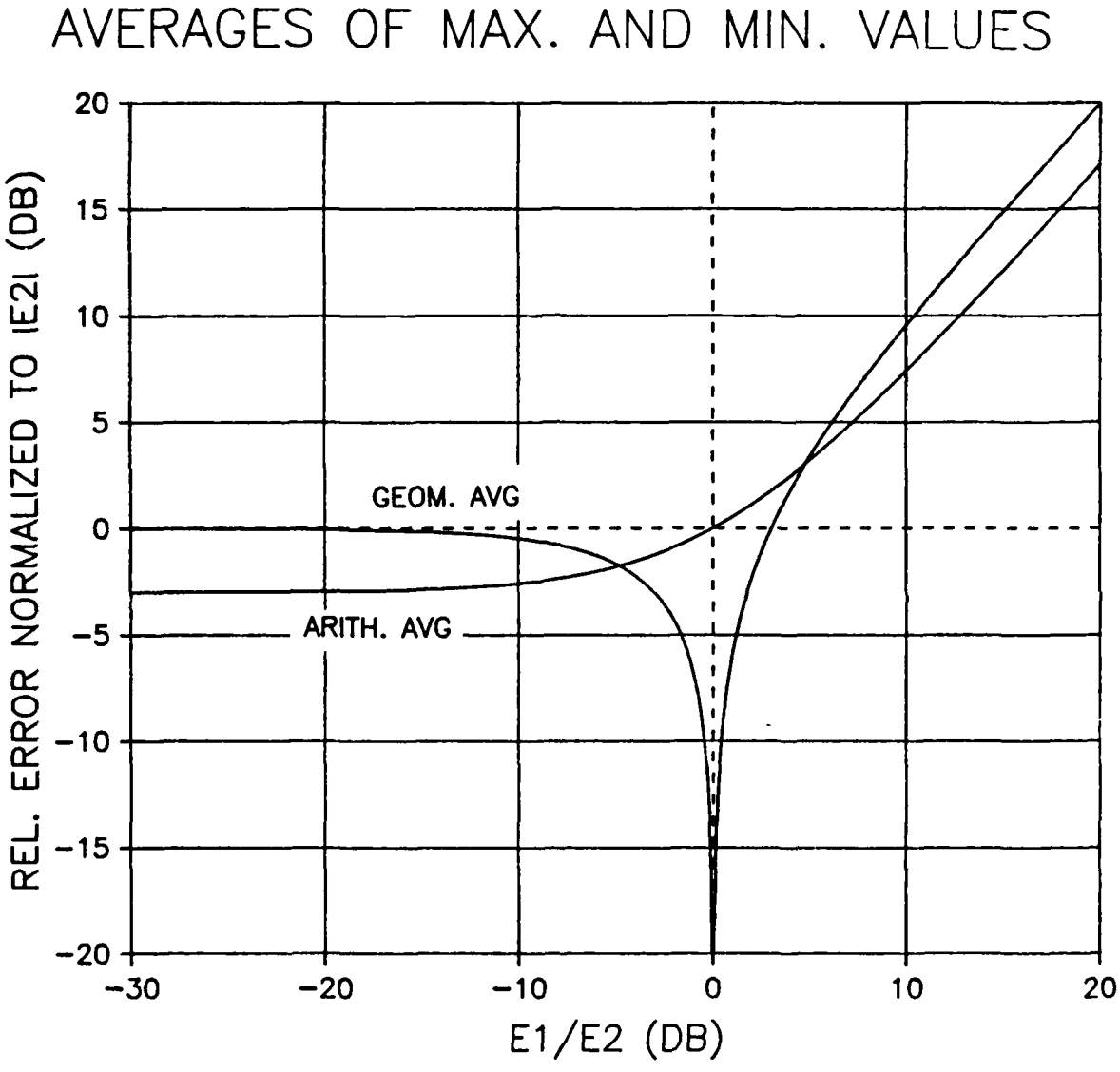

Fig. 3.5. The geometric and arithmetic means of the maximum and minimum error levels used for error reduction.

shows the result of taking the arithmetic and geometric means of the maximum and minimum values measured. The geometric average represents a closer value to the correct result than the arithmetic average for ratios smaller than -5 dB. For ratios greater than 0 dB neither of the above averaging methods work well. One problem is in determining whether E_1/E_2 is positive or negative.

To help in determining the relative error coupling levels present for typical measurement arch setups, a simple experiment was conducted at one of the absorber vendor's manufacturing facilities during a visit to that facility. A 16 foot radius arch, which was being used to test 24 inch pyramidal absorbers at 1 GHz, was observed during a routine reflectivity measurement. The antennas used in the arch formed a +/- 10 degree bistatic angle about the normal to the test sample. Four pieces (a 4 by 4 foot section) of absorber were being tested at one time. The routine measurement results gave maximum and minimum reflectivity values of -47 and -57 dB respectively with the up and down motion of the test table. Using the vendor's measurement procedure, this 10 dB swing in the measured result correlated to a recorded performance level of -50.6 dB. It was also assumed that the actual absorber reflectivity was larger in magnitude than the error signals. To check the validity of this assumption, a metal hand tool approximately 8 inches in length was placed between two of

the pyramids within the test sample to degrade the performance of the material and the measurement was repeated. If the absorber returns were larger than the error signal returns, then the variations in the response should decrease and the measured response level increase. Instead, the results were opposite, and a 21 dB variation was measured (from -46 to -67 db). This suggests that the true level of the unmodified absorber performance was actually much lower than the recorded level and that the errors associated with the arch measurement prohibited the true levels from being measured for this particular case and arch. It is felt that these same limitations are present for most arches in use today for evaluating high performance anechoic absorber materials.

e) Another limitation with the arch technique is in the calibration of the absorber performance levels. Using reflectivity values relative to an arbitrary flat metal surface does not always result in adequate information about the absorber. This is especially a problem for monostatic and off-specular angles of interest. Actually, the flat metal surface used for comparison often returns less monostatic energy away from normal incidence than does the absorber. The results are also highly dependent on the positioning accuracy of the measurement and on the illumination of the flat plate. A more standard calibration technique similar to what is done with RCS measurements

would offer more directly applicable results in most cases.

f) The arch method also does not indicate the reason for degraded absorber performance since it is basically a "go" or "no go" type test. A better method which gives some type of diagnostic results about the sample is desirable so that problem areas can be found and quick performance improvements can be implemented.

3.3 MODERN RCS METHODS

The free-space evaluation of absorber materials consists of measuring the reflected or scattered energy coming from the absorber caused by illuminating it with incident energy. Energy which is not returned by the absorber is assumed to be absorbed or scattered in another direction. This same technique is used to measure the RCS of various targets and structures, and quite elaborate and accurate techniques exist for conducting such measurements, even for very-low-scattering targets. Therefore, it is reasonable to apply these RCS measurement techniques to the evaluation of absorber materials. Such measurement techniques were used during this absorber evaluation to study the performance of anechoic absorber materials. A description of these techniques is included in this Section.

The basic operation of the NRL arch is really nothing

more than a simple RCS measurement of the absorber sample. There are several advantages with using modern RCS methods over the arch technique. These include:

a) The need for conducting RCS measurements on extremely large (even full scale aircraft) targets has resulted in illumination techniques and facilities where large targets can be placed in a true far-field environment. One such technique used for generating large indoor far-field environments is the employment of a compact range. Compact ranges are discussed in Section 3.3.1. A method by which a large sample of absorber can be evaluated in such a compact range is to simply mount a large wall of material on the same target support devices used for RCS targets. This technique makes full use of the benefits of existing positioning equipment and standard test facility procedures. One such absorber testing configuration, as used during this study, is addressed in Section 3.3.2.

b) The techniques used for measuring RCS are well documented and used throughout the industry, and many more RCS facilities are in existence than are facilities using arch techniques. The methods used to perform such tests are also well accepted.

c) Standard calibration techniques exist which can be used to specify the absorber performance independent of aspect angle and angle of incidence. RCS results are usually calibrated to the known RCS values of a calibration

target and are given in units of area (usually dBsm or dB with respect to 1 sq. meter). Absorber results calibrated in this way have more universal meaning and are much simpler to interpret when using the results to construct chamber performance models or comparisons.

d) Probably the most important advantage of using RCS measurement techniques is in the application of existing coherent wideband radar instrumentation. These techniques generally allow for a complete diagnostic evaluation of the test target and are typically used to identify or determine the scattering components and mechanisms present with the scattering target. These methods make use of time-domain or range-resolved scattering results to isolate or identify these various scattering components. Inverse synthetic aperture imaging is one technique which makes full use of the range resolution capability of a coherent wideband radar and its associated signal processing. The specific application of such wideband radar techniques to the testing of absorbers is presented in Section 3.3.3.

3.3.1 Compact Range Illumination

The concepts for compact range technology have existed since 1964, but not until the past several years has this technology been widely received and implemented. The idea of a compact range is to make use of a microwave reflector

or lens in the near-field to collimate a typical spherical-wave from a source antenna into a plane wave. The size of this plane wave can be nearly as large as the reflector or lens aperture. Details of the technique are well published in the literature. Two recent articles are excellent summaries of the current status of these types of ranges [2],[28].

At least three different approaches to the compact range are commonly used. In general, all three approaches generate a large plane wave test zone (or quiet zone) within the chamber. The specific compact range technique which was used to conduct the absorber evaluations during this study is illustrated in Figure 3.6.

This range was selected because of its availability. The range makes use of a dual parabolic-cylinder reflector configuration. These reflectors collimate the incident spherical wave in elevation with the first or sub-reflector and in azimuth with the second or main-reflector. The plane wave zone or test zone is shown in the center of the room approximately 5 meters from the center of the main reflector. The main reflector for this particular range was 3.0 meters wide and 2.5 meters high. The size of the plane-wave zone generated is about 4 feet wide and 4 feet high by greater than 8 feet deep at 5 Ghz. At 15 GHz, the test zone size increases to almost 6 feet wide and 5 feet high by 8 feet deep. The specifications on the quality of the plane

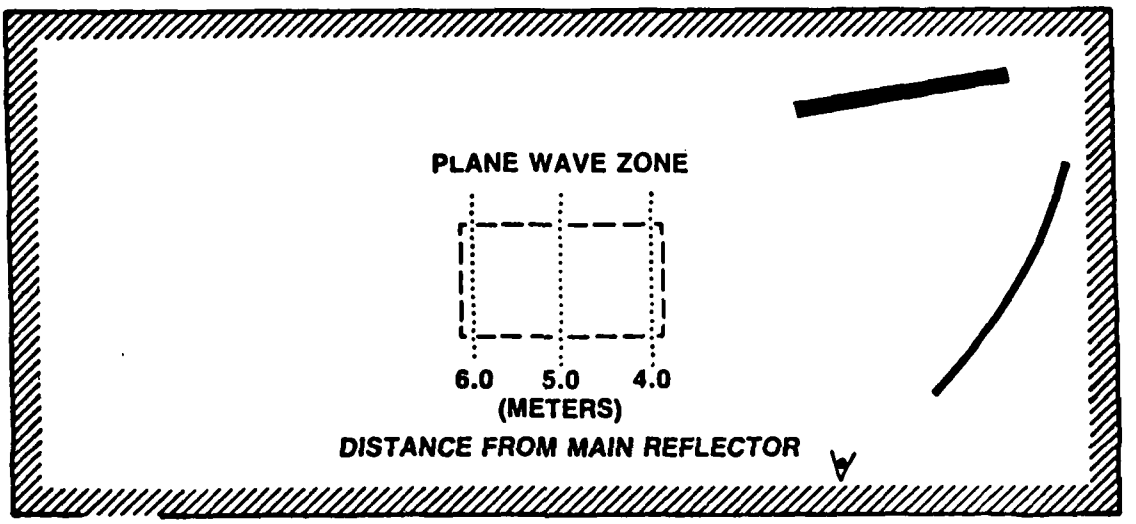

Fig. 3.6. Dual parabolic cylinder compact range used to conduct the absorber evaluations.

wave for this quiet zone size are a total amplitude variation of less than 0.75 dB and phase within 10 degrees.

The use of such a large plane wave allows for far-field conditions to be present over an absorber sample up to the size of the plane wave. Another advantage of the compact range is that the incident field beyond the edge of the test zone rolls off very fast, thus minimizing the illumination of the test sample outside of the test zone and also reducing edge effects. Figure 3.7 shows both measured and predicted plane-wave amplitude performance as a function of the vertical position along the test zone. The two-way field is shown to decrease by almost 40 dB beyond 2 feet from the edge of the test zone at 10 GHz. Two-way results account for both the transmit and receive paths within the room.

3.3.2 Test Sample Configuration

The absorber evaluations conducted during this study were performed in the compact range discussed in Section 3.3.1. To make use of the entire test zone size, many of the evaluations were made using an 8 by 8 foot test wall mounted in the chamber which allowed 16 pieces of absorber to be tested at one time. Various types and sizes of absorbers were then mounted on this wall and numerous tests

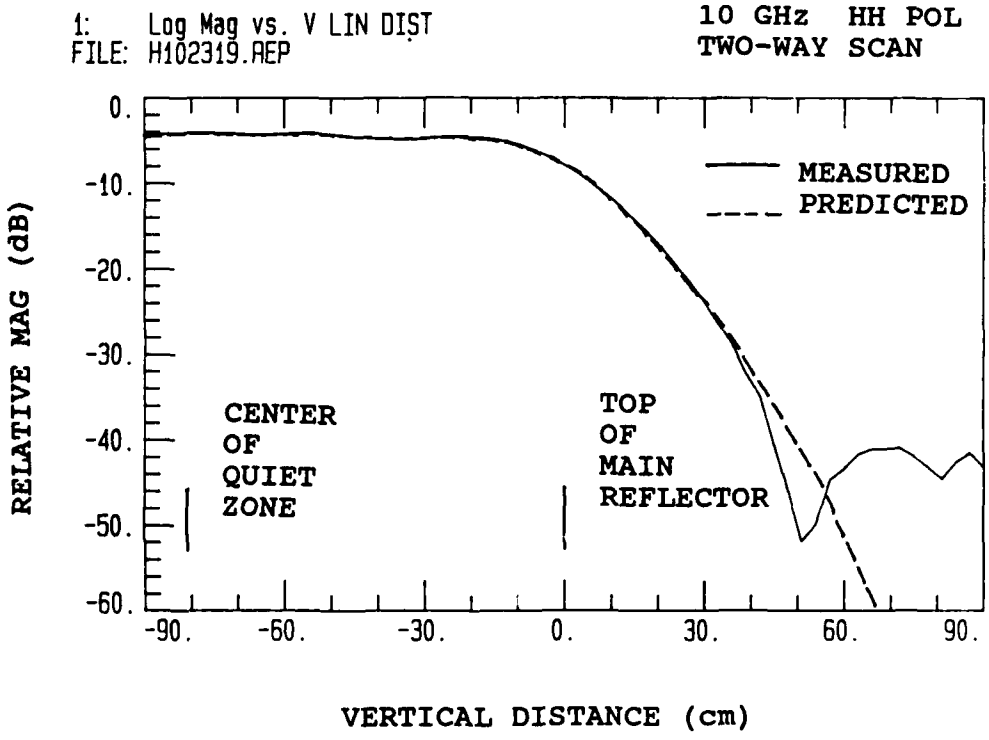

Fig. 3.7. Compact range plane-wave amplitude variations as a function of vertical position in the chamber.

were performed. Unlike an actual wall of absorber in the chamber, the test wall could be moved and oriented in almost any position so that tests at various angles and directions could be conducted. One disadvantage of the compact range and test wall measurement configuration is that bistatic measurements are not easily conducted. Only monostatic absorber evaluations were conducted using this setup because of this limitation. Other absorber tests were also conducted in the compact range on smaller samples and configurations; these will be discussed throughout this chapter.

The construction of the test wall and its positioning and supporting structure are shown in Figure 3.8. The wall is mounted on a low-backscattering metal support column and is placed in the compact-range chamber. The wall was built from plywood with a wooden backup structure. The azimuth (AZ) positioner, shown mounted on the top of the support column, was attached to a wooden structure which allowed for additional elevation (EL) and azimuth (AZ) control. Thus, forming complete AZ/EL/AZ control of the wall. The bottom positioner being computer controlled and the top two axes being manually set. A digital inclinometer, with an accuracy of 0.1 degrees, was used for aligning the wall. However, the wooden wall structure itself was not flat enough to allow for better than a 0.25 degree alignment accuracy. Figure 3.9 illustrates the movement of the wall and

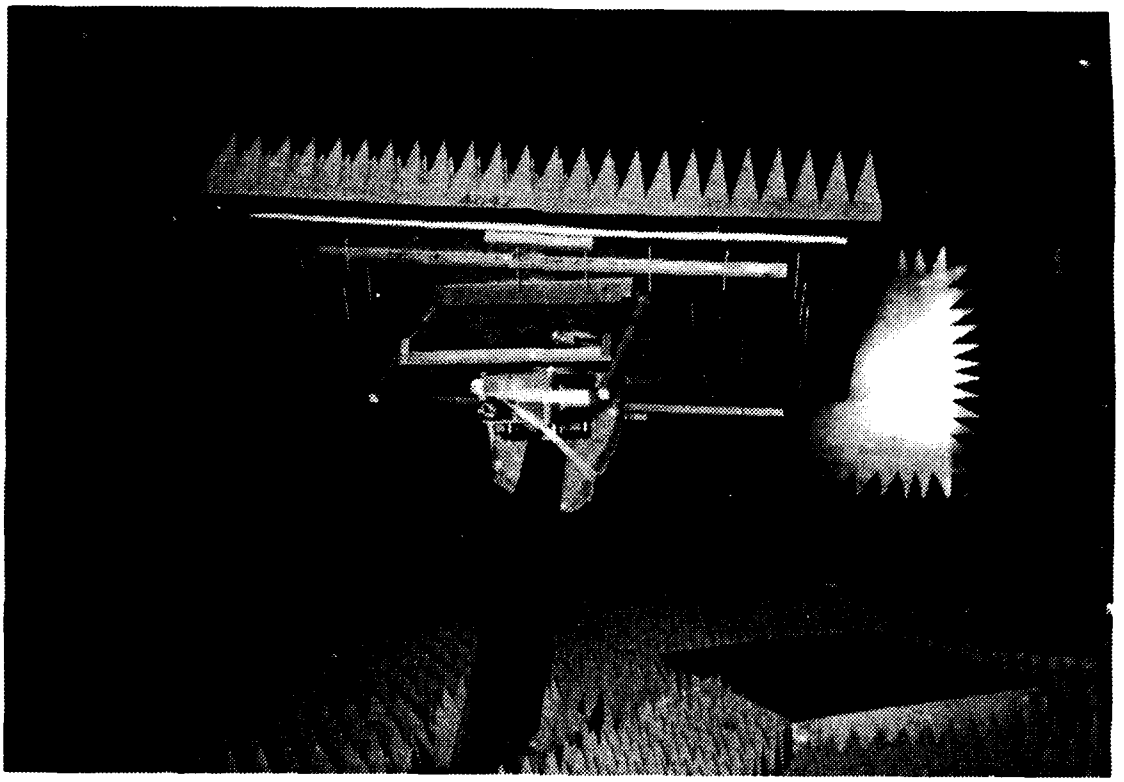

Fig. 3.8. The absorber test wall shown mounted on low backscattering metal support with positioning equipment.

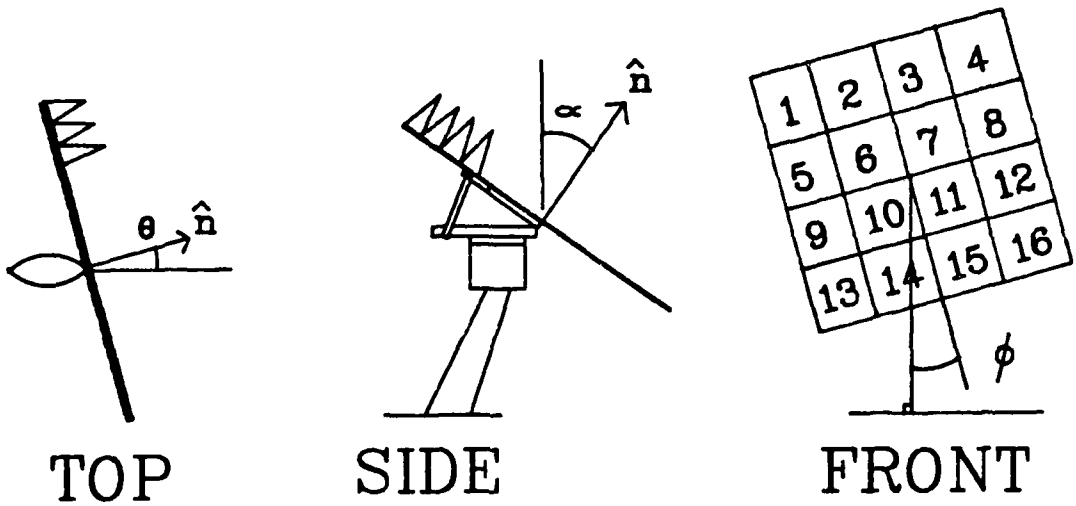

Fig. 3.9. Definition of the test wall's orientation with respect to the incident plane-wave direction and compact range.

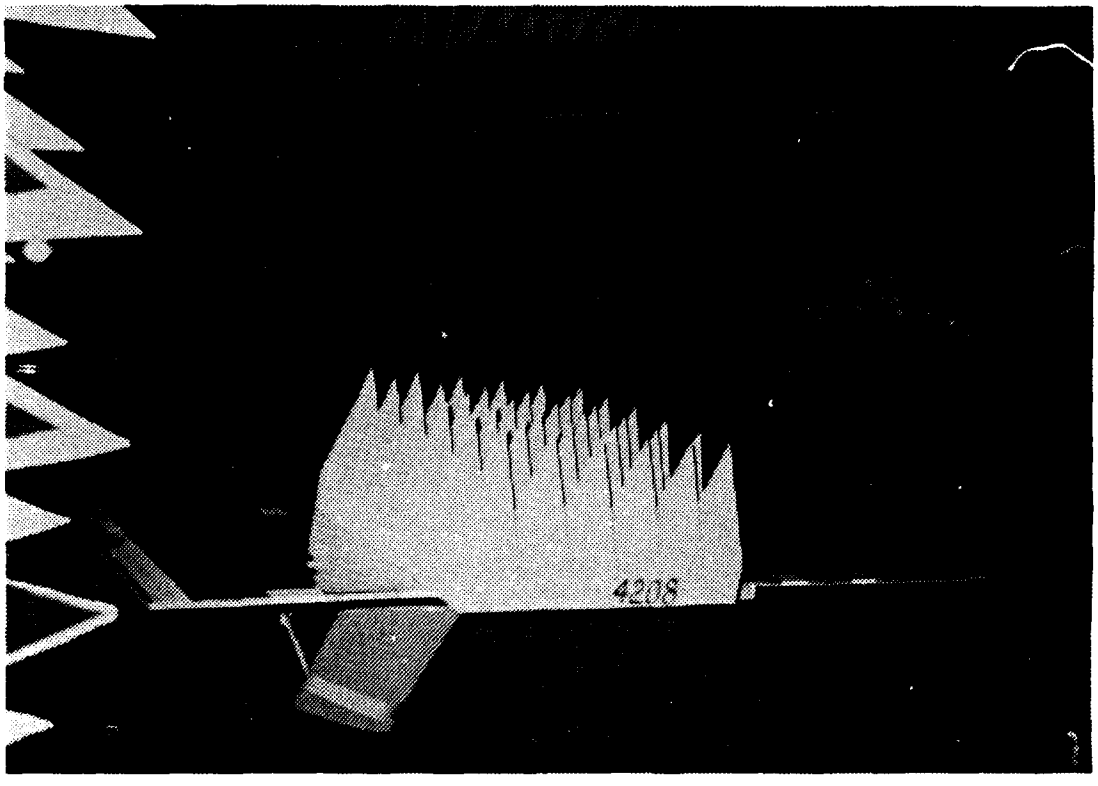

Fig. 3.10. Test wall shown with metal covered surface and single 12 inch pyramidal absorber piece.

defines the appropriate angles used to describe the wall's position.

Evaluations involved both the absorber placed over the bare wooden wall, and with the wall covered with a thin metal surface, as shown in Figure 3.10. This was done to help determine the importance of the metal backplane on the absorber's performance.

The size of the wooden wall was 7 by 7 foot so that the absorber samples would extend over and cover the edges of the supporting wood structure. The absorber shown in Figures 3.8, 3.10 and 3.11 is a 12 inch pyramidal absorber. The absorber was mounted on the wall by protruding several small 0.25 inch wooden dow pins, sharpened on one end, through the back of the wall a distance far enough to extend into the absorber base and hold the material in place as shown in Figure 3.8. Figure 3.11 shows this same absorber wall as viewed from the front with phi=0, and alpha=20 degrees.

3.3.3 Coherent Wideband Radar Techniques

The advantages of using coherent wideband radar instrumentation and techniques for absorber evaluations have already been addressed. They are mostly associated with the wide frequency bandwidth over which such radars can

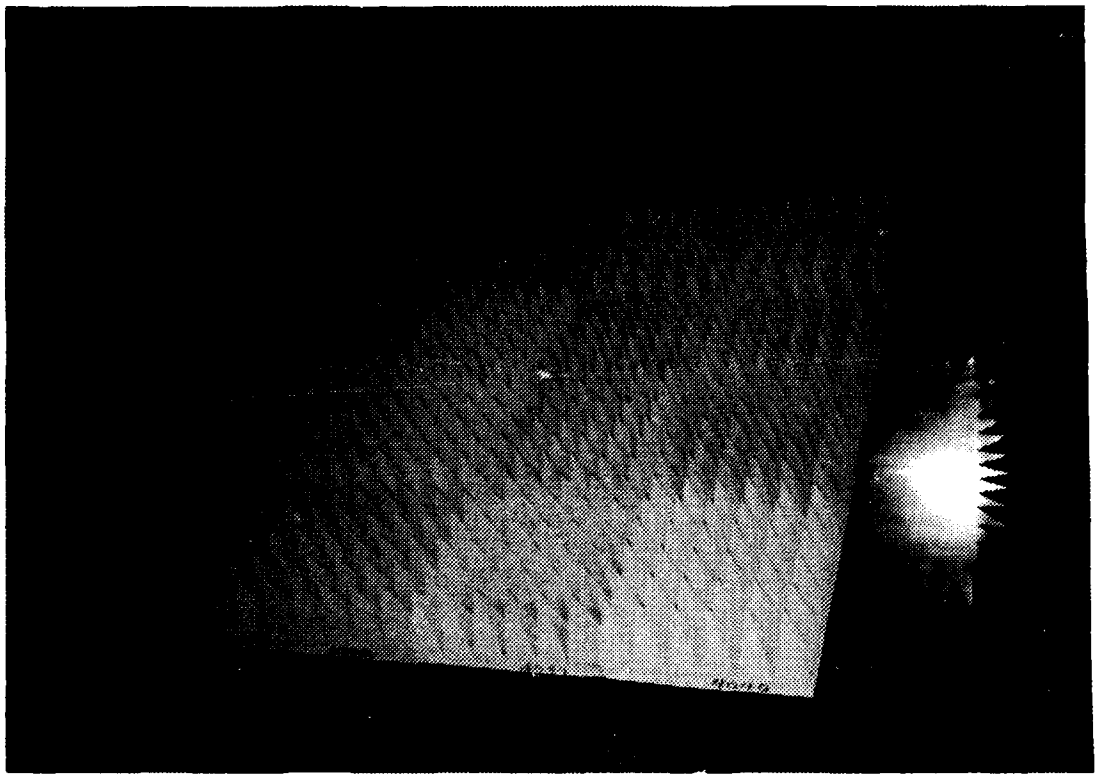

Fig. 3.11. Front view of absorber covered test wall shown mounted in compact range.

operate. The capability to generate time-domain results from this frequency-domain information then allows such techniques as range-gating or range resolved measurements to be conducted. Generally, the more frequency information which is available the more range resolution also available. Many different types of wideband radars and processing techniques are commonly used today. These systems range from the simple short pulse radars and FM/CW or chirp techniques to advanced synthetic or frequency stepped approaches. The synthetic approaches have the benefit that large instantaneous bandwidth is not required; however, accurate frequency stepping is needed. Using this technique, much more effective frequency bandwidth can be achieved and better range resolution obtained. These various radar systems are well addressed in the literature [29]-[32]. The system used to conduct the absorber evaluations for this study was a stepped frequency or synthetic short pulse technique. The system instrumentation is described in Section 3.3.3.1.

With appropriate signal processing, imaging techniques can be conducted with the use of a coherent wideband radar. Imaging allows for a range-resolved presentation of the measured target in at least two different simultaneous planes. An imaging technique known as Inverse Synthetic Aperture Radar (ISAR) imaging was used to perform many of the absorber evaluations of this study and is discussed

further in this Section and in Appendix A. Other typical frequency and time domain techniques are also presented along with some significant measured absorber results obtained with these techniques.

3.3.3.1 Measurement Instrumentation

The instrumentation setup used to conduct the absorber evaluations for this study is shown in Figure 3.12. The system was based around the use of a Hewlett-Packard vector network analyzer (HP-8510) as the principal receiver. A synthesized microwave source (HP-8340) was used to generate the transmitted signal as well as a phase-lock and reference signal. A solid-state amplifier (HP-8349) was used to increase the transmitted power level to around 100 milliwatts. The antenna feeds, which were used to illuminate the compact range and thus the target, were simple corrugated conical horn antennas. Four antennas were used to form a feed cluster with mechanical switches to select the proper polarizations for the measurement.

All of the test equipment including the target positioner controller were controlled by a DEC MicrovaxII computer via an IEEE-488 communications bus. The controller computer had facilities for user-interfacing, data storage and data presentation through the appropriate devices as

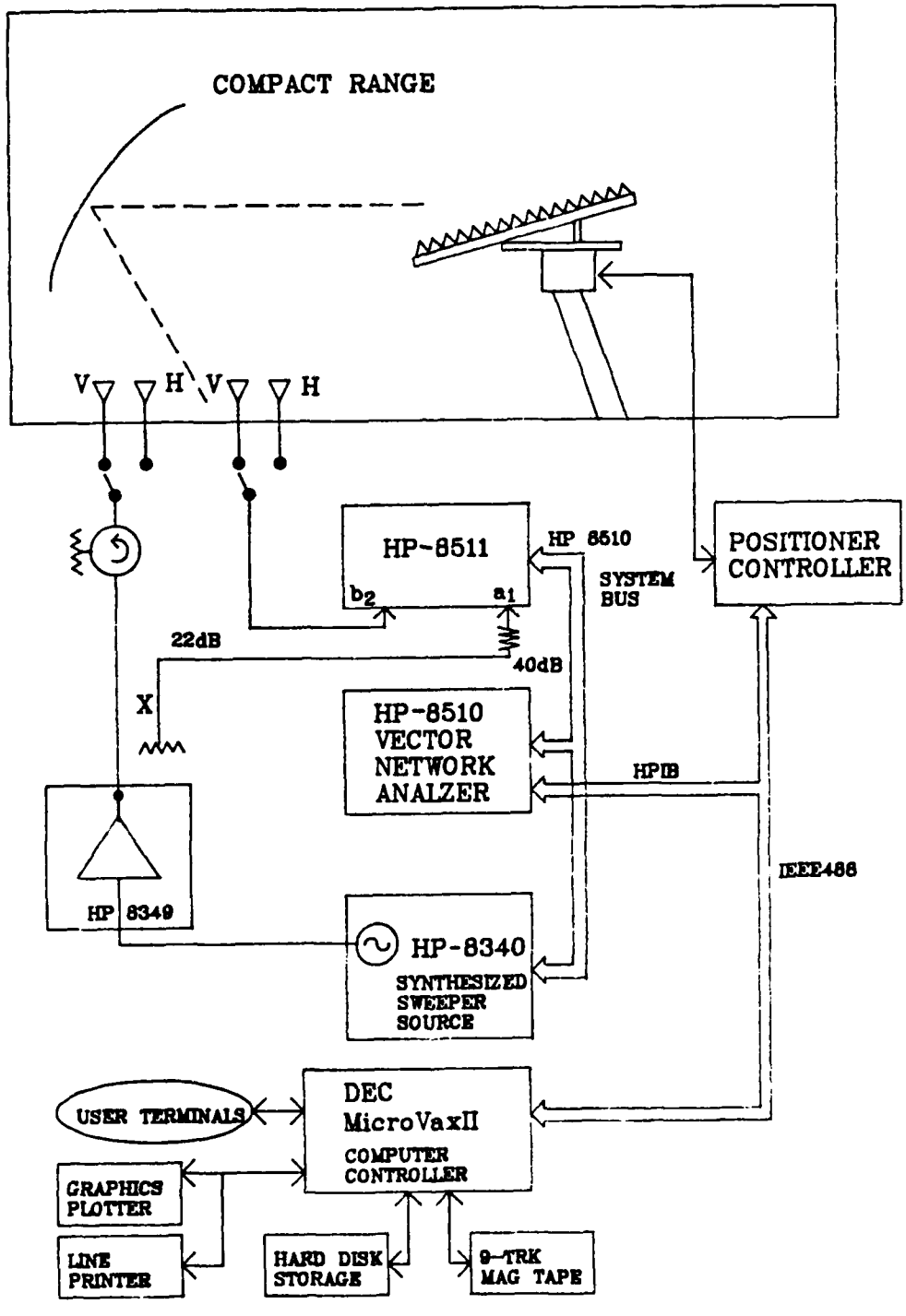

Fig. 3.12. The RCS measurement instrumentation setup used to conduct the absorber evaluations.

shown.

The HP-8510 is a commonly used instrument to conduct RCS measurements [33],[34]. For image processing, this device is used as a frequency stepped radar receiver. The advantages of the HP-8510 are its vector representation and time-domain processing capabilities. The stability, dynamic range and accuracy of the device also make it a good candidate for RCS evaluations. In addition to the time-domain processing capability of the HP-8510, additional signal processing can be conducted on the measured data within the computer controller, which employs a dedicated matrix array processor. Using this particular setup, with additional signal processing, ISAR type images can be formed. A software package known as ARCS (Automated RCS) [35] is used to control the HP-8510 and perform many of the signal processing and data presentation functions through the Microvax computer.

3.3.3.2 Inverse Synthetic Aperture Radar (ISAR) Imaging

Imaging techniques have already been introduced as methods by which diagnostic type information about the scattering behavior of a complex target can be obtained. ISAR imaging is one such technique which was considerably used during this absorber evaluation to determine the

off-normal performance of various absorbers. The results obtained from the image data have been used to help explain some of the nonhomogeneous nature of the absorber samples as well determine the importance of certain installation alignment techniques and procedures. Other significant advantages of the imaging techniques are their capability to isolate and separate error signals from the measurement, and their improved sensitivity performance which leads to more accurate results especially for low-scattering, high-performance absorber materials. Example ISAR images which were measured during this study are illustrated in this section demonstrating the advantages of the technique.

The theoretical relationships behind ISAR imaging are found in Appendix A. In general, with ISAR imaging, a complex scattering target can be characterized by the exact location of its isolated scatterers in both slant (down) range and cross range. The construction of an image, using the stepped frequency radar approach, involves collecting scattering data from a complex target as a function of both frequency and angular rotation. For each angular sample, the frequency data is used to obtain the slant-range profile of the target through an inverse Fourier transform. When the profiles for all the angular sample points are collected they are again processed through a Fourier transform to extract the Doppler frequency content of each scatterer and the cross range information is obtained. Thus, an

image is formed. The resolution of the image is basically determined by the frequency bandwidth over which the scattered signal is measured and the total angular deviation over which it is taken. For the images constructed on the absorber samples, a frequency bandwidth of 4 GHz was used, resulting in a slant-range resolution of about 5 cm after application of the proper weighting function to reduce the sidelobes in the time domain result. To achieve the same cross-range resolution, an angular rotation of 32 degrees was used for the 2.9 to 6.9 GHz frequency band and 15 degrees for the 13.8 to 17.8 GHz band.

Other uses of ISAR imaging techniques, relative to absorber evaluations, include their use for incoming inspection and quality assurance. Several pieces of absorber materials can be evaluated during one single measurement and the exact performance of each piece can be extracted. Synthetic imaging techniques can also be useful for chamber verification and check-out, since an image of a complete wall section of a chamber can be evaluated to check for problem areas or faulty absorber pieces.

3.3.3.2.1 Absorber Images

During the absorber evaluation, several different types and sizes of absorber materials were imaged using the ISAR system discussed above. Over 1400 images were

constructed and numerous useful and interesting results were obtained. Images were constructed for various orientation angles on the absorber samples ranging from 10 to 50 degrees from grazing incidence. A few of the actual images and their significant results will be presented in this section in order to demonstrate the usefulness of the technique. Other imaging results from the absorber evaluation are summarized in Chapter 4.

Images can be presented in the form of a 3-D waterfall plot or a contour plot showing the magnitude or phase of the resolved scatterers making up the image as a function of their slant range and cross range. Presentation of the images in this way provides an immediate method of determining which parts of the target sample demonstrate the best or worst performance. However, because of the enormous number of images taken during this study and the amount of information contained in each image, a method of summarizing the overall result of a given image had to be employed.

The method used to summarize the images was to calculate, using the image data files and a computer, the averages, medians and standard deviations of the returns of all the range cells which made up the image. Only the part of the image which represented the 4 by 4 foot area of the center of the test wall and not along the zero cross range line were used. The reasons for this selection follow. The

number of range cells within this test area is a function of the range resolution of the image and the tilt angle of the wall (alpha). For the images conducted during this study, 930 range cells were used in the analysis for tilt angles of 10 to 20 degrees and 750 range cells for a tilt angle of 40 degrees.

An ISAR image of the test wall, covered with 18 inch pyramidal absorber, at an aspect of phi=0, theta=0, and alpha=30 degrees, is shown in the waterfall plot of Figure 3.13. The imaged region includes an area which is larger than the actual test wall (+/- 2 m.) and the boundaries of the test wall are clearly shown in the image (recall that the test wall is 8 by 8 feet or 2.4 by 2.4 meters). The larger returns shown along the cross range of the image at a slant range of about -1 meter are caused by the relatively large flat absorber surfaces along the front edges of the absorber covered wall. The returns from this area are shown to be about 20 dB higher than the returns from the rest of the wall. One big advantage of the imaging technique is that these large returns, which are not found with an actual absorber wall, can be excluded or separated from the part of the test wall where the desired performance data is being evaluated. The levels over the rest of the absorber wall are around -60 dBsm. As stated earlier, only the area of the test wall representing the 4 foot square center section of the wall was used in the actual

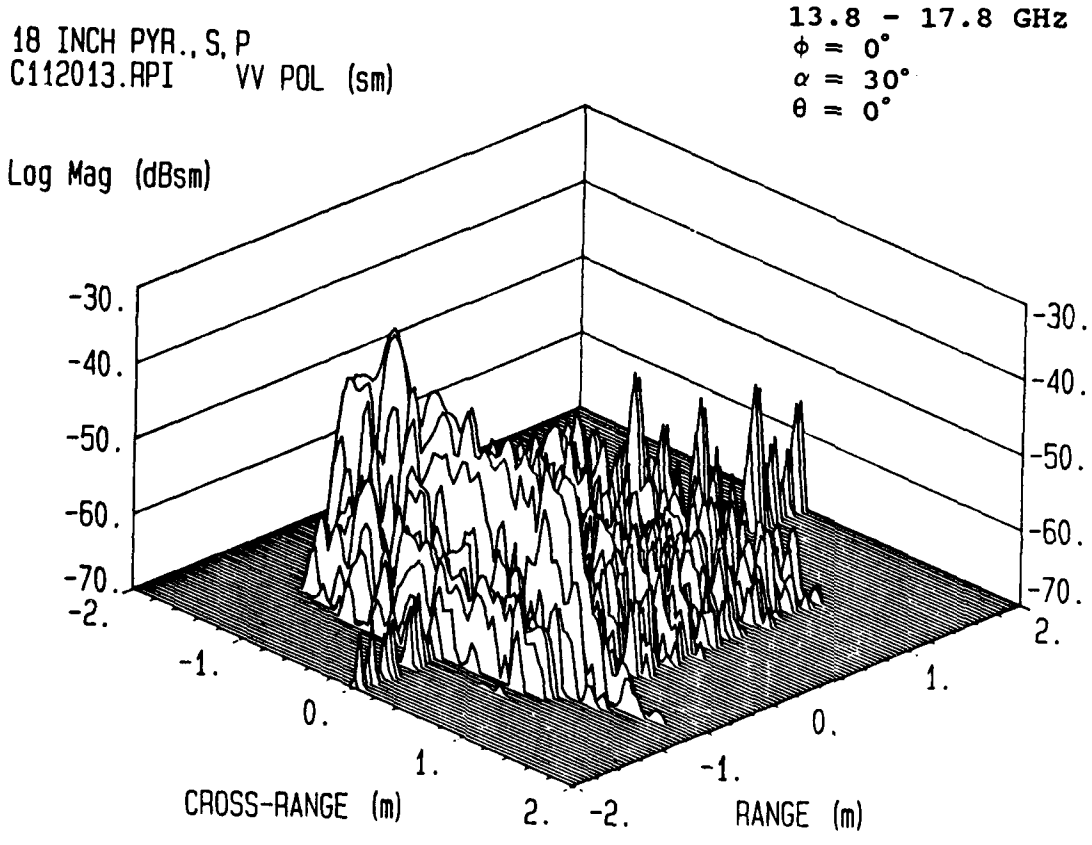

Fig. 3.13. ISAR image of test wall covered with 18 inch pyramidal absorber for Phi=0 and Alpha=30 degrees.

absorber evaluation and performance summary. This was done to discriminate against the unwanted edge contributions and also because of the compact range illumination and test zone size.

The sensitivity or the lowest measurable level for a given S/N ratio is shown in the image to be below -70 dbsm, which allows extremely small scattering levels to be detected. This is very important when evaluating the low-level scattering nature of absorber materials. The ability to measure such low-scattering levels is related to the transmit power used, the receiver sensitivity, and the signal processing (integration via the Fourier transform) used to generate the image. Such integration has the same effect as coherent integration or averaging to improve the S/N ratio; however, because weighting and time-gating are usually used, the result is a weighted average involving the number of discrete data points used in the transform. Another benefit of imaging is the isolation and discrimination of the testing environment and unwanted error signals not associated with the test wall. This is achieved by the use of both range gating and Doppler filtering. Because the returns associated with the chamber environment and instrumentation do not rotate or move with the target rotation, they have no Doppler content and can be separated from signals which do have Doppler. The presence of the error signals are shown in Figure 3.13 along the zero cross-

range line. Without being able to separate these error signals, the smallest measurable absorber return would be much higher than -70 dBsm. The returns along this zero cross range line were ignored in the evaluation of the image. No form of background subtraction was used for these measurements.

Using the measured images of different absorber configurations, comparisons can be made between the relative absorber performance of the various configurations. Figure 3.14 shows a measured image of the same test wall and absorber as in Figure 3.13 but for a phi angle of 45 degrees. Using a computer to compare the differences between the scattering of these two cases it was shown that the material turned 45 degrees offered an average of 3 dB improved monostatic performance for this particular aspect, frequency and polarization. Figure 3.15 shows an image of the 18 inch wedge materials at the same aspect as for Figure 3.13. The improvements with this case are easily seen. Again note the large returns associated with the front edge of the test wall.

Another image of the 18 inch pyramidal absorber wall is shown in Figure 3.16 for an alpha of 10.6 degrees (phi and theta of 0). This orientation represents the half-angle of the absorber pyramids and is the aspect where the radar is directed normal to the pyramid's flat sides. As a result, the returns from the absorber for this case are

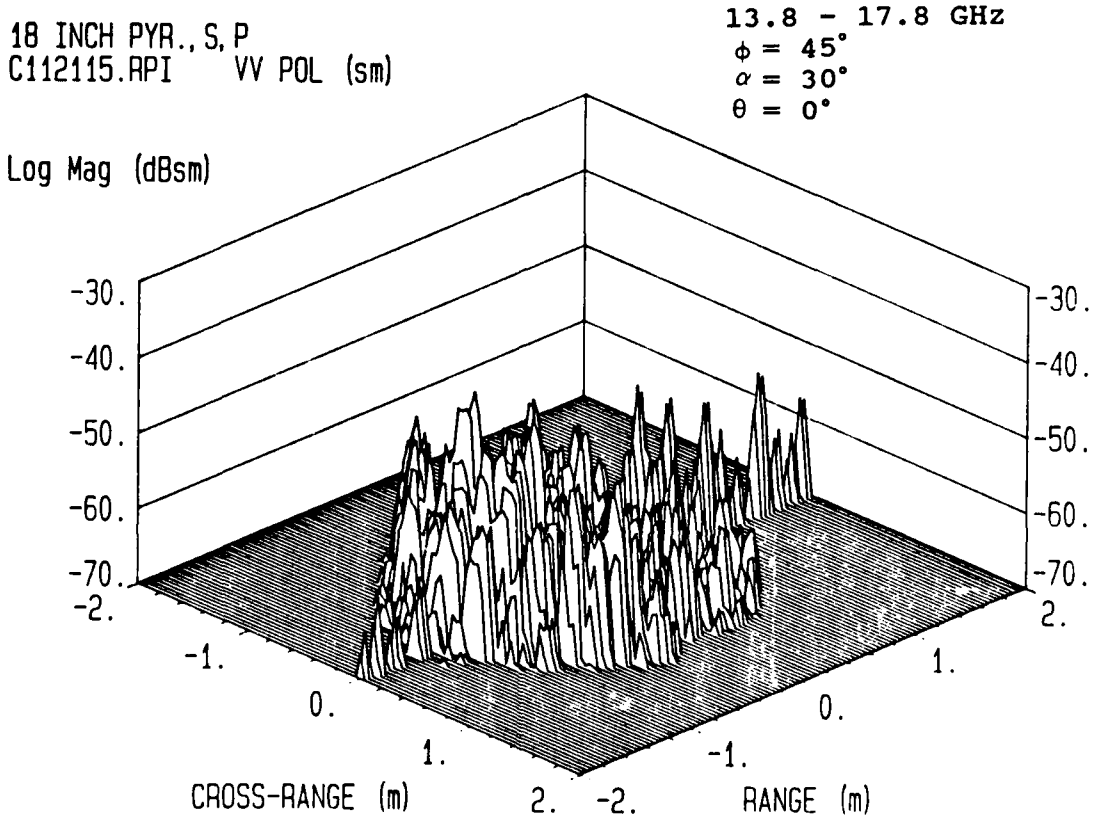

Fig. 3.14. ISAR image of test wall covered with 18 inch pyramidal absorber for Phi=45 and Alpha=30 degrees.

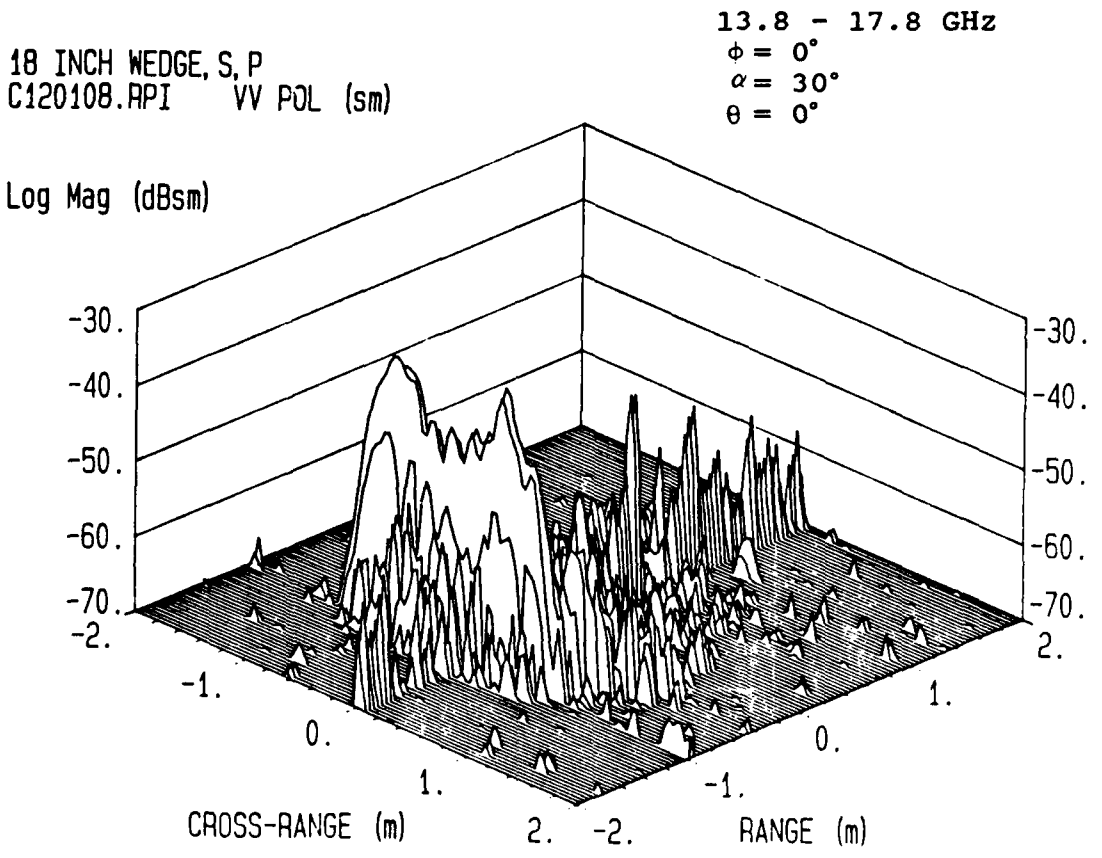

Fig. 3.15. ISAR image of test wall covered with 18 inch wedge absorber for Phi=0 and Alpha=30 degrees.

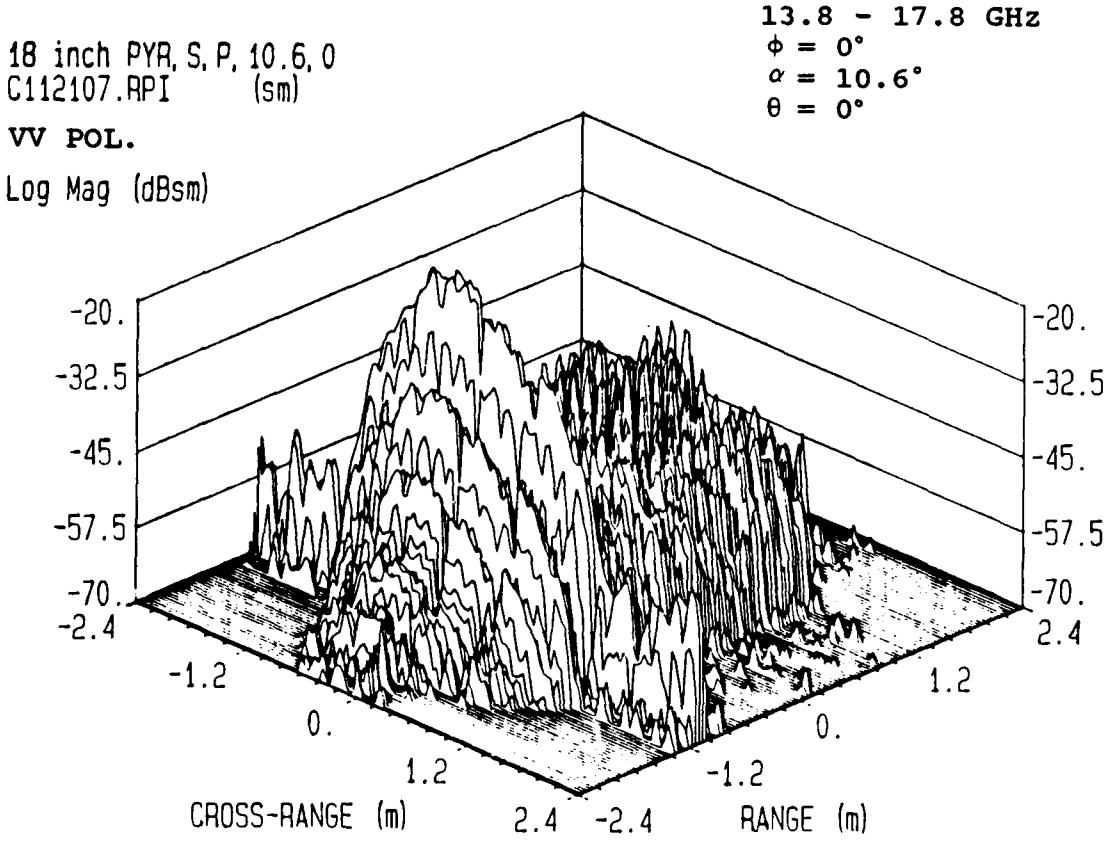

Fig. 3.16. ISAR image of 18 inch pyramidal absorber showing the large return from the flat sides of the shapes for Phi=0 and Alpha=10.6 degrees.

more than 20 dB higher than for the case of alpha= 30 degrees. The large return from the flat surfaces along the front of the wall are clearly shown and are as big as -10 dBsm. Figure 3.17 shows the same image data but in the form of a contour plot.

To illustrate the diagnostic benefits of the ISAR technique, Figure 3.18 shows a close-up contour view of the four pieces of material in the center of the wall (a 4 by 4 foot section). A piece of 18 inch pyramidal material is 2 by 2 feet at the base and has 16 individual pyramids (cones). The image clearly shows the return from each individual cone and also shows that the returns from the cones are not uniform. It is also shown that each piece of material has a different scattering performance. The inconsistent and nonhomogeneous nature of the material has not been so clearly presented by any other evaluation method. Section 4.2 addresses the nonhomogeneities of the material in greater detail.

3.3.3.2.2 ISAR Image Focusing

One important characteristic of the ISAR imaging technique which must always be considered is the issue of the image's quality or sharpness. There are several factors which cause an ISAR image to not be the exact representation of the target. These image errors are referred to

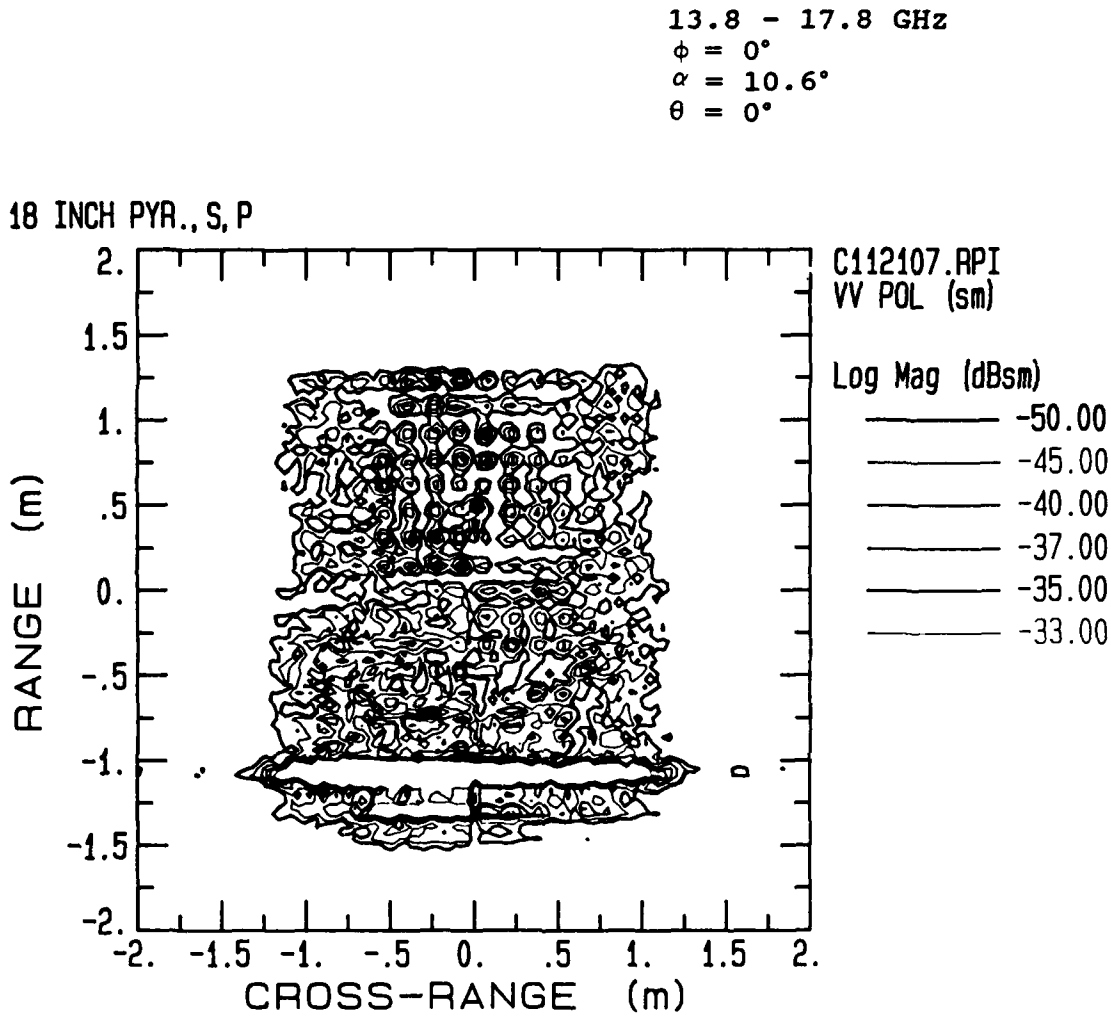

Fig. 3.17. Same ISAR image data as in Figure 3.16 but shown as contour plot.

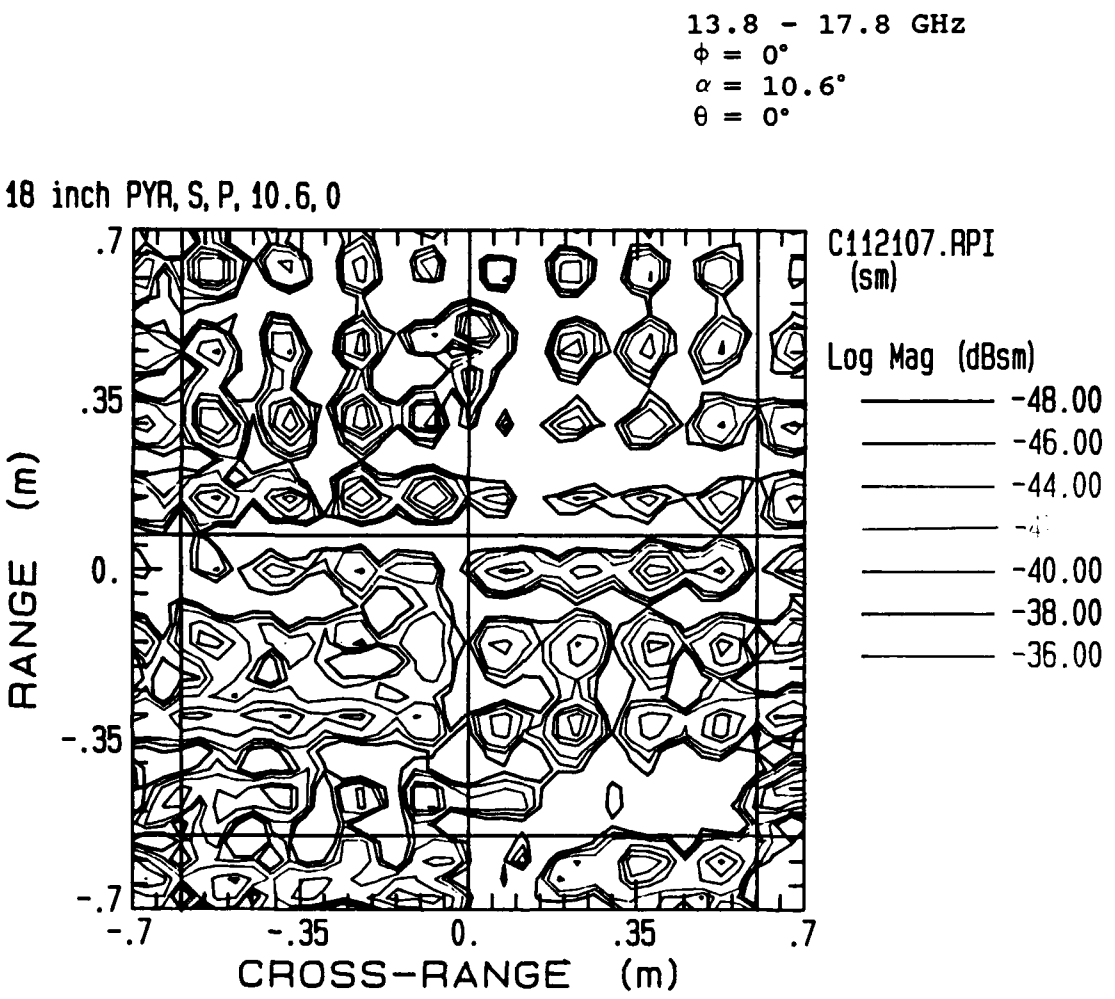

Fig. 3.18. Contour plot showing the returns from the four center pieces of absorber for the same image data as in Figure 3.16. The return from each pyramidal shape is shown.

as image defocusing. The effects of nonfocused images are discussed in this section. Focused processing techniques can be used to improve the quality of most images. These focusing techniques are discussed in Appendix A.

Many of the causes of unfocused images are associated with the motion or rotation of the target. For non-cooperative targets the motion of the target cannot be controlled and motion compensation techniques must be employed to correct for image defocusing. Other causes of defocusing are related to the signal processing and measurement sampling techniques used to construct the image. For the imaging of cooperative RCS targets, as with the case for the absorber evaluations, the motion behavior of the target can be well controlled, resulting in very little image degradation of this type. Thus, the source of most image errors, for the absorber evaluations, was in the signal processing techniques employed. This type of image defocusing results in range cell blurring and amplitude or phase variations across the image being worse at the edges and diminishing toward the center region of the image (center of rotation).

The ISAR signal processing techniques used during this study made use of a stepped frequency or synthetic short pulse radar to collect reflectivity data over a band of frequencies and range of angular samples. For practical purposes, evenly spaced frequency and angular spacings were

used. This data was then processed using standard discrete Fourier transforms (DFT) to first generate the synthetic slant range profiles for each angular position and, secondly, to find the Doppler frequency content of each scatterer in cross range. This process involves a 2-dimensional DFT. A DFT will convert one set of complex values into another exact transform-pair set of values as long as the values are at uniformly spaced intervals. Thus for this case, the 2-D transform requires a rectangular grid of uniformly spaced measured data in the spatial frequency domain (see Appendix A). A problem arises because the uniformly spaced data in frequency and angle, measured with the radar, form a polar grid when transformed to the spatial frequency coordinates. Transforming this polar grid can cause the image to be distorted or unfocused.

Focusing techniques exist where the measured polar-grid data can be reformatted to, or approximated by, a rectangular grid (see Appendix A). The polar reformatting method requires additional processing and usually involves a loss in effective resolution; however, perfectly focused images can be constructed. The approximation approach assumes that the target data is collected over small angular regions and that small frequency bandwidths, compared to the center frequency, are used. Under these limitations, adequately focused images can be constructed, especially for images of relatively small targets, high center operat-

ing frequency, or minimum resolution requirements. A method generally used to determine the adequacy of the approach is to define a blur radius of the image, or the radius at which a scatterer would migrate through a complete range cell over its total rotation. If the target size is smaller than the blur radius then the approximations result in nicely focused images. However, using this technique does not indicate what performance degradations occur when the target is larger than the blur radius or if usable results can still be obtained even though some defocusing occurs.

A method, by which the effects of image defocusing can be observed and analyzed, is by generating images of known targets with defined scattering characteristics and correlating the measured results with the expected results. This method is most effective with the use of computer simulated images of perfect theoretical targets. The advantages of this technique are that the targets are completely defined and theoretical or classical targets can be modeled. Computer simulations are also a valuable development tool for trying new or different processing algorithms.

The effects of defocusing on the absorber images were evaluated by simulated ISAR images of arrays of point source targets, simulating an absorber wall. The simulated images were constructed using the image system parameters (frequency bandwidth, angular sampling, weighting and test

sample size). For this case a square resolution of 1.5 inches was assumed.

A wall of pyramidal absorber was modeled using one point source to represent each cone of absorber positioned at the appropriate location on the 8 by 8 foot wall. As an example, the simulated wall of 18 inch pyramidal absorber had 16 by 16 point sources (256 total) spaced 6 inches apart. Figure 3.19 shows the simulated image of this particular wall using fully focused processing at the 13.8 to 17.8 GHz band. This contour plot shows the return levels of -1 and -5 dbsm (the value of each point source was normalized to 0 dBsm) over a +/- 1 meter area of the wall. The four pieces of material representing the middle sample area of the wall are also identified in the figure. For the focused case, the image is essentially perfect. Figure 3.20 shows the result of the same simulated wall except with unfocused image processing. The same four pieces of material in the center of the wall are marked. The contour lines in this image are for -1,-3, and -5 dBsm. Notice the effect of defocusing starting to blur the image at its edges. The center sample area is only slightly blurred to the -5 dBsm level, even though the calculated blur radius for this case is only 5.6 inches.

Figure 3.20 also shows that the amplitude of the responses is reduced for those point sources away from the center of the image. To see the effect more clearly, Figure

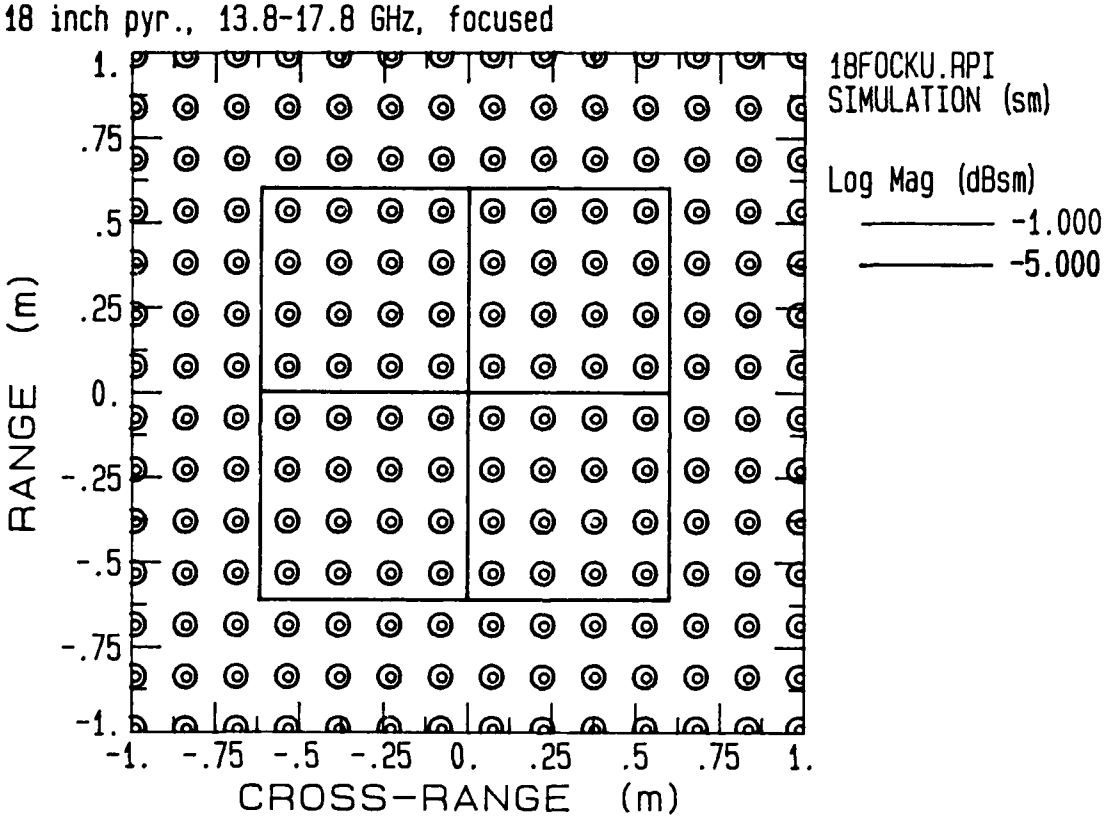

Fig. 3.19. Simulated ISAR image of 18 inch pyramidal absorber test wall using point-source model and fully focused processing.

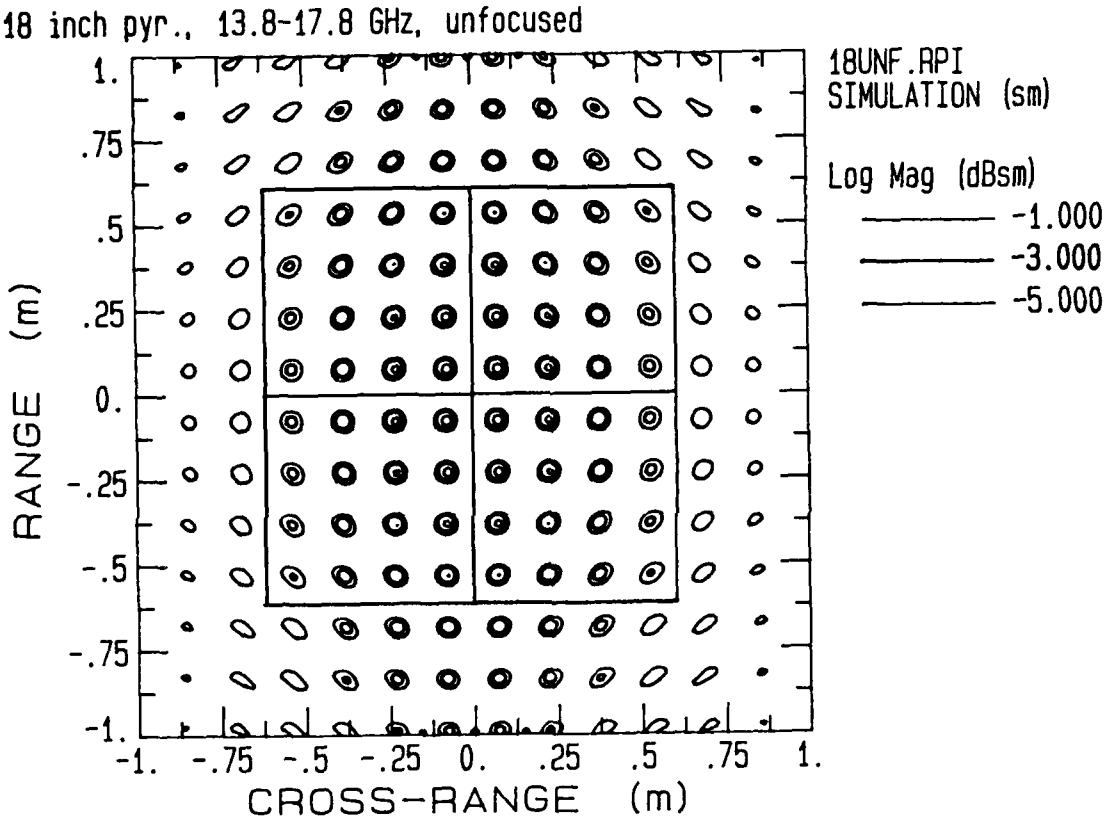

Fig. 3.20. The same simulated ISAR image as for figure 3.19 except using unfocused image processing.

3.21 shows three different plots of a single down range or cross range profile of the image with a fixed value of range or cross range. These plots represent cuts through the image showing the effects of defocusing at the edges. The overall effect is that the worse case amplitude error, within the 4 by 4 foot sample area, is only 2.8 dB. Repeating this same procedure, for the 2.9 to 6.9 GHz band, results in slightly more image blurring and a worse case amplitude error at the edges of 4.9 dB. For the same image parameters with simulated images of point sources spaced more closely than that of the 18 inch simulated wall, defocusing resulted in increased blurring at the image's edges but in the same amount of amplitude error. Figure 3.22 illustrates the image defocusing for a single cross-range row of 12 inch simulated cones within the four foot sample area (12 cones spaced four inches apart).

Based on these simulated results, and considering the intended application of the absorber images, the minor effects of defocusing were not considered to be limiting; even though the blur radius had significantly been violated. It was decided that unfocused image processing could be used for the absorber evaluations since the processing algorithms were already available and the data acquisition time would be significantly less for the same amount of image resolution. Improved image sharpness could, however,

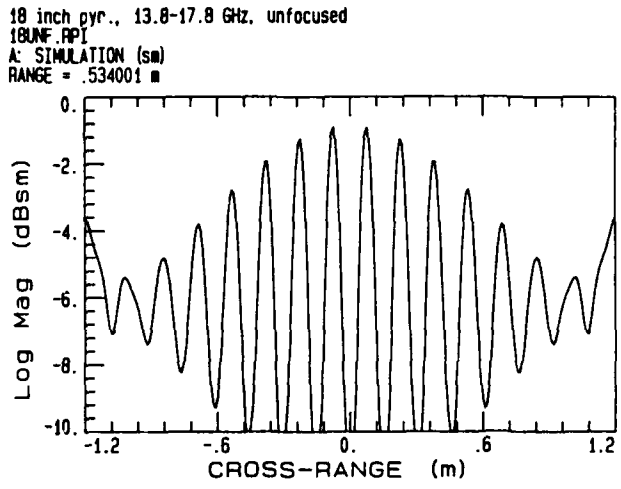

a) Fixed slant range= 0.53m

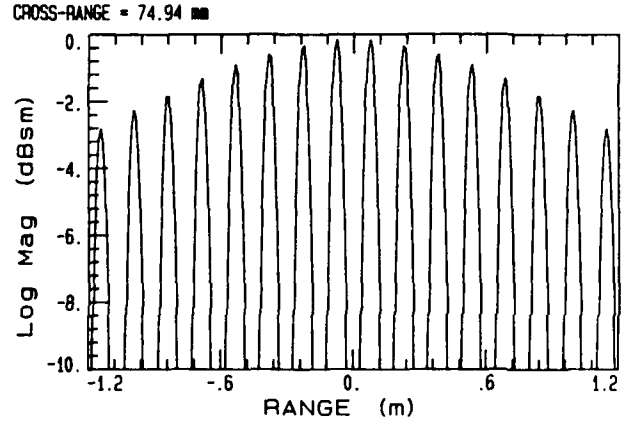

b) Fixed cross range= 75mm

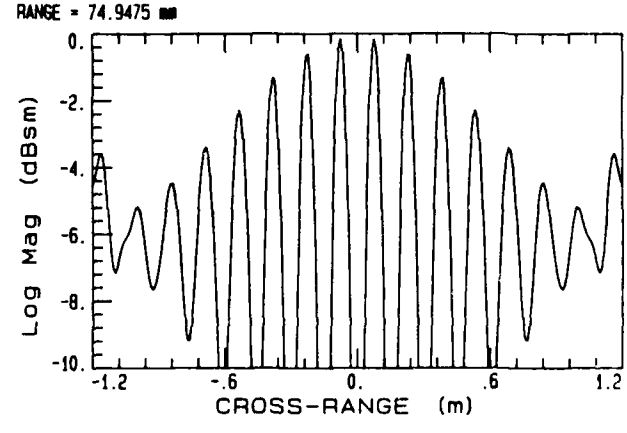

c) Fixed slant range= 75mm

Fig. 3.21. Amplitude plots of the simulated image data shown in Figure 3.20 for fixed values of either slant range or cross range showing the extent of amplitude variations caused by defocusing.

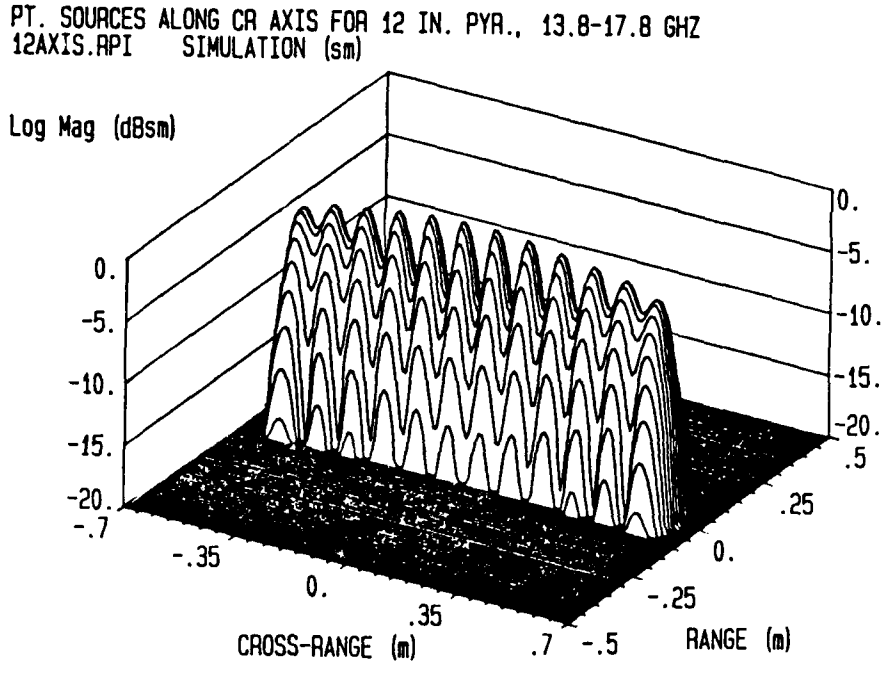

a) Waterfall amplitude plot

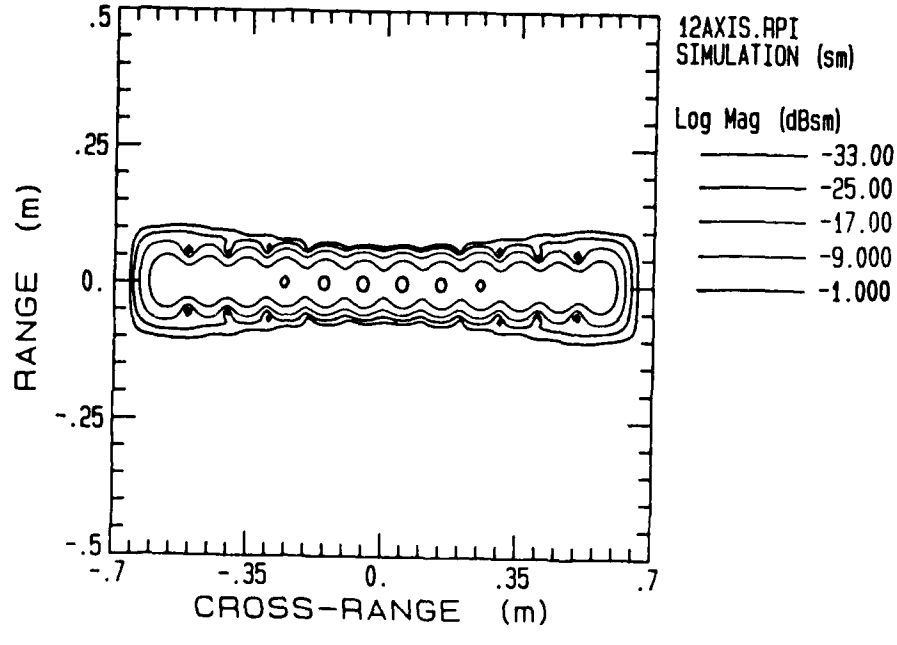

b) Contour amplitude plot

Fig. 3.22. Simulated ISAR image of a single row of 12 inch pyramidal absorbers showing effects of defocusing for more closely spaced scatterers.

be achieved by the use of focusing techniques in the future.

3.3.3.3 Frequency-Domain Time-Gated RCS

One technique used to evaluate the performance of the absorber samples at normal or near-normal incidence (alpha=90 degrees), was to conduct standard RCS versus aspect and frequency measurements on the complete test wall in the compact range. Range gating techniques were used to eliminate the unwanted responses of the chamber, test wall edges, and instrumentation. A range gate of 2.0 meters was used. The total backscatter signal was recorded as a function of the aspect position of the wall (varying theta) for fixed frequency values. The measurements were calibrated using standard RCS calibration techniques and the results were recorded in units of dBsm.

The effective result of such a measurement is to measure the RCS of the absorber wall, versus aspect angle, in a plane including the normal to the wall. Figure 3.23 illustrates the results of one such measurement conducted on the test wall covered with 12 inch pyramidal absorbers at 15 GHz. The test wall was covered with a metal surface beneath the absorber sample. Both polarizations are shown. The results show that the scattering from the wall changes only slightly over the entire +/- 40 degrees from normal

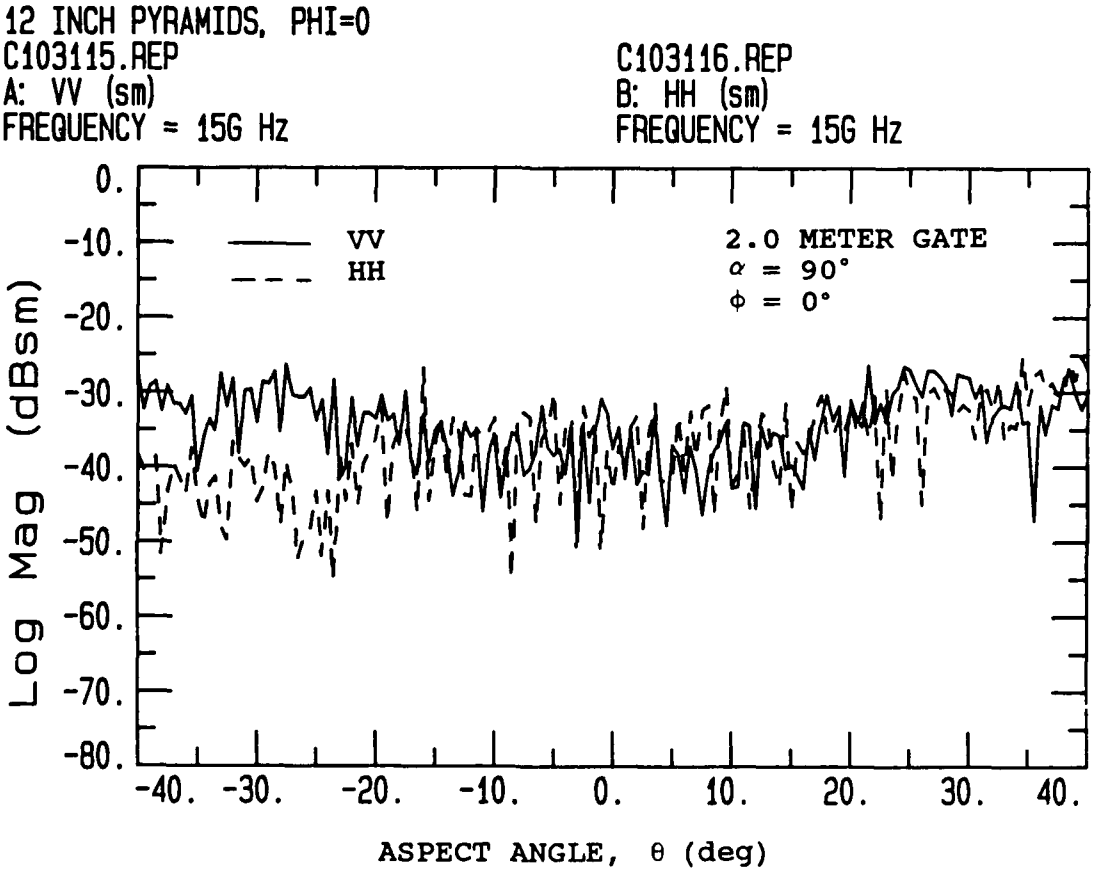

Fig. 3.23. RCS versus aspect angle measurement results for the complete test wall covered with 12 inch pyramidal absorber.

incidence. Also shown is that no specular scattering component is present at normal incidence. This is an important result in that it suggests that the material works uniformly over a very broad monostatic angular region. This somewhat contradicts previously published data [1],[36] which indicates that the material's reflectivity increases roughly with the cosine of the incidence angle from normal incidence, although it is not clear whether bistatic or monostatic conditions are assumed in the references.

A specular reflection from the absorber sample could be caused by two things. It could be due to energy penetrating the absorber and reflecting from the metal backplane or due to specular reflections from the surface of the absorber itself. At the frequencies used and for the sizes of materials evaluated, it is suspected that any energy which enters the absorber is almost entirely attenuated before it can reflect back through the material from the metal backplane (see Section 4.4). Specular reflections caused by the absorber surfaces are controlled by shaping of the absorbers and the number of shapes used to diffuse the incident energy. Within the angular region of +/- 40 degrees, the radar never approaches aspects where it looks normally into the absorber's flat surfaces. However, the straight edges and bases of the shapes, and diffraction effects are also present and must be considered as well as secondary reflections. This diffuse scattering

nature of the absorber actually improves its performance and is discussed further in Section 4.2.

All of the numerous measurements conducted at both frequency bands on the 6 inch convoluted, and the 8 and 12 inch pyramidal and some of the 18 inch pyramidal absorbers demonstrated similar performance to that of Figure 3.23. A few of the measurements conducted on the 18 inch pyramidal absorbers and all of the wedge absorbers, however, showed slightly more specular behavior at near normal incidence. Figure 3.24 shows results for one of the 18 inch pyramidal absorbers. The reason for these specular components is suspected to be due to the larger straight edges at the pyramid's base which causes a higher reflection or diffraction toward the radar at some aspects. The pyramids of 18 inch absorbers have much larger surface areas and longer straight edges along their sides as well, but this effect should tend to improve the backscattering performance of these materials. There are also fewer cones to help diffuse the incident energy. For materials longer than 18 inches this becomes even more of a problem and specular conditions start to degrade the absorber's performance at some aspect angles. The wedge absorbers have constant edges along the tip and valleys of their shapes and thus scatter energy from these long straight edges accordingly. To improve the performance of such materials requires that either the material be installed or aligned so that the specular

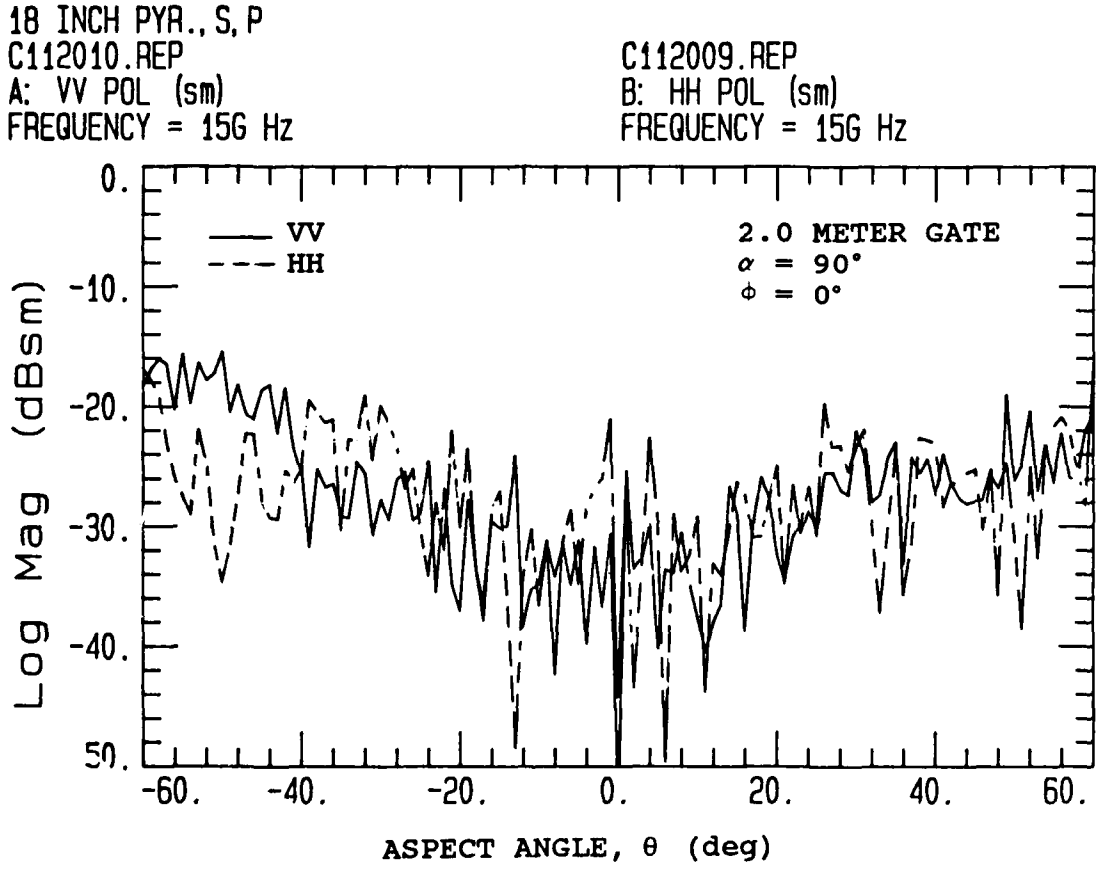

Fig. 3.24. RCS versus aspect angle results for the complete test wall covered with 18 inch pyramidal absorber showing increased specular reflections near normal incidence.

reflections are directed away from the area of interest or that new material shapes or designs be implemented.

It is also possible to obtain phase information about the scattering from such absorber surfaces using this measurement technique. However, all of the phase data taken shows that there is a highly random phase relationship, at all incidence angles including normal incidence, between the bare metal wall and the absorber sample. The reason being associated with the presence of the many distributed scattering sources of the absorber covered wall.

There are two reasons to be slightly cautious about the absolute levels in the measured results shown above. First, the sensitivity of the measurement system under the conditions of these tests was approximately -40 to -45 dBsm, resulting in a S/N ratio of only 10 to 15 dB for the particular measurements in Figures 3.23 and 3.24. Thus, these measurements may be somewhat corrupted with noise because of the low-level scattering from the absorber samples. And secondly, the angular samples used in some of the measurements, especially for the 18 inch pyramids, were taken every 1.0 degree resulting in too coarsely stepped samples to see very narrow spikes. The problem with the coarsely spaced angular samples was not discovered until after the data had been taken and it was too late to repeat any of these tests. Future work in this area should try to improve on these two deficiencies.

For flat absorber materials or for frequencies where the depth of the absorbers becomes less than a wavelength, another problem occurs with this measurement technique. Under these conditions, part of incident energy can penetrate the absorber and reflect from the large metal backplane. In this case, the return of the sample wall alone has a very narrow RCS pattern because of the its size and the frequency at which it is being tested and is very difficult to detect (measure). For flat absorbers, the specular reflection from the absorber's surface causes the same problem. Figure 3.25 shows the measured RCS pattern of the bare metal test wall at 15 GHz. It is shown that the main response of the metal wall is less than 0.5 degrees wide. The alignment accuracy of the test wall is believed to be only slightly better than this same value. With such alignment accuracy, RCS measurements of this type could very easily miss the peak return from the wall and an error in the conclusions could result. For this reason, a smaller test sample would have to be used for these cases.

Using measured RCS results as shown in Figures 3.23 and 3.25, reflectivity values can be determined using the same method as done with the NRL arch. Instead of reporting the performance of the samples by their RCS level, the reflectivities of the samples can be determined by comparing their RCS value with the RCS of the metal wall alone. As noted in Section 3.3.3.3, care must used in ob-

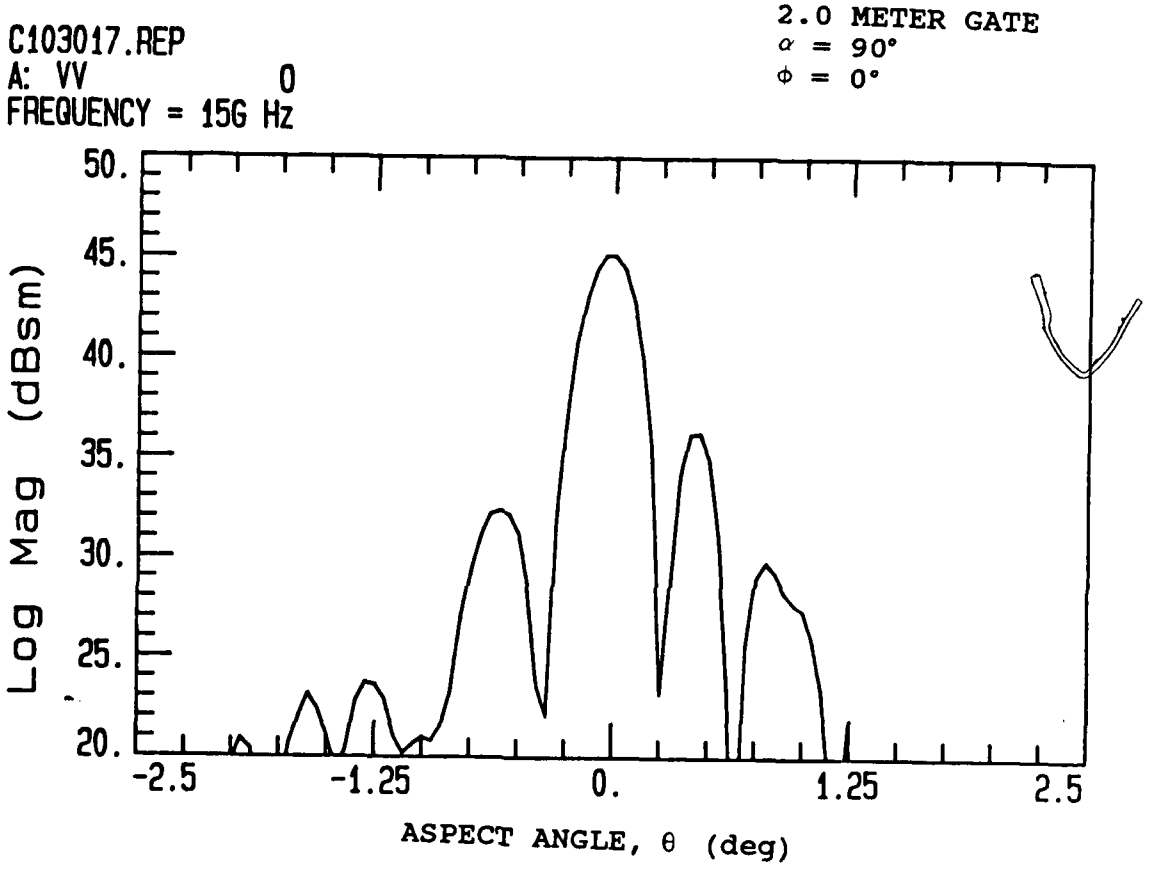

Fig. 3.25. The measured RCS versus aspect angle response of the bare metal test wall.

taining the bare metal wall measurement and in obtaining the accurate response of the absorber test sample. Reflectivity values for many of the absorbers evaluated using this technique are presented in Chapter 4. Since many of the absorbers had nearly uniform performance over a very large angular region, the arithmetic average of the absorber's RCS over a +/- 40 degree sector was used to represent their scattering performance.

As an example, for the data in Figures 3.23 and 3.25, the return of the bare metal wall is +45 dBsm at normal incidence whereas the absorber sample is below -30 dBsm for both polarizations. This results in a reflectivity value less than -75 dB, which is 25 dB better than all of the vendors report for this material. In all the cases evaluated, the reflectivity results measured during this study show better performance than the vendor's published values. One reason for these differences is related to the measurement methods used and to the limitations associated with the NRL arch method. The size of the test sample being tested, and the type of illuminating source used, also contribute to these differences.

For a random and noncoherent scattering surface, as assumed for the absorber samples shown above, the backscattered power level increases linearly with the size of the sample. This is generally true whether the sample is illuminated with a plane wave or a spherical wave (see sec-

tion 4.2). However, for the coherent flat metal surface, used as the reference, the return increases as the square of the area and is dependent on the type of illumination being used. Thus, for the case of the compact range illuminating the test sample with a plane wave, the return from the metal reference may be much larger than the reference return for the arch technique while the total scattering from identical absorber samples remains nearly the same. This would result in a lower reflectivity value for the compact range measurement. In any case, it is shown that more benefit is realized from a random scattering absorber when a plane wave condition is present.

3.3.3.4 Time Domain RCS

The third category of RCS measurement techniques, used for the absorber evaluations, are those known as time domain or RCS versus down-range measurements. As with imaging, the use of a coherent wideband radar to obtain high-range-resolution, time-domain profiles of a complex target is a common technique to determine scattering mechanisms associated with the target. For the absorber evaluations, these techniques were used to look at various test samples at normal or near-normal incidence aspect angles and at fixed positions. Such measurements were conducted in a com-

pact range RCS chamber. The degree of range resolution obtained is directly determined by the amount of frequency bandwidth used. A resolution of approximately 1 inch can be obtained for an unweighted frequency bandwidth of 6 GHz.

Results from this type of measurement are presented in Figure 3.26 which shows the time-domain backscattering profile of a single 12 inch unpainted-tip pyramidal absorber shape. The range scale is in meters and shows the location of the isolated down range scatters of the absorber sample. The zero range value is determined during calibration of the instrumentation and represents the center of the styrofoam column used to support the test sample. Figure 3.26 also shows the mounting technique used to attach the absorber pyramid to the column. A piece of masking tape was used to support the absorber shape. A weighted bandwidth of 7 GHz (test frequencies from 11 to 18 GHz) was used for this measurement, resulting in a down-range resolution of approximately 1.4 inches. Both the transmitted and the received polarizations were horizontal. The calibrated RCS values (in dBsm) of each isolated scatterer is shown in the data. The data clearly shows the relative contributions of each different part of the absorber. The contribution from the tip is at least 10 dB below the contributions from the back edges of the sample and several other scattering returns are shown to appear from areas along the length of the pyramid. Many of these

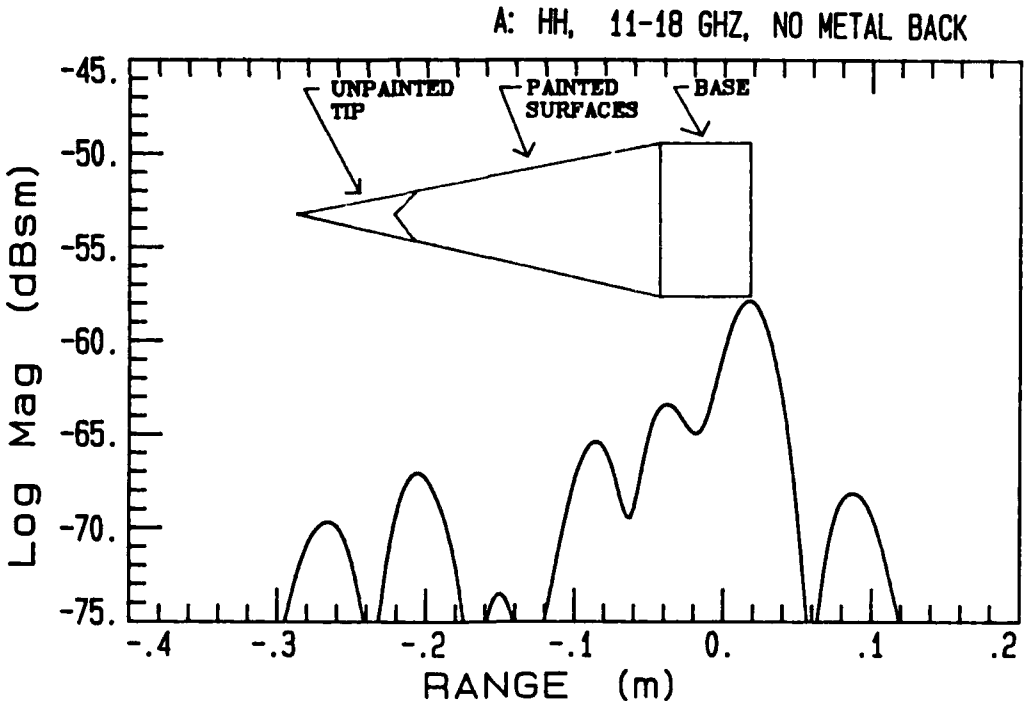

a) Measured time-domain profile

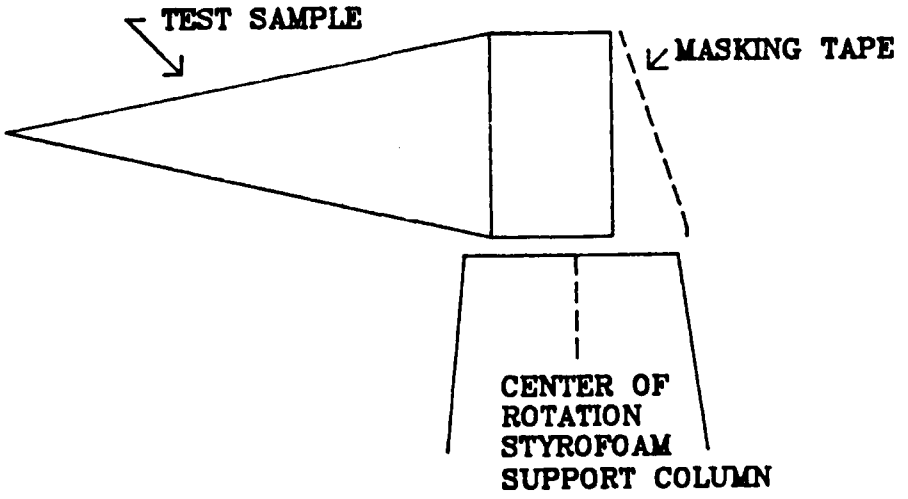

b) Measurement setup showing mounting technique

Fig. 3.26. Time-domain RCS results and measurement setup for a single unpainted-tip 12 inch pyramid absorber shape.

scattering mechanisms are discussed further in Chapter 4.

Using this technique, levels down to -75 dBsm can be detected with the use of subtraction. Such sensitivities are required in order to measure the returns from a low-level scatterer such as an absorber shape. Figure 3.27 shows the measured baseline results of the empty chamber and styrofoam column demonstrating the sensitivity levels obtainable over the range window from -1 to +1 meters.

To see the effect of the absorber sample mounting technique shown in Figure 3.26, a simple experiment was conducted which measured the return from a 1 square inch piece of standard masking tape attached to the back side of the styrofoam column. Figure 3.28 shows this result. The return from the tape is greater than -55 dBsm and is located at a range of +0.7 meters. The scattering from the tape alone is greater than any of the scatterers shown in Figure 3.26. For this reason care was taken in mounting the absorber samples so that a minimum of supporting tape or any other material was used. Figure 3.26 also shows the effect of masking tape on the back side of the column.

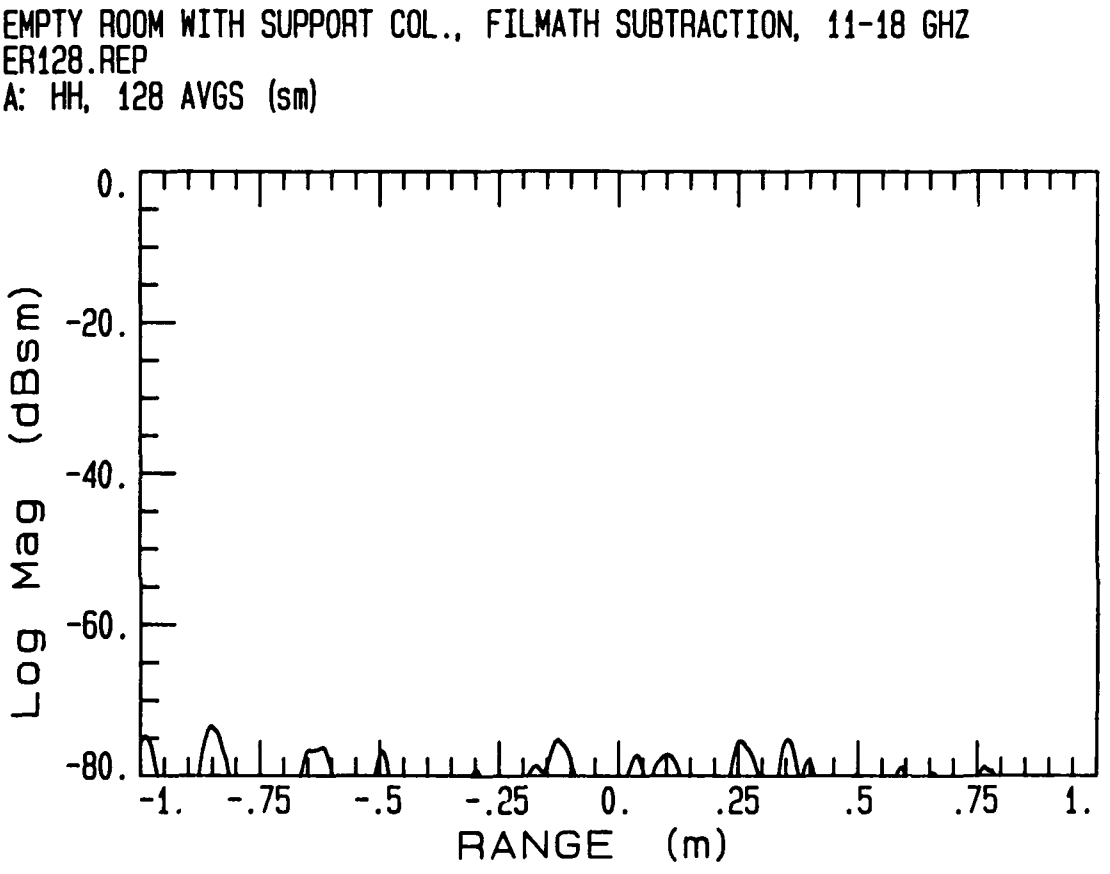

Fig. 3.27. The measured time-domain baseline levels of the empty chamber and styrofoam column demonstrating the sensitivity levels achievable.

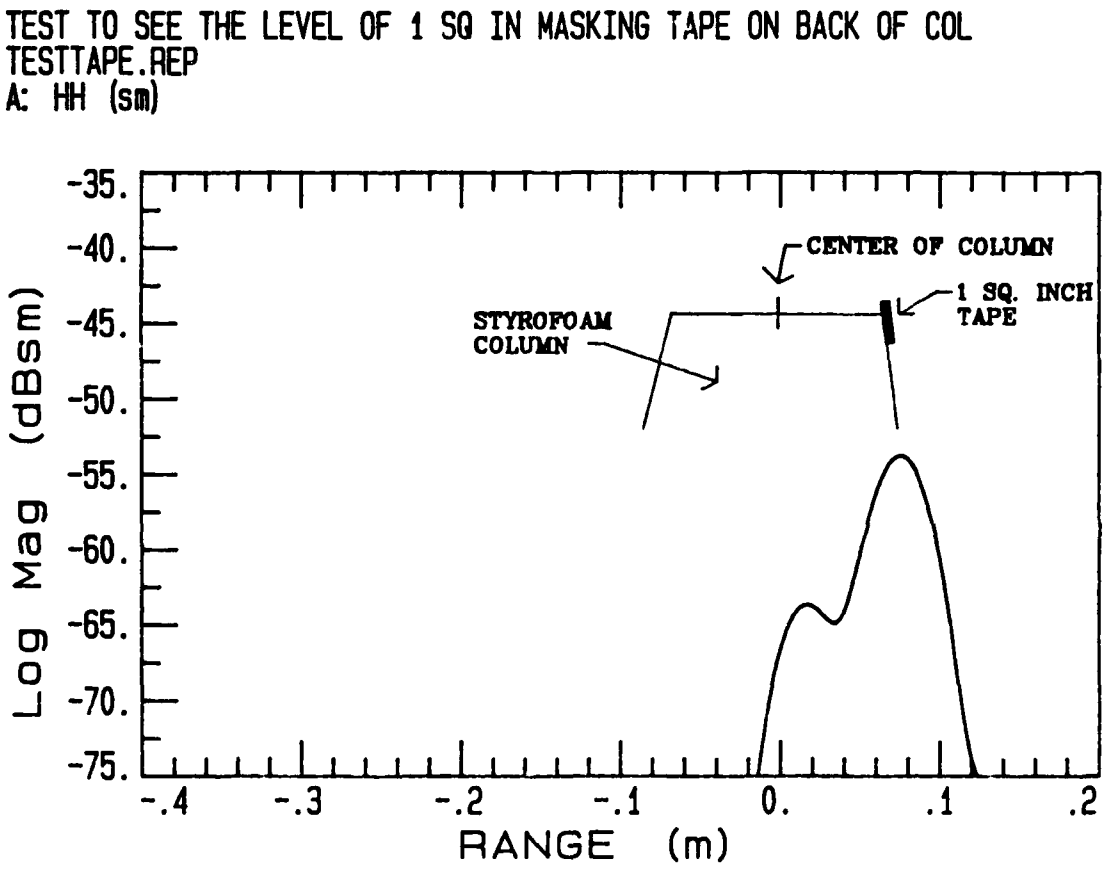

Fig. 3.28. The measured time-domain response of a single 1 square inch piece of masking tape attached to the back side of the column.

4.0 ABSORBER PERFORMANCE RESULTS

4.1 INTRODUCTION

As discussed in Chapter 1, the general knowledge of carbon loaded foam absorbers has changed very little since their first application, over 25 years ago. It has also been demonstrated that many chamber designers and users have determined that this level of understanding is inadequate for addressing modern chamber performance requirements and techniques, especially for low-level RCS measurements. Better absorber characterization is needed to properly determine if present absorber designs are adequate to meet these modern requirements or if new material types and designs should be investigated. Thus, the goals of this research study, and the purpose for evaluating anechoic absorbing materials, were to obtain a better understanding and characterization of the performance levels of these materials. The approach taken for this evaluation was to conduct numerous performance measurements, using improved and modern measurement techniques, on various absorber types and sizes as described in Chapters 2 and 3. This chapter addresses and presents many of these measurements and the most significant of the absorber performance results.

Measured results are presented which demonstrate the performance of different shapes and sizes of absorbers for

various incidence angles and orientations. The evaluations conducted involved mostly monostatic or backscattering conditions and only monostatic measured results are presented. However, in some cases the expected bistatic nature of the material can be extracted. Future work in this area should further address the absorber's bistatic performance. Also, since most microwave test facilities make use of absorbers which are at least one to two wavelengths in thickness, only absorber evaluations under these conditions were conducted.

In general, the performance of absorbing materials is determined by both their absorbing and scattering behaviors. Section 4.2 of this chapter presents measured data which illustrates some of these mechanisms for various materials and also discusses the nonhomogeneous and diffuse scattering nature of the material. Section 4.3 compares results for various shapes, sizes and orientations of the materials. The remaining parts of this chapter address the effects of metal backings, fire retarding chemicals, paints, and installation techniques on resultant performance levels. The chapter ends with a comparison of the performance of similar materials from three absorber vendors which provide most of the materials presently available. Other absorber performance results are also presented in Chapter 3 which illustrate the usefulness and advantages of the absorber evaluation techniques used throughout this

study.

4.2 ABSORBER SCATTERING BEHAVIOR

In order to better understand the behavior of absorbers, measurements were conducted on various absorbers to determine and identify the scattering mechanisms which dictate the overall performance of the material. The results presented throughout this chapter basically show that for materials with thicknesses greater than one or two wavelengths, the predominant effect on performance is the scattering from the absorber surface itself and not by insufficient absorbing properties within the materials.

Scattering from the absorber is caused by both reflections at the air to dielectric interfaces (impedance mismatches) and by edge and tip diffractions. Better impedance matching at the interfaces would greatly improve the amount of incident energy which enters the absorbing material and is dissipated as heat. Graded material loading or matching techniques could be used to achieve such an improved impedance match, however, the complication and cost of fabricating the materials would also increase. Diffraction effects are best controlled by shaping of the edges but are also determined by the material's electrical properties.

Another parameter of the material which affects its scattering behavior is its nonhomogeneous nature. The material's composition is sometimes found to be non-uniform in carbon density (loading) and physical size. The reasons for such inconsistencies are mainly associated with the fabrication processes used. This nonhomogeneity causes the scattering from different parts of the material to vary and gives the material a somewhat random (in both phase and amplitude) scattering nature. Because of these inconsistencies and the large number of shapes and pieces of material usually used, a diffuse scattering nature from the absorber covered surface can also occur. The overall effects of diffuse and random scattering tend to improve absorber performance; however, a controlled and predictable method for obtaining such results is required for consistent performance levels to be reached. These scattering mechanisms are further discussed in this section.

Another effect of these inconsistencies is that an adequate number of samples should be evaluated in order to determine the expected performance of a given lot or quantity of materials covering a surface. Many of the absorber evaluations conducted during this study used a sample size of at least four individual pieces of material (4 x 4 foot section). The results presented are generally determined by the performance of this limited four piece sample.

4.2.1 Scattering Mechanisms

Tests were conducted on numerous absorber samples to determine the actual backscattering mechanisms associated with standard pyramidal and wedge absorbers and to observe their relative scattering levels. One method used was to measure the absorber's monostatic time-domain RCS response at fixed incidence angles. Other tests were conducted using standard RCS versus aspect angle measurements and ISAR images. The procedures used for these evaluations are discussed in Chapter 3.

The measured backscattering time-domain response of a single 12 inch pyramid is shown in Figure 4.1. The pyramid is aligned so that the illuminating fields are incident along the axis of the shape or perpendicular to the flat back of the absorber. This orientation is usually referred to as normal incidence. The polarization of both the transmitted and received field is horizontal (HH pol) and the stepped frequency bandwidth used was from 11 to 18 GHz. For this angle of incidence, no specularly reflected scattering from the absorber surfaces is reflected back in the incident direction. The edge and tip diffraction effects should be the significant contributors. The results show that for the single pyramid, most of the returned energy is from the back straight edges at the base. The level of these returns are about -57 dBsm and both the front and

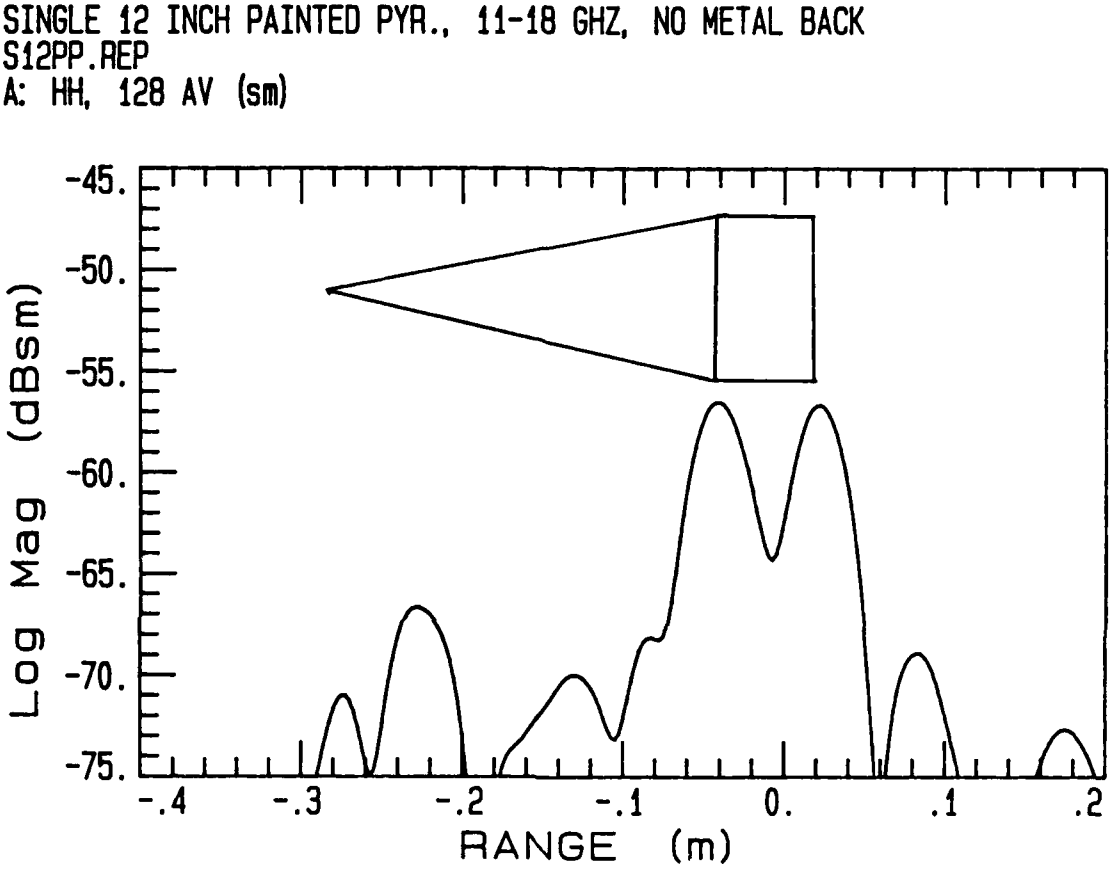

Fig. 4.1. Time-domain response of single 12 inch pyramid at normal incidence.

back edges of the base are clearly visible. The contribution from the tip is below -70 dBsm and is small compared to the base components. Several other smaller scattering returns are shown to come from areas between the base and the tip. These returns are actually associated with the absorber and are not caused by test environment error returns (see Section 3.3.3.4). The cause of these returns are believed to be from resonant structure conditions and from scattering caused by nonhomogeneous areas and the rough surfaces of the absorber itself. The return at +0.8 meters is caused by the mounting technique used to support the sample (see Section 3.3.3.4).

Using the same test conditions, the results for a piece of absorber with four 12 inch pyramids is shown in Figure 4.2. These results should include the effects of multiple interactions between the pyramids, however at this angle, no multiple monostatic specular reflection path between the shapes should exist. The base edge returns remain the strongest contributors even though the response of a full wall of absorber would not show the same effect. The tip contribution from the sum of the four tips increased 7 dB and the scattering from the middle section of the absorber also increased and is about the same level as the tip component. The most significant result from this measurement is that the nonspecular scattering from the absorber sample is composed from several scattering sources

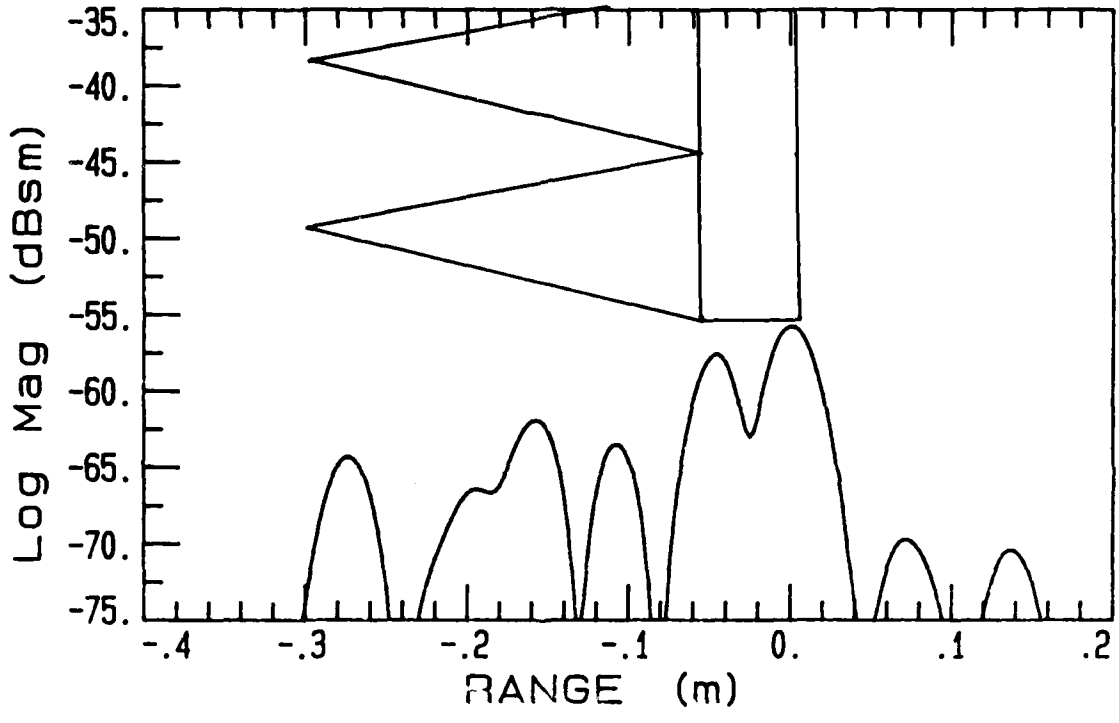

Fig. 4.2. Time-domain response of four 12 inch pyramids at normal incidence.

and one part or area of the material does not dictate its performance, except for the base edge components which are not expected to be as severe for a continuous section of absorber. Thus, reduction of the scattering level of the absorber requires that all of the separate individual components must be reduced. This includes, as a minimum, the tip and edge diffractions.

Similar results for a single 24 inch pyramidal shape and a section of four pyramids are shown in Figures 4.3 and 4.4. The results are not much different from those of the 12 inch materials except that a higher number of returns are shown.

To illustrate the scattering *from* the absorber surface for angles away from normal incidence, a time-gated RCS measurement of a single 24 inch pyramid is shown in Figure 4.5 at 5 GHz. A 1.5 meter time-gate was used, therefore, the total return from the entire pyramid is displayed as a function of aspect or azimuth angle. The total return is the vector sum of the individual responses as shown in Figure 4.3. Zero degrees azimuth represents normal incidence and -90 degrees is for incidence normal to the flat sides of the pyramid's base. The results show that the total return from the standard pyramid changes only slightly from -5 degrees out to -50 or -60 degrees but increases significantly beyond that point until the angle where the normal to the large flat side surface is reached. This

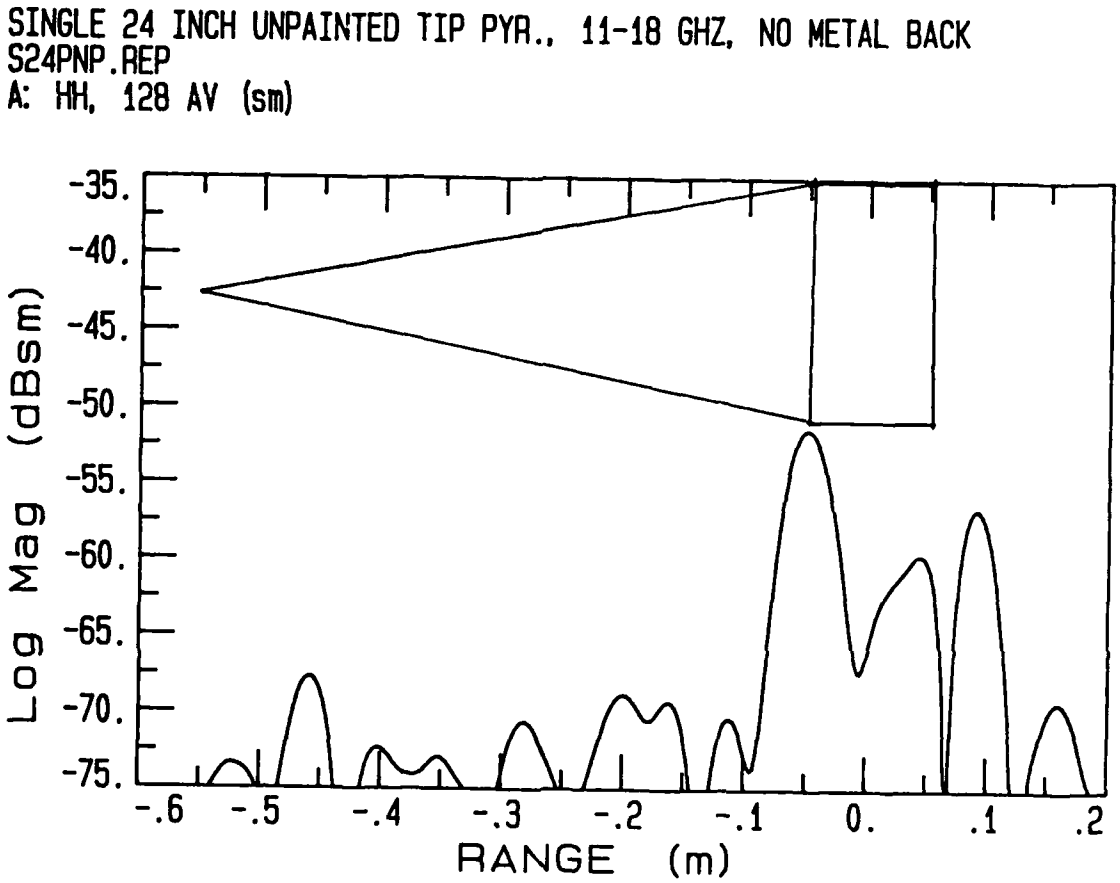

Fig. 4.3. Time-domain response of single 24 inch pyramid at normal incidence.

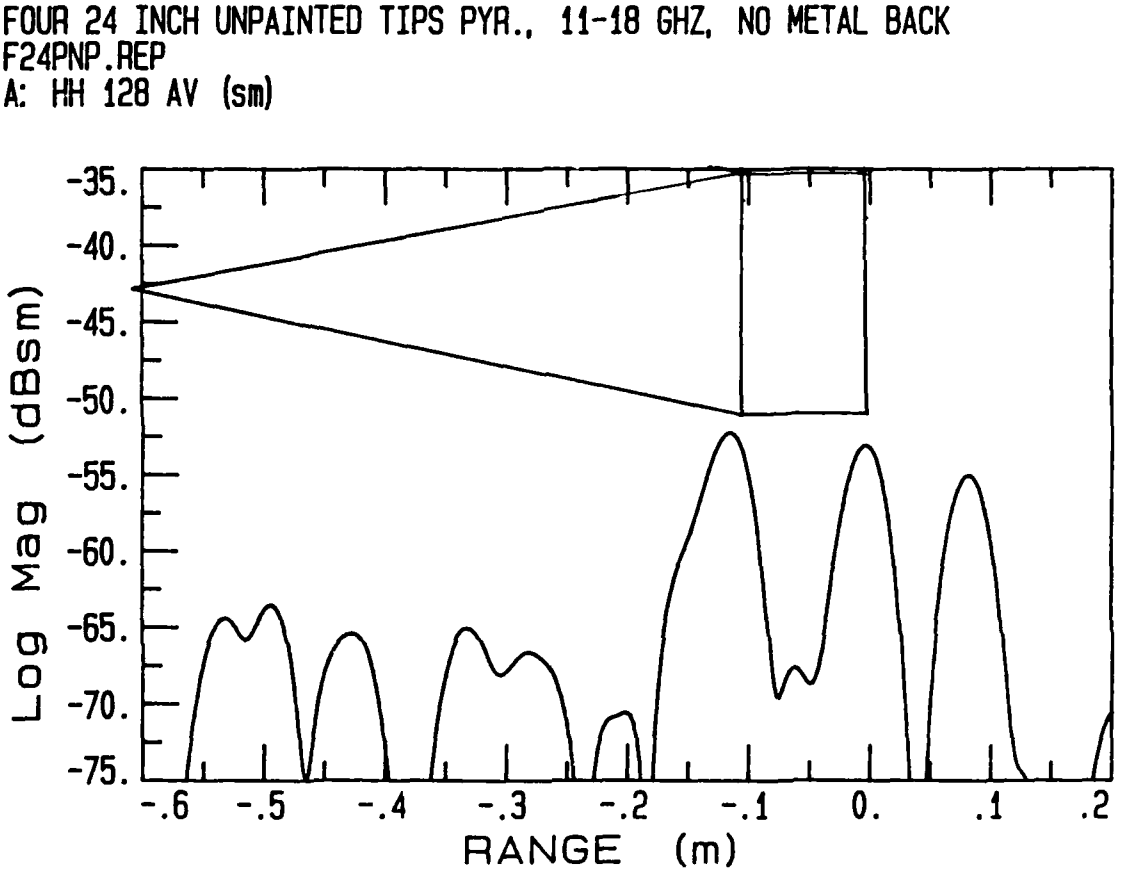

Fig. 4.4. Time-domain response of four 24 inch pyramids at normal incidence.

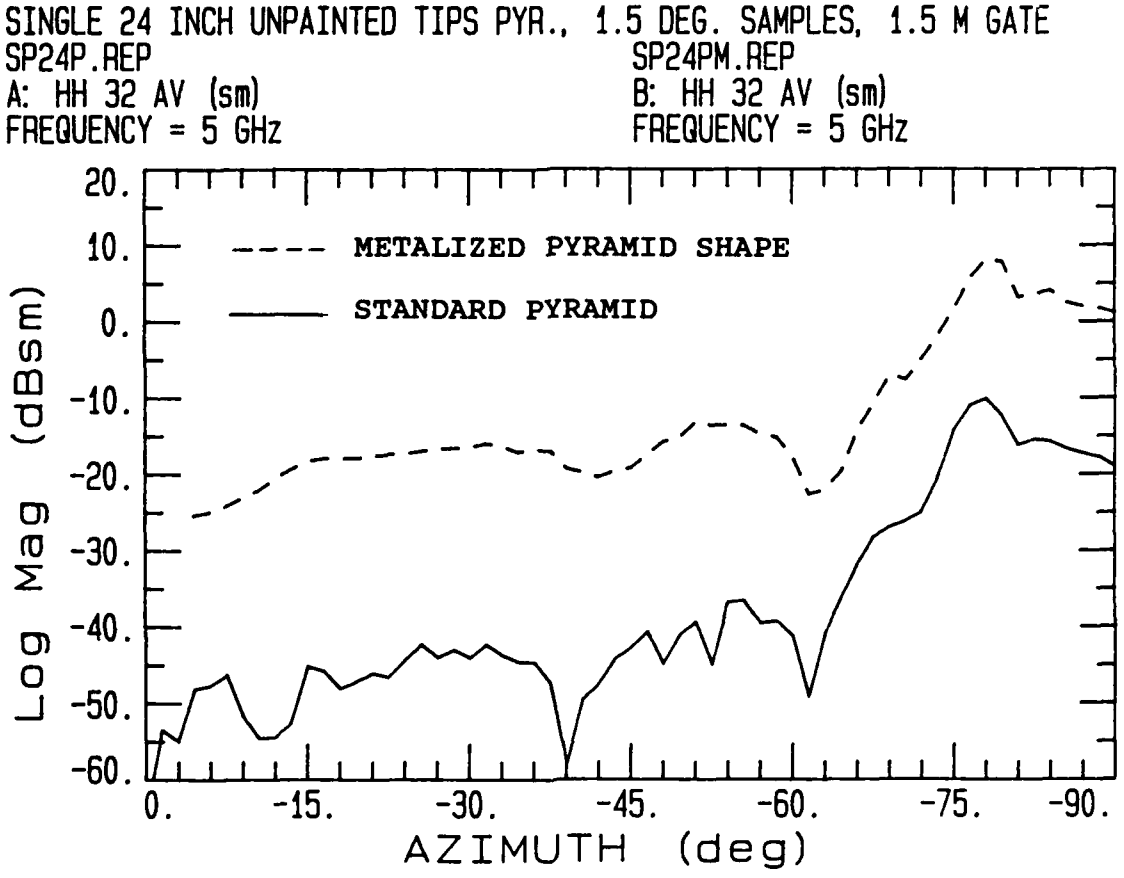

Fig. 4.5. Time-gated RCS versus aspect measurement of single 24 inch pyramid.

angle occurs at -78.7 degrees. The specular return from the large flat side is more than 40 dB larger than for the return at normal (on axis) and is at -10 dbsm. Such a high return level would be unacceptable from the absorber within an anechoic chamber even if an entire wall demonstrated such levels. Fortunately with proper absorber orientation and with multiple pyramids always being used, the overall effects of such specular reflections can be decreased. Section 4.3 illustrates the net effects for a complete wall section and shows techniques for improving performance.

Also shown in Figure 4.5 is the measured RCS of a single 24 inch pyramidal absorber cone which was metalized by covering its surface with metal tape. The response is very similar to that of the non-metalized sample except that the levels are from 18 to 25 dB higher. By comparing the relative level of the two returns at -78.7 degrees, the magnitude of the reflection coefficient at the absorber surface for normal incidence can be determined. Doing so, a magnitude of the reflection coefficient of 0.12 is obtained. This value is in reasonably good agreement with results published in [9] which show a reflection coefficient of 0.16 using $\epsilon_r = 1.5 - j\ 0.69$ for the carbon loaded foam material at 3 GHz.

This high frequency specular scattering nature of the material is a very useful concept for predicting the general performance of a given absorber shape or

orientation. Both monostatic and bistatic performance can be estimated in this way.

Time-domain RCS results for wedge shaped materials were also obtained during this study. Figure 4.6 shows the backscattering results for a single 12 inch wedge having the same sized base as a single 12 inch pyramid (4 x 4 inch). The wedge was aligned so that the incident horizontally polarized field was parallel to the length of the wedge (referred to as soft polarization). The large scattering return from the front edge of the wedge is shown to appear because of the specular edge scattering contribution. Specular edge diffraction is more significant than is tip diffraction, especially for the case of soft polarization on a leading edge. The edge contribution of the wedge absorber is shown to be almost 15 dB larger than the tip contribution for the pyramid shape. The edges of the base are also shown to contribute to the overall scattering level and are at roughly the same level as for the single 12 inch pyramid. Results for the case of the incident field being perpendicular to the edge of the wedge (hard polarization) are shown in Figure 4.7. The front edge component for this case is 9 dB lower than for the soft polarization case but still 6 dB higher than for the tip diffraction. The returns from the base are also slightly smaller since only hard polarized edges at the base are present.

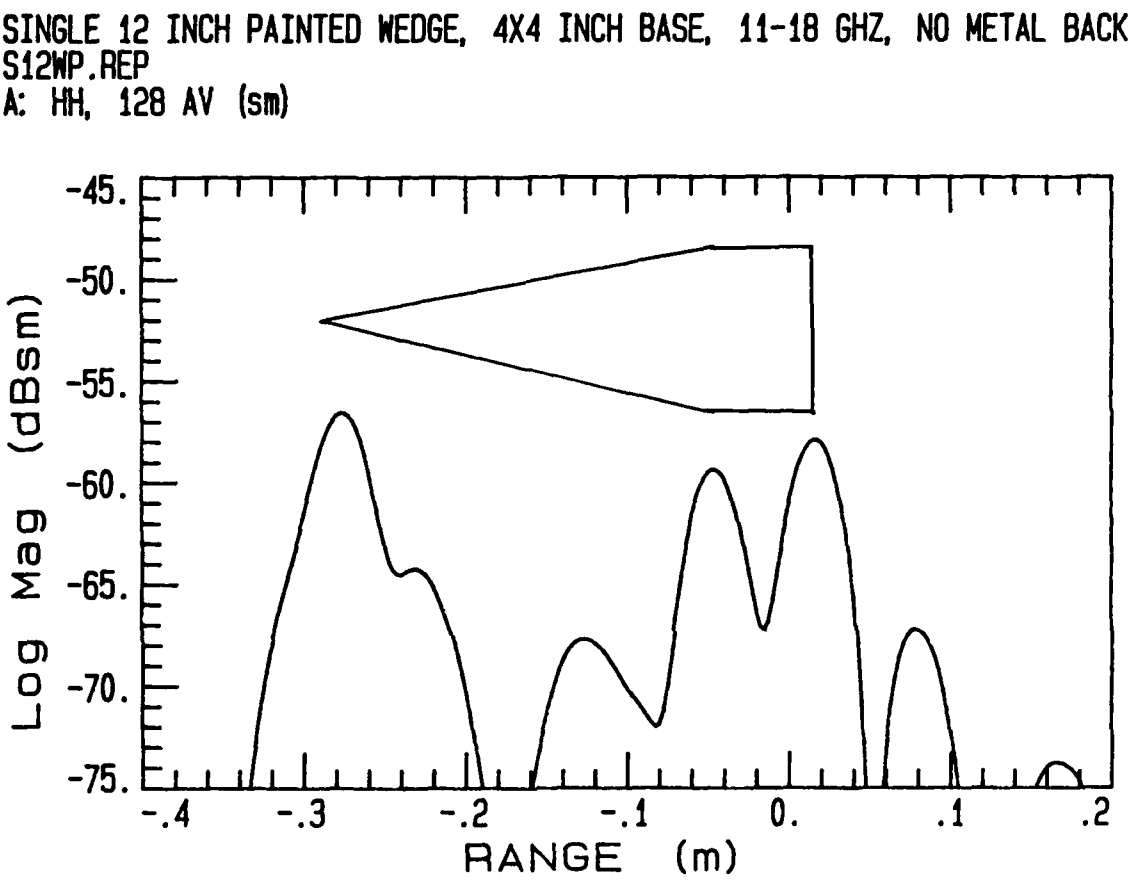

Fig. 4.6. Time-domain response of single 12 inch wedge section for soft polarization.

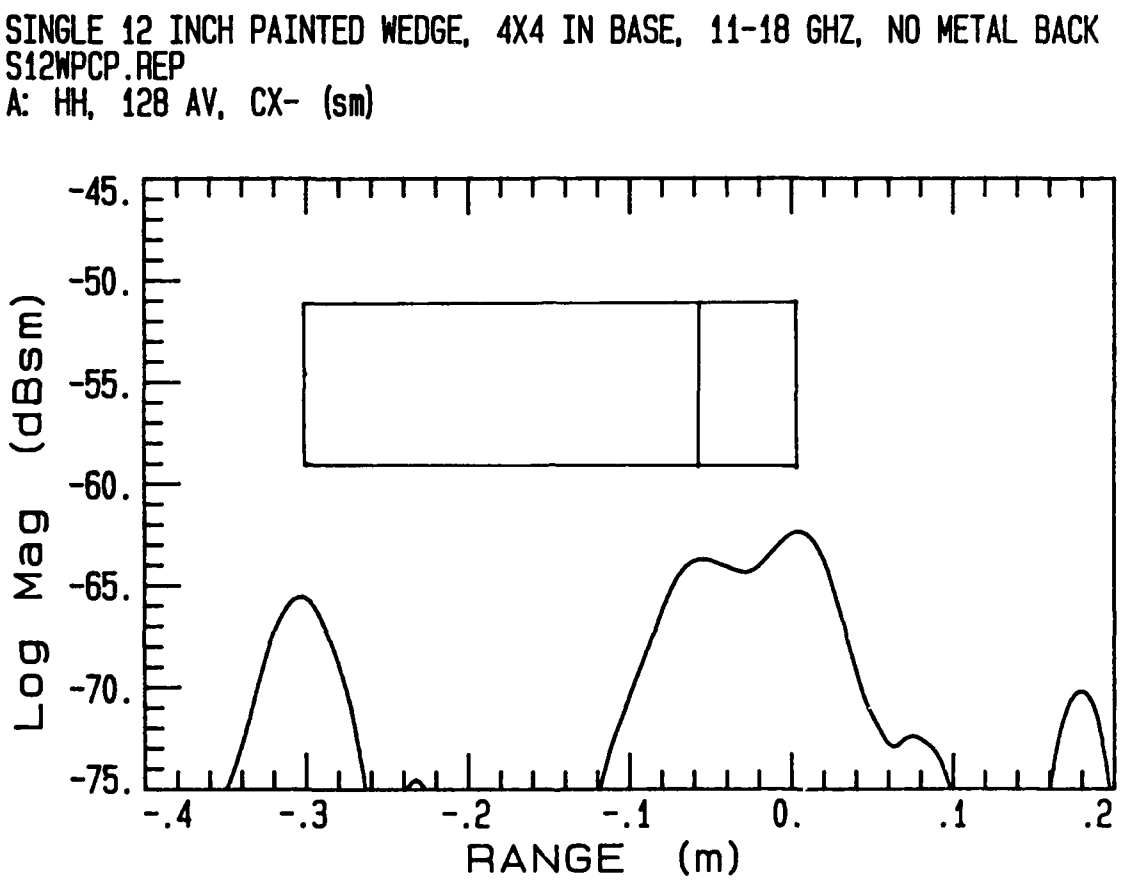

Fig. 4.7. Time-domain response of single 12 inch wedge section for hard polarization.

Wedge results for a larger section of 12 inch material having two wedges, and a base the same size as four 12 inch pyramids, is show in Figure 4.8. Both hard and soft polarizations are shown. The results are similar to the single wedge samples except a smaller difference is obtained between the two polarizations for the leading edge contribution. The hard polarized leading edge case is only 6 dB lower than for the soft polarized edge. Both cases show the significant contributor to be the front edge of the wedge for normal incidence, and that the wedge material should have an overall higher backscattering level for both polarizations than the pyramidal material (compared to Figure 4.2). The backscattering from the wedge material for off-normal incidence in the plane of the wedge shapes, however, is generally lower than for the pyramidal case because of the high degree of specular surface and edge bistatic scattering from the wedge shapes.

Convoluted materials were also investigated. Figure 4.9 shows normal incidence time-domain results for a section of 3 inch convoluted absorber with an 8 by 8 inch base. Most of the scattering for this case is shown to be caused by reflections from the rounded front surfaces of the convoluted shapes. The rounded valleys between the shapes also contribute to the overall scattering level. The back-edge component is negligible for this case. It is shown that the contribution from the front surface alone is

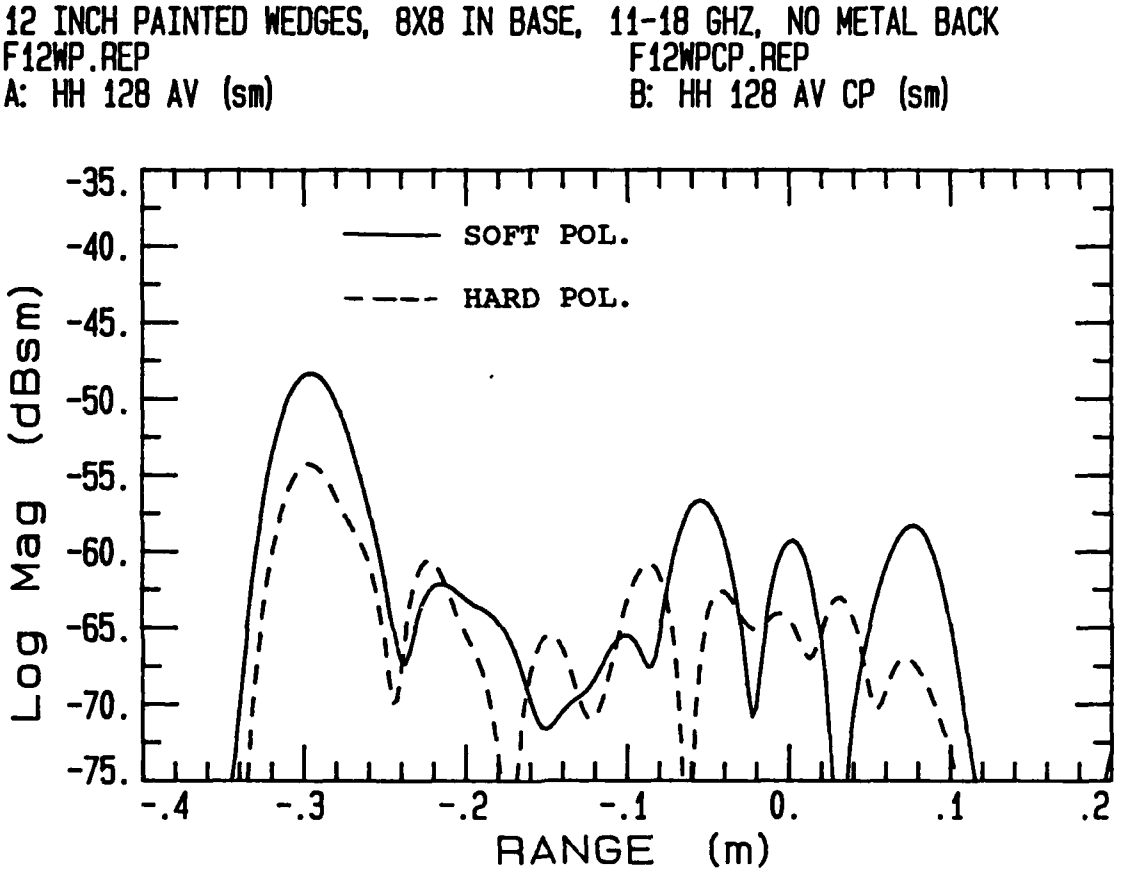

Fig. 4.8. Time-domain response of 12 inch double wedge section (8x8 inch base) for both hard and soft polarizations.

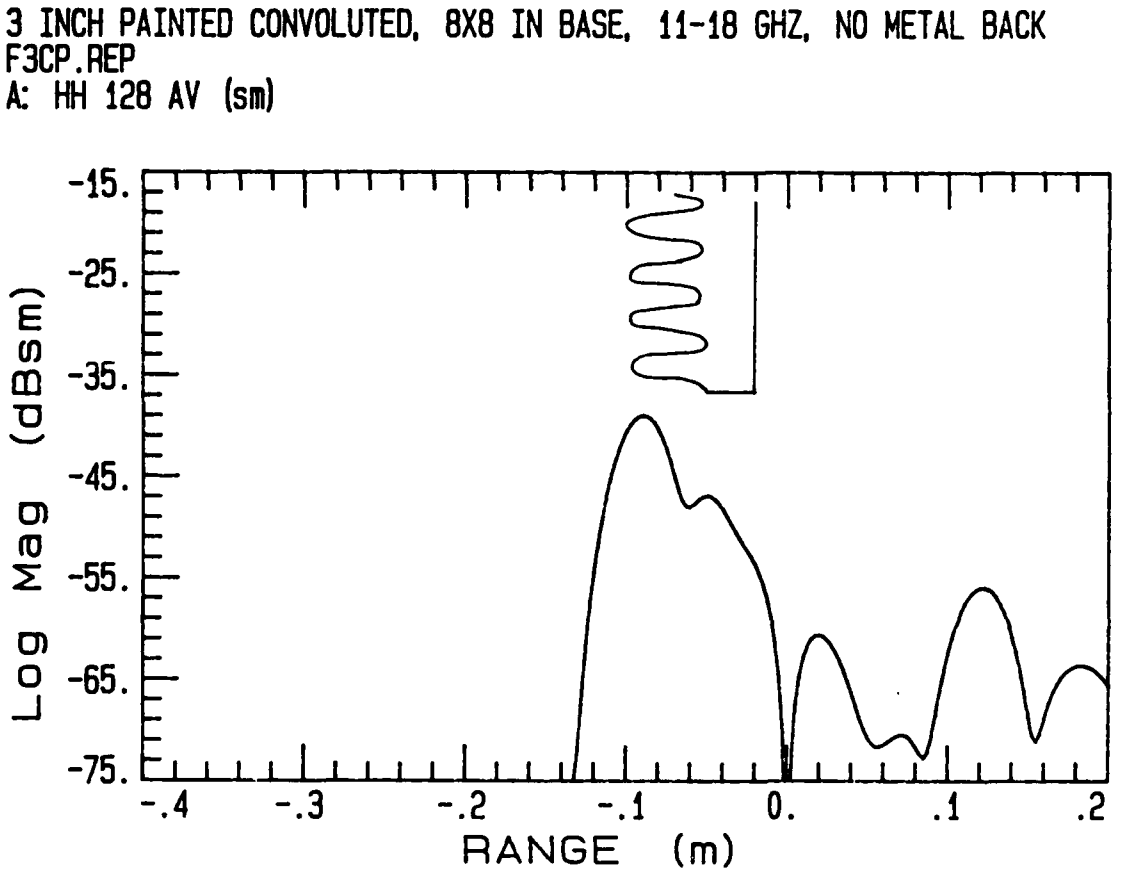

Fig. 4.9. Time-domain response of 3 inch convoluted absorber for normal incidence.

higher than -40 dBsm resulting in much worse overall performance than for the pyramidal or wedge shapes. Due to the rounded nature of the convoluted shape, this increased backscattering condition exists over extremely wide angular regions and especially for higher operating frequencies. This contradicts the fact that convoluted materials are usually recommended, by some of the vendors, for use at millimeter wavelengths or higher. Some of the results of this study show the reasons for such a recommendation is not clear and a smaller pyramidal cone may offer better performance.

4.2.2 Nonhomogeneities

One of the significant results of this study was in clearly showing and displaying the nonhomogeneities which exist with almost all currently available absorbers. The use of ISAR imaging techniques nicely shows these inconsistencies between different sections of absorber pieces and between absorber pieces as described in Chapter 3. The fact that nonhomogeneities within the absorber exist is not a new discovery and has been previously reported [8],[9].

One such ISAR plot is shown in Figure 4.10 for the test wall covered with 18 inch pyramidal absorbers. The four pieces of absorber in the middle of the test wall were

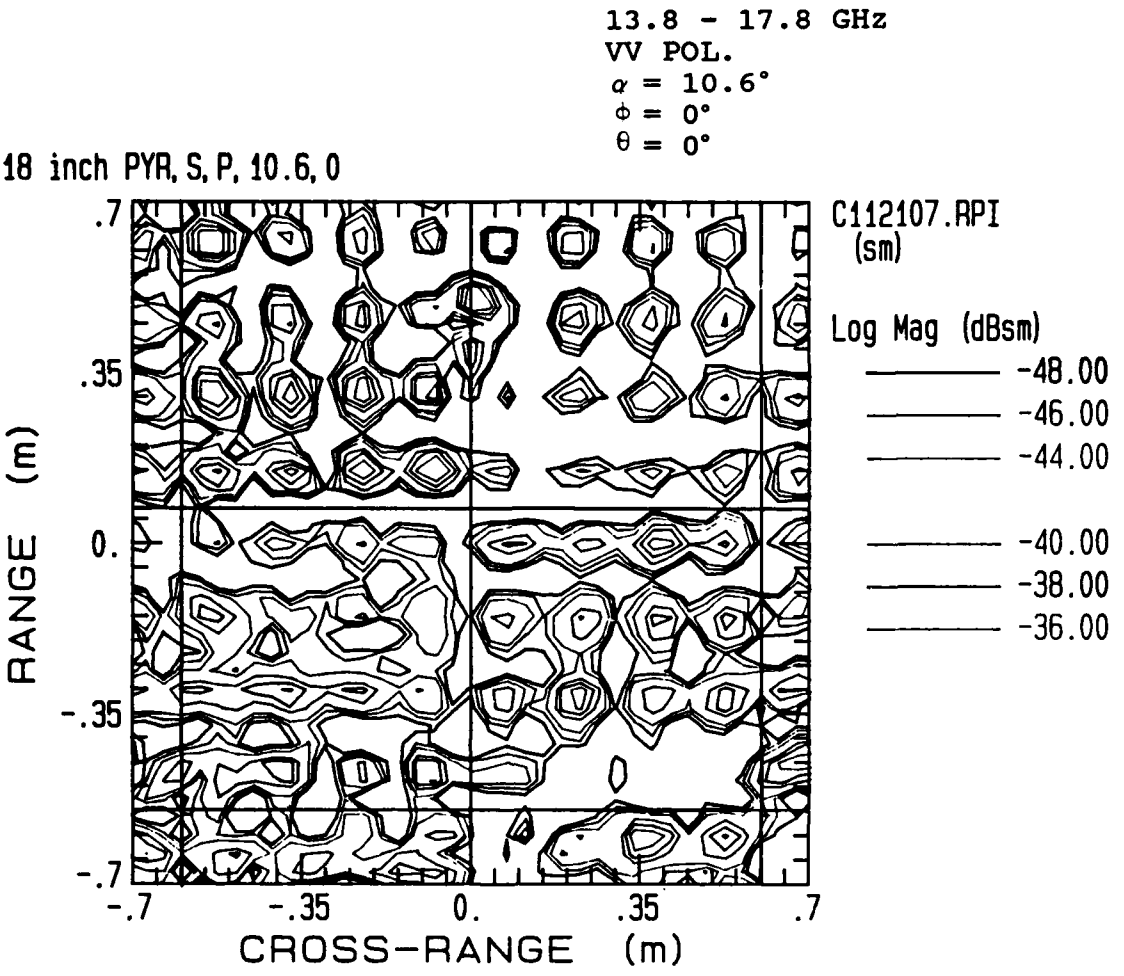

Fig. 4.10. ISAR image results of test wall covered with 18 inch pyramidal absorber showing material non-homogeneities.

used as the test sample and are outlined in the image data. Each piece of 18 inch pyramidal material has 16 individual pyramids. Each of these shapes are clearly shown in the figure. The use of imaging allows the magnitude and phase response from each individual shape to be separately evaluated. The magnitude variations across the sample, shown in the figure, clearly illustrate the inconsistencies in performance caused by differences with the material. Performance variations are shown for both individual shapes within the same 2 by 2 foot piece of material as well as between complete pieces. Amplitude variations as high as 5 dB are shown between pyramids within the same piece of material and variations greater than 12 dB are found between separate pieces of material. The variations between pieces are found to be more significant. The four pieces of material used for this evaluation were from two separate lot numbers but from the same vendor. Greater than 12 dB variations were found between the different vendors. In most cases, no physical difference could be detected between the absorbers from the same vendor which demonstrated the most variations.

Phase variations between the separate pyramids of this same test sample are not shown in a figure because of the difficulty in displaying this information in a single one color plot. The phase plot is highly random. However, the phase results show that variations as high as 60 degrees

occur between pyramids of the same piece of material and for the same down range row. Variations between down range rows are randomly spaced between 0 and 360 degrees as would be expected because of the spatial offset of these rows with respect to the imaging radar. Between pieces of absorbers for the same down range row, phase variations also appear random in nature with variations as high as 210 degrees.

The results of such a measurement clearly show the inconsistent performances of the material. Similar results were found for the different absorber sizes and shapes. The presence of such nonhomogeneities is not necessary bad. Performance improvements can actually be obtained because of the random scattering nature of the absorbers. Random scatterers tend to avoid coherent conditions which constructively increase scattering levels. However, the random nature of the material should be controllable and predictable in order to achieve consistent and optimum performance. Currently, the causes of many of the material's inconsistencies are associated with the fabrication processes used and occur largely by chance. Absorber installation techniques also introduce some of these inconsistencies.

4.2.2.1 Fabrication Related Nonhomogeneities

To help determine the causes of material inconsis-

tencies, several of the vendor's manufacturing facilities were visited during this study. From the surveys, it was apparent that several techniques and processes used in fabrication can lead to performance inconsistencies. The techniques and resultant level of inconsistencies vary form vendor to vendor as well. The exact processes used by the various vendors will not be discussed in this thesis in fairness to the vendors. However, it is recommended that users of such materials become familiar with the fabrication techniques used in their construction.

4.2.2.2 Installation and Alignment Related Nonhomogeneities

When a section of absorber is installed on a surface, some inconsistencies can be caused by the installation methods used. This is especially true for the case of wedge absorbers. Many wedge absorbers vary in size in both height and width due to the fabrication methods used. When several pieces are placed end to end to cover a complete wall section, it is quite common for a misalignment to occur between the individual wedge pieces. Typical misalignment up to 1 inch in any direction can result if proper attention is not given to forcing the alignment of the pieces. Tests conducted during this study show that degradations in performance, for these misaligned areas,

can be as high as 5 dB. With proper absorber selection and installation such misalignments can be reduced to amounts which insignificantly degrade the absorber's performance.

In some cases, an application of glue or adhesive between absorber pieces is commonly used to aid in alignment or to attach absorber sections to selected areas. The use of such glue also has the potential for causing performance variations over the absorber covered surface. The exact effect of such variations should be evaluated by the individual user for his own unique application or requirement.

In an attempt to improve the performance of wedge type absorbers, a new fabrication process was implemented by one absorber vendor during this study. Wedge pieces 6 foot in length, instead of the standard 2 foot pieces, were constructed using post-jigging impregnating techniques and making use of a numerical-controlled cutting saw. Post-jigging techniques infer that the material's shape is cut from the bulk foam material after it has been impregnated with carbon. These techniques resulted in a much superior absorber alignment and in a more consistent material.

4.2.3 Diffuse Scattering

Because of the inconsistent nature of the absorber materials and because of the large number of individual

shapes used for most applications, the high frequency scattering nature of the material tends to be highly diffuse. In other words, scattered energy is radiated in many directions and in a rather random fashion. The specular reflections from the large number of shapes contribute to much of this diffuse scattering. However, shadowing, multiple interactions, and diffractions also contribute. The total diffuse result is dependent on incidence angle, polarization and frequency. The effect of diffuse scattering is improved absorber and anechoic chamber performance.

Even with this diffuse nature, for many materials, orientations and incident directions still exist where an increased amount of energy is still scattered in undesirable directions. Such conditions exist ,for example, when the angle of incidence is normal to the large flat surfaces of the absorber shapes. An important parameter to consider when evaluating such conditions is the phase relationship of the various scatterers which contribute to this scattering.

In general the total scattered power or energy which is directed in a given direction by a wall or section of absorber, and which is caused by a incident field on the absorber, can be described by the total radar cross-section, σ_T, of the wall as:

$$\sigma_T = \left| \sum_{n=1}^{N} \sqrt{\sigma_n} \; e^{jK\theta_n} \right|^2 \qquad (1)$$

where N is the total number of individual scatterers which contribute to the total scattering and σ_n and θ_n are the RCS and relative phases of each individual scatterer. The result is then the squared magnitude voltage vector summation of all the scatterers.

Since the amplitudes of the various scatterers are generally random and vary less than 10 dB or so for the monostatic case, as shown in Figure 4.10, the phase relationship between the individual scatters has a large effect on the overall result. Two phase conditions are assumed. The worse case scattering level will occur if all of the individual scatterers add coherently or in-phase. Under these conditions, assuming equal amplitudes, the net result is:

$$\sigma_T = \left| N \sqrt{\sigma_n} \right|^2 = N^2 \sigma_n \qquad (2)$$

and the total result is simply 20*log(N) greater than the level for a single scatterer. Because of the random and diffuse scattering nature of the material it is reasonable to assume that this condition is not likely to exist, even for normal incidence on the material, and thus places a conservative upper bound on the level expected.

The other condition which is possible, is for the scatterers to have a truly random phase relationship where the phases of the individual returns are uniformly distributed from 0 to 360 degrees. The result for this case is:

$$\sigma_T = N \left| \sqrt{\sigma_n} \right|^2 = N \sigma_n \qquad (3)$$

and the total scattering level is only 10*log(N) greater than the level for a single scatterer. This condition is referred to as addition of powers only and sets the lower limit on the scattering level expected. The actual level will fall somewhere between these two limits. The more random the scattering from the individual scatterers, the closer to the lower limit will be the result. The amplitude variations, however, must also be considered. In practice, the average magnitude level over the sample area is usually

used to represent σ_n.

4.3 SHAPING AND ORIENTATION EFFECTS

Some of the important issues regarding anechoic absorbing materials are the performance dependencies on their shape and size, and whether or not preferred orientations exist which improve their performance. These issues are among some of the more recent questions being asked by chamber users and designers, especially regarding the use of compact ranges. Compact ranges place slightly different performance requirements on the absorber materials than for conventional ranges [4],[37]. One example of this is the increased interest in the near-grazing incidence performance of the absorber materials placed on the side walls of the chamber. Most compact ranges tend to illuminate the side walls at incidence angles from 5 to 20 degrees from grazing (grazing is 90 degrees from normal). Depending on the particular design used, the low-angle incidence performance of the absorber can have a significant impact on the performance of the chamber with regard to both its backscatter and bistatic scattering levels. This is especially true if extremely low ambient chamber RCS background levels are required. A problem in designing such ranges is that adequate data on the performance of the absorbers for these

conditions has not existed in the past.

To help obtain some of this badly needed performance data on the absorbers, measurements were conducted during this study to evaluate the monostatic performance of commonly used materials at both near grazing and near normal incidences and for various sizes and shapes. Various material orientations, with respect to the incident fields, were also evaluated. Some of these results are shown in this section. The techniques used to conduct such tests involved both ISAR imaging and reflectivity measurements as described in Chapter 3. The angles defining the positions and orientations of the test samples are also defined in that chapter.

4.3.1 12 Inch Wedge and Pyramidal Materials

Using the 8 by 8 foot test wall of absorber, ISAR images were generated at various incidence and orientation angles on both 12 inch pyramidal and wedge absorbers. These images were obtained for both principle polarizations and at two different frequency bands, 2.9 - 6.9 GHz (low-band) and 13.8 - 17.8 GHz (high-band). For comparison purposes, the average backscatter return per unit range cell over the test sample was used to represent the performance of these materials for the different angles and orientations. Only the 4 by 4 foot area in the center of the test wall was

used for these comparisons. All the materials were from the same vendor and were all painted and contained no fire retarding salts. The measured results clearly illustrate the relative performance levels of the various cases.

Figure 4.11 presents the measured results at the high frequency band. The results show the average RCS, in dBsm, per unit range cell for both 12 inch pyramidal and wedge materials and for different orientation angles (phi) as a function of the incidence angle from grazing (alpha). All the data shown is for theta= 0 degrees. A large variation in performance is shown for the different cases.

The 12 inch pyramid results are shown for phi angles of 0, 10 and 45 degrees. A phi angle of 0 degrees (for theta=0) is the plane which includes the normal to the flat side of the pyramid shapes. Normal incidence to the pyramid's surfaces occurs at alpha = 11.3 degrees. A phi angle of 45 degrees is a plane which includes the normal to the straight edges of the pyramids. The normal to these edges occurs at alpha = 15.8 degrees. The results show that at the angles where the radar looks into the flat sides or the straight edges of the absorber shapes the backscattering from the materials is increased. This result is as would be expected by intuition. The level of increased scattering is approximately 20 dB higher than at angles greater than 20 degrees from these normals. The performance

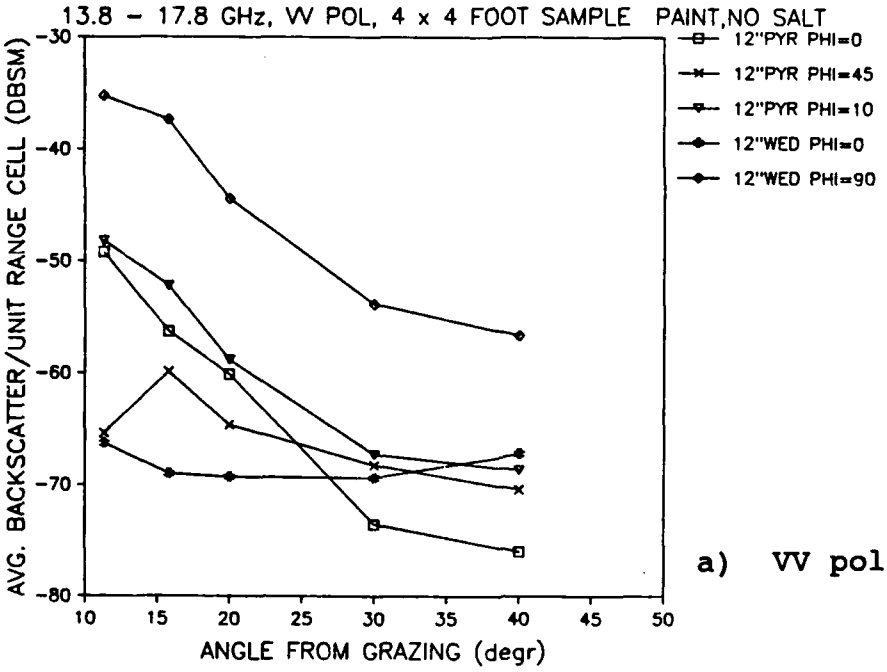

a) VV polarization

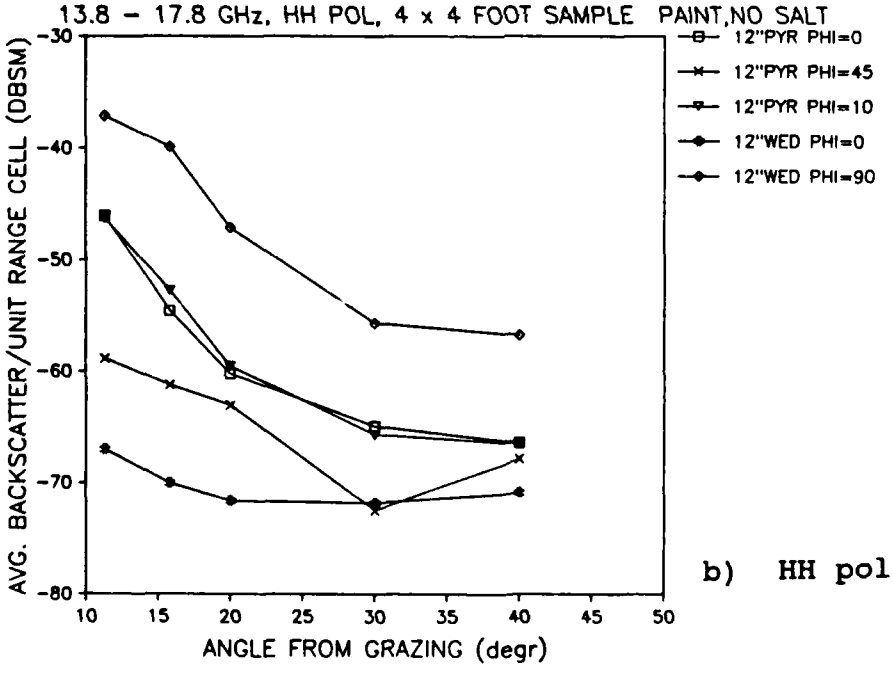

b) HH polarization

Fig. 4.11. Measured high-band backscattering performance of various 12 inch pyramidal and wedge absorbers as a function of incidence angle from grazing.

of the pyramidal material, turned phi= 45 degrees, is also shown to be as much as 10 dB better than for the phi= 0 case, especially at angles of alpha less than 20 degrees. Turning the pyramidal material only 10 degrees is shown to actually degrade its performance somewhat since additional edges are exposed to the radar.

The performance of the wedge materials, for the back-scatter case and for this frequency band, is shown to be up to 10 dB better than for the pyramids at incidence angles below 30 degrees for phi = 0, but no clear advantage is shown in using these materials above 30 degrees. In fact the pyramidal materials offer better performance beyond these angles. Turning the wedges 90 degrees obviously results in the worse case performance.

The performance results for these same materials at the low frequency band is shown in Figure 4.12. For the 12 inch materials, at this frequency, the wedge absorber at phi = 0 is much better than all the other configurations by as much as 30 dB. The performance of the pyramidal absorb-ers and the wedge turned at phi = 90, all show about the same performance level. The dependency of the performance on incidence angle for this frequency band is also shown to be much different. The response forms a slight peak about 15 degrees from grazing and falls off almost as the cosine of the angle beyond that point. This is believed to be a result of the much broader scattering response from the

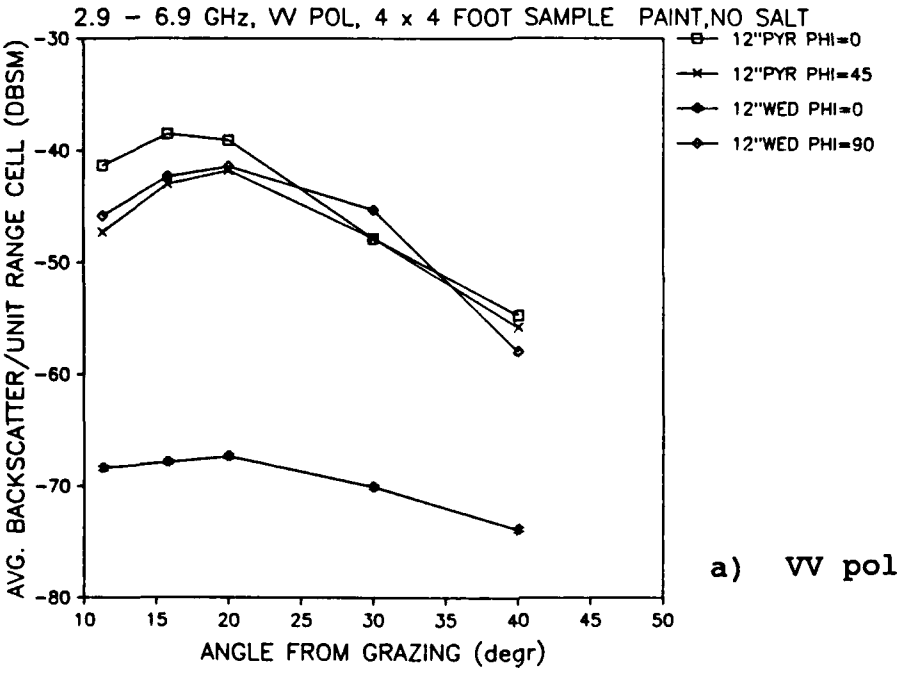

a) VV polarization

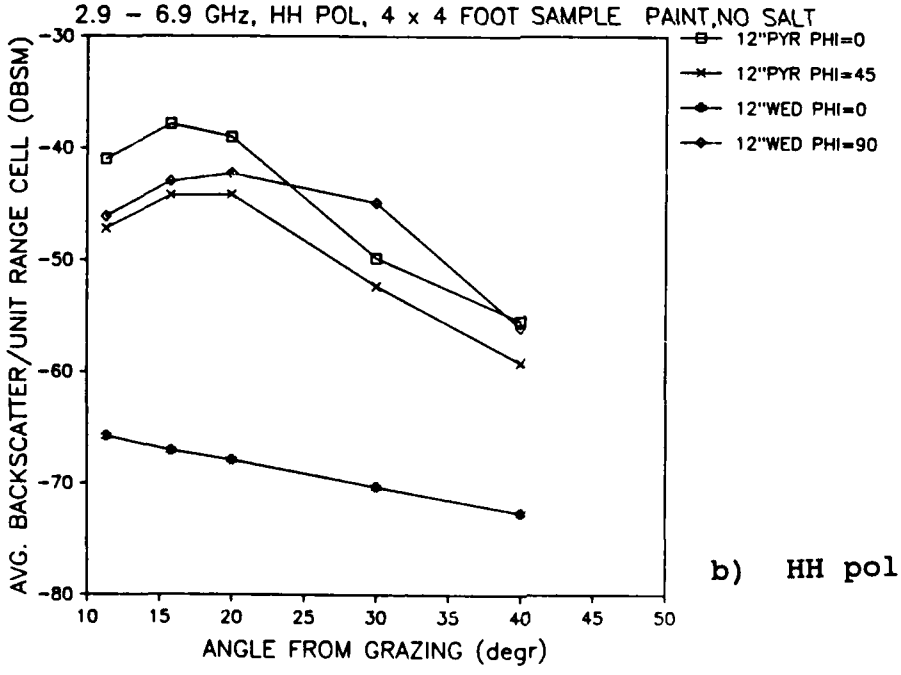

b) HH polarization

Fig. 4.12. Measured low-band backscattering performance of various 12 inch pyramidal and wedge absorbers as a function of incidence angle from grazing.

absorber's surfaces at these lower frequencies.

Figure 4.13 presents measured reflectivity results for these same absorbers at both the lower and upper frequency bands. This data was obtained using the techniques described in Section 3.3.3.3. Also shown in the figure is the typical vendor specified performance levels [24]-[27]. The results show that in all cases levels much better than the vendor's published levels were measured. This is due mostly to the evaluation procedures and techniques used.

The data in Figure 4.13 shows that the 12 inch pyramid absorber at phi= 45 degrees demonstrated the best performance with reflectivity levels better than -85 dB. The reason being that the straight edges along the bases and edges of the shapes are partially cross-polarized with in the incident energy for this case. The wedge materials at phi = 0 are shown to be as much as 15 dB worse than the pyramids turned 45 degrees for this polarization. However, the pyramids turned phi = 0 and the wedges at phi = 90 degrees perform at about the same level as would be expected. The reason for the degraded performance of the wedge materials is the specular scattering from the long straight edges of the wedge's tips and bases.

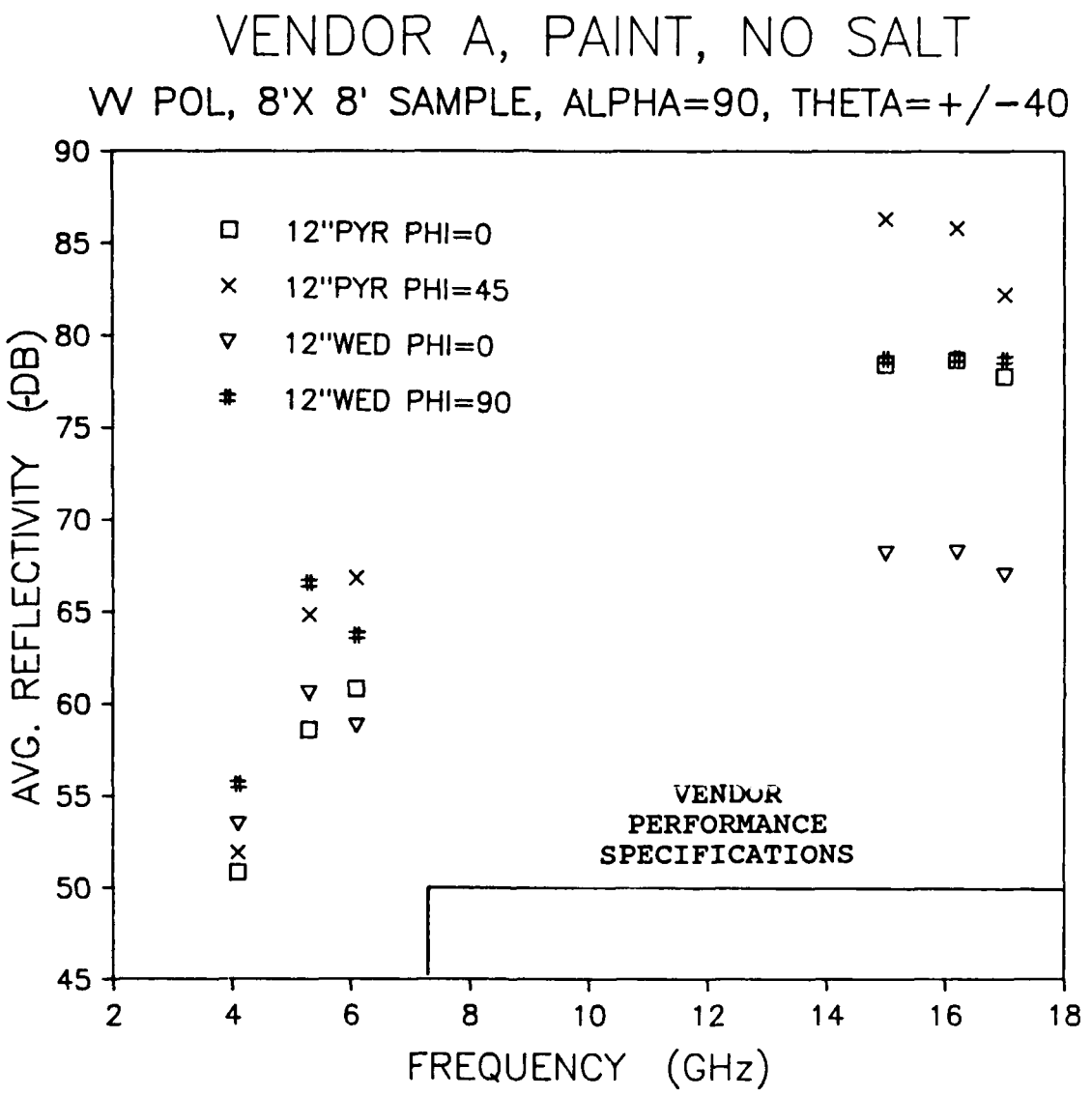

Fig. 4.13. Measured reflectivity of various 12 inch pyramidal and wedge absorbers.

4.3.2 18 Inch Wedge and Pyramidal Materials

Similar evaluations were conducted on 18 inch materials as with the 12 inch absorbers. The results of these measurements are presented in Figures 4.14 through 4.16. The 18 inch materials generally perform similar to the 12 inch materials except for the slight differences in the absolute scattering levels. Other differences include the fact that the variations in scattering between the 18 inch wedge and pyramidal test samples are shown to be less than with the 12 inch materials. Part of the reason for these differences is the larger absorber shape as described in Section 4.2, and also that the 18 inch samples were obtained from a different vendor than the 12 inch samples and contained fire retarding salts. Section 4.5 discusses the effect of these salts on performance. The alignment of the 18 inch wedges was also fairly poor from piece to piece because of the inconsistencies in the absorber's size.

4.3.3 6 and 8 Inch Materials

Smaller absorbing materials were also evaluated. Both 6 inch convoluted and 8 inch pyramidal and wedge absorbers were measured in the same way as for the larger materials for both frequency bands and polarizations. The smaller ab-

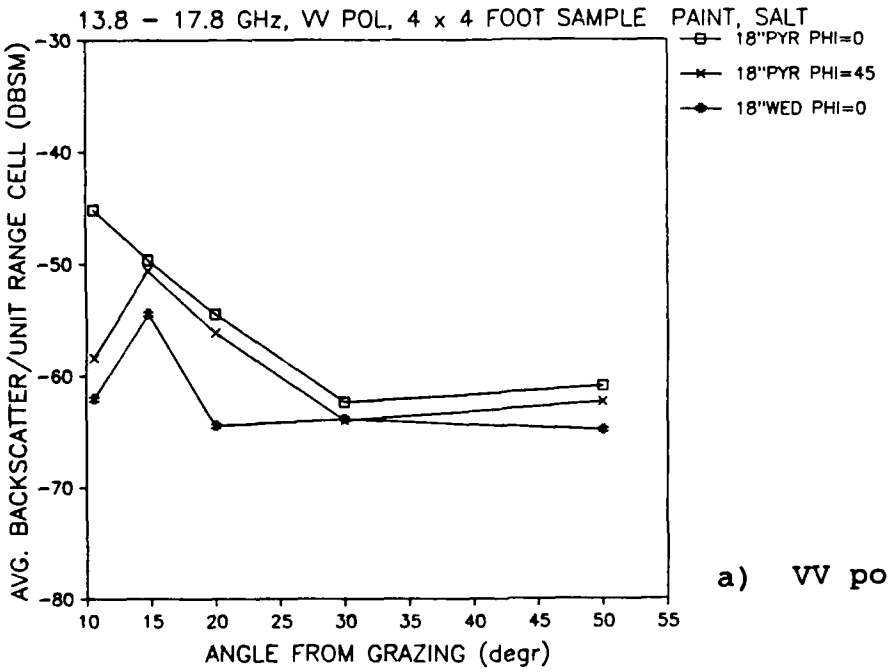

a) VV polarization

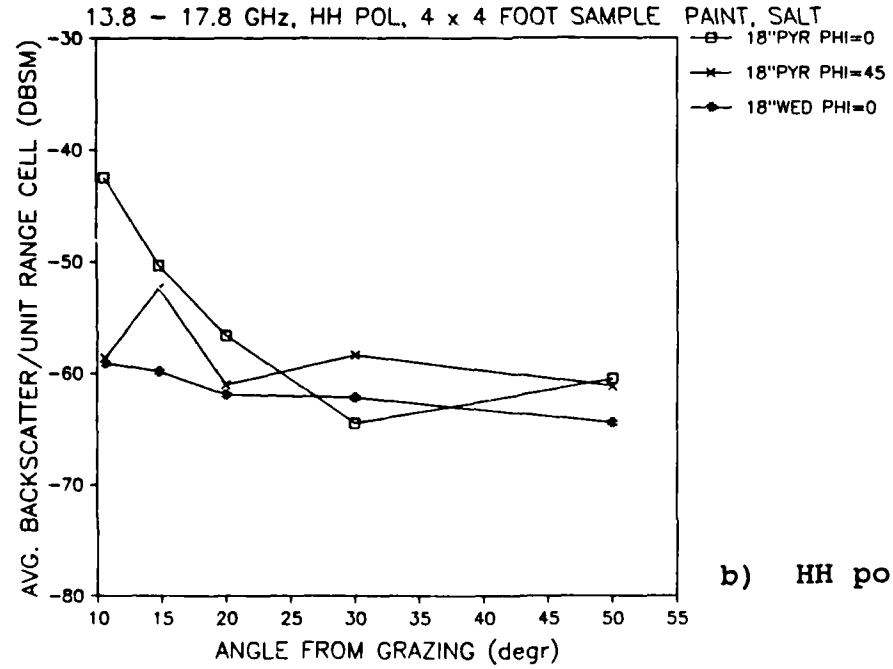

b) HH polarization

Fig. 4.14. Measured high-band backscattering performance of various 18 inch pyramidal and wedge absorbers as a function of incidence angle from grazing.

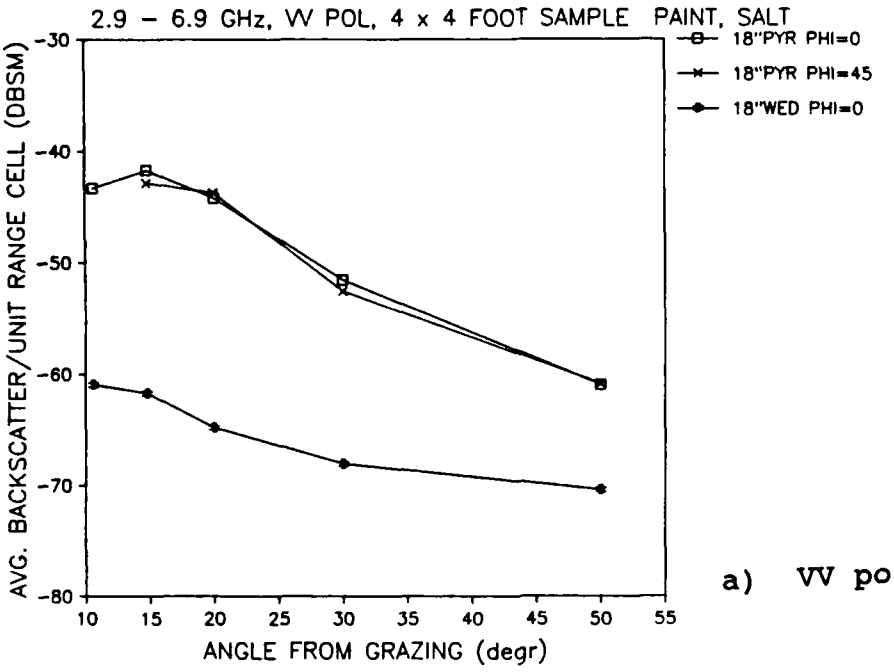

a) VV polarization

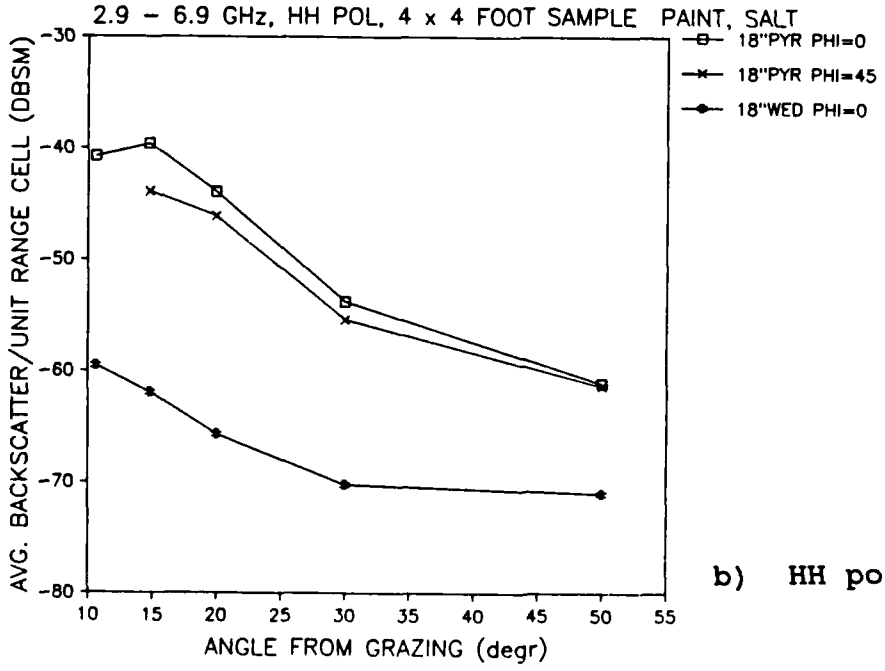

b) HH polarization

Fig. 4.15. Measured low-band backscattering performance of various 18 inch pyramidal and wedge absorbers as a function of incidence angle from grazing.

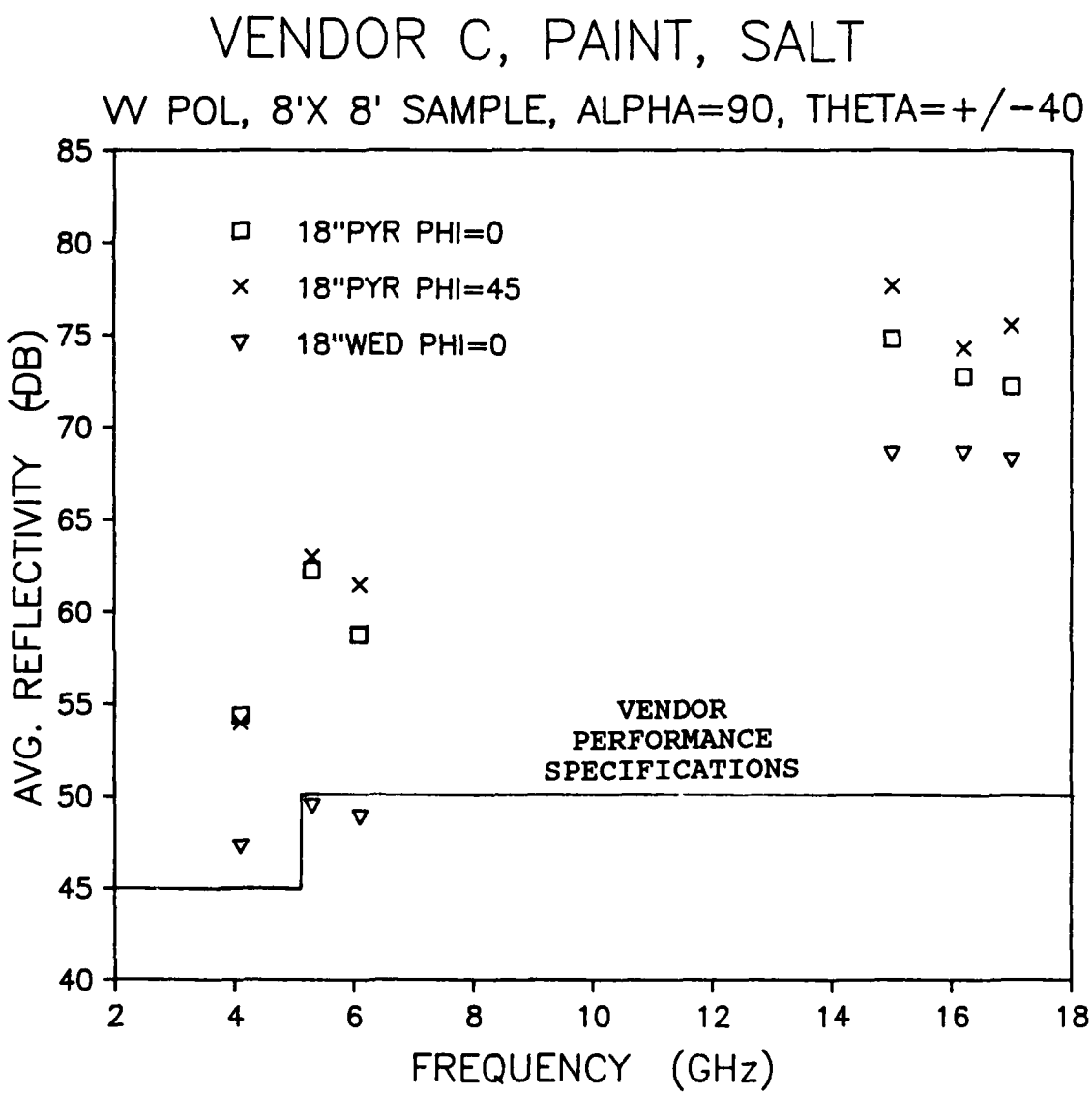

Fig. 4.16. Measured reflectivity of various 18 inch pyramidal and wedge absorbers.

sorbers have shorter shapes but a higher number of shapes per piece. The half-cone angle for the 8 inch materials is 13 degrees as opposed to 11.3 degrees with the 12 inch and 10.6 degrees for the 18 inch absorbers. All of the 6 and 8 inch materials were form the same vendor and had fire retarding salts.

The backscattering results for these materials at the upper frequency band are presented in Figure 4.17. Once again the wedge absorber turned at phi=0 offers the best performance with up to 20 dB improvement at the near grazing incidence angles. At alpha = 40 degrees, however, only slight differences between any of the materials is observed. The pyramidal materials turned both at phi= 0 and 45 degrees offer nearly the same performance as for the convoluted materials except at the very low incidence angles. For this case, turning the material phi=45 degrees offers no real advantage except for alpha angles below 18 degrees and for HH polarization. The relative level of these materials is also shown to be higher than for the 12 inch materials; again, partially due to the use of fire retarding salts, but also partially caused by the differences in the shape's sizes and the number of shapes used.

The lower frequency band results are shown in Figure 4.18. The response of these materials for this frequency band is somewhat surprising. The different orientations and

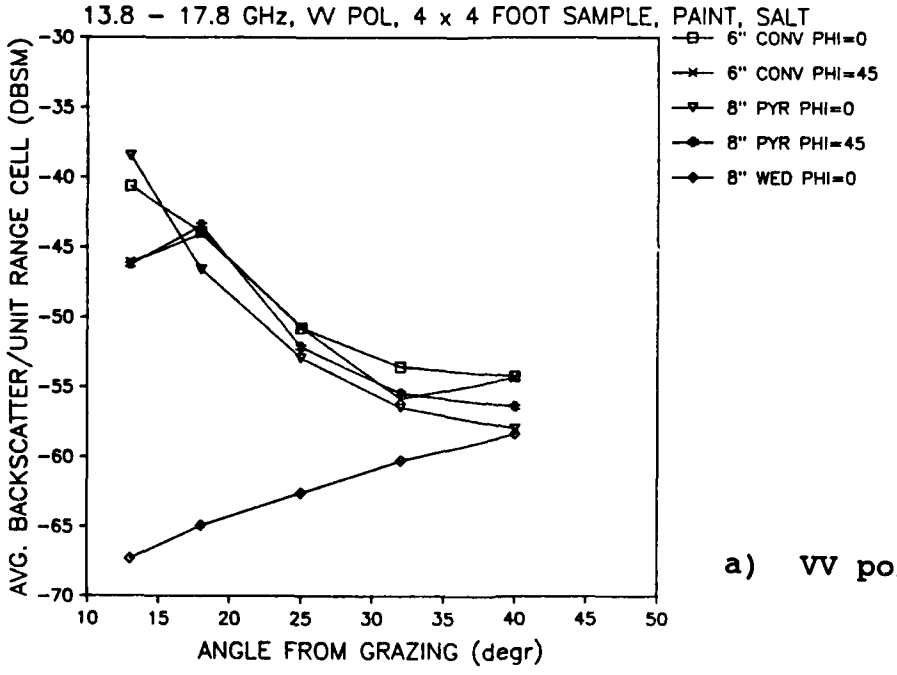

a) VV polarization

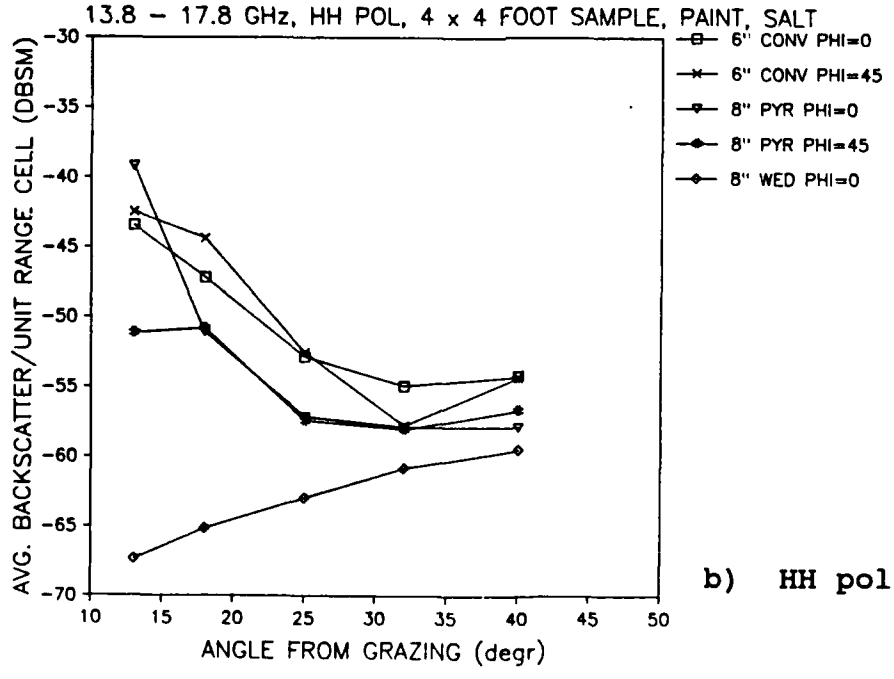

b) HH polarization

Fig. 4.17. Measured high-band backscattering performance of various 6 and 8 inch absorbers as a function of incidence angle from grazing.

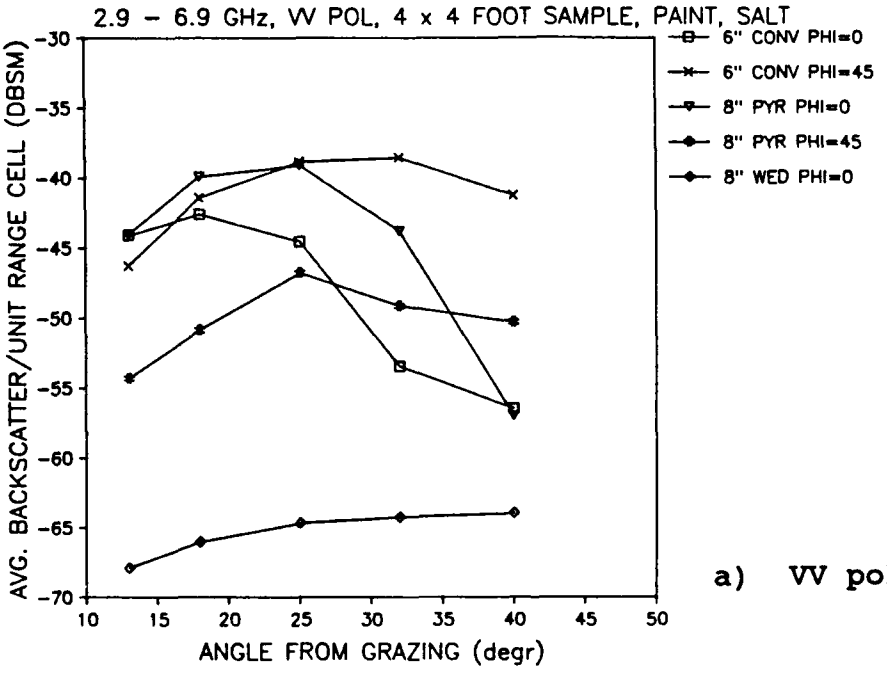

a) VV polarization

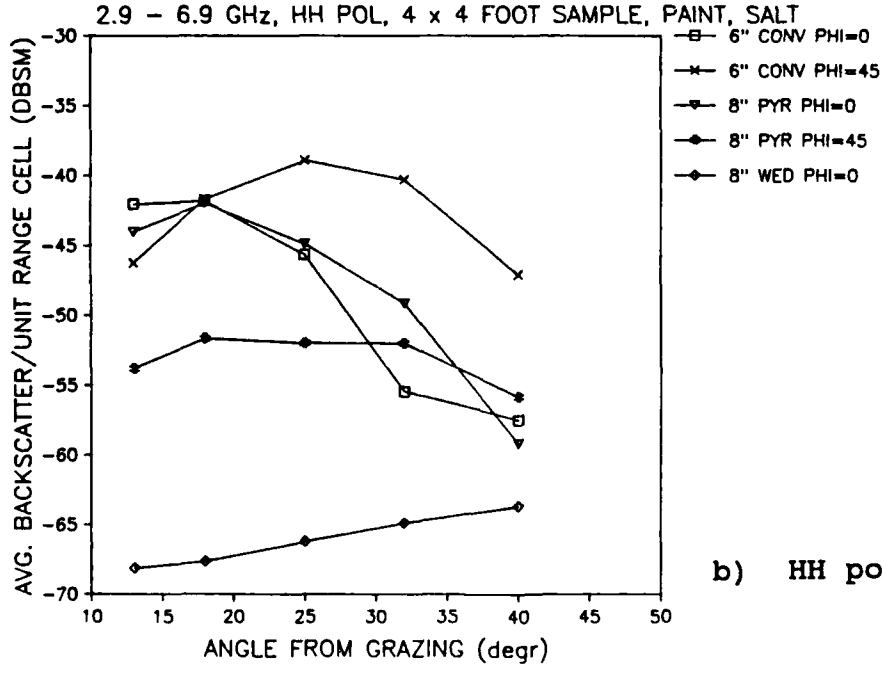

b) HH polarization

Fig. 4.18. Measured low-band backscattering performance of various 6 and 8 inch absorbers as a function of incidence angle from grazing.

sizes of material have much more of an effect on performance than they did for the higher frequency band. The exact reason is unclear but it may be due to resonant scattering conditions on the absorber and an improved air-to-dielectric impedance match at some incidence angles. A deeper penetration into the absorber at these frequencies is also present. The results again show that the wedge absorber is clearly best out to 40 degrees from grazing. The pyramidal material turned at phi= 45 degrees offers the next best performance below alpha = 30 degrees and the 6 inch convoluted works fairly well above alpha = 30 degrees. The worst absorber performance is from the 6 inch convoluted materials at phi= 45 degrees.

The reflectivity results in Figure 4.19 show that the wedge materials perform from 10 to 15 dB worse than the pyramidal and convoluted shapes toward normal incidence but that all the other materials have very similar performance. The results are again shown to be much better than the vendor's published specifications except for the wedge absorber.

4.3.4 New 12 Inch Material Designs

During this study an experiment was conducted in an effort to find an improved pyramidal absorber design. The goal was to obtain a pyramidal shaped absorber which had

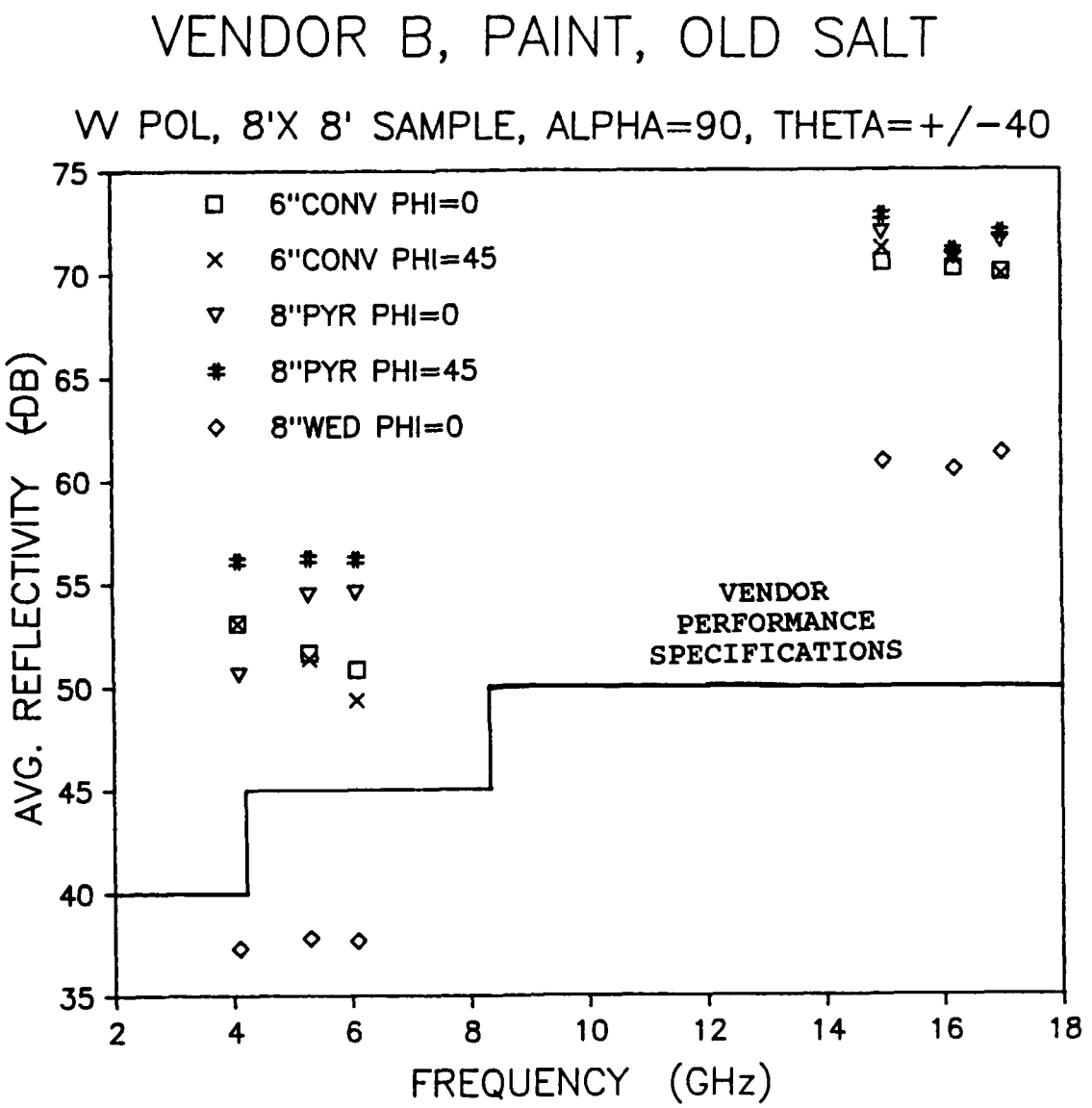

Fig. 4.19. Measured reflectivity of various 6 and 8 inch absorbers.

improved performance at both near-grazing and normal incidence, especially at the lower frequency band. The use of such a material should provide better chamber performance without having to use wedge materials. Wedge absorbers, although they offer better backscattering performance at the near-grazing angles, cause increased target or chamber coupling in some situations because of their increased specular bistatic scattering.

In modifying the design of pyramidal type absorbers only a few parameters can be changed without making the material impractical or too expensive to produce. The issue of fabrication has always played a big role in the design of absorbers. Specific shapes and graded or layered absorbers can be conceived which would offer better performance for specific applications; however, such shapes or absorbers may be very difficult to fabricate, especially in enormous quantities and at low costs.

The urethane foam material, for suspending the lossy carbon, is believed to be an adequate and acceptable base material unless major changes in the absorber design are to take place. The carbon loading solution used in present materials has been experimented with for many years by most of the vendors and it is believed that for a single solution application a near optimum concentration of carbon and binder has been reached. The only improvement which could be implemented would possibly be the addition of magnetic

lossy materials [38] or improved impedance matching techniques such as with layered or graded absorbers. The only other design parameter available for variation is material shaping.

To try to improve the performance of pyramidal type absorbers, with only a minimal impact on fabrication requirements, designs which had a larger number or density of pyramids per piece were fabricated. Two of the vendors produced and supplied 12 inch materials which had 49 and 64 individual pyramids per absorber piece as opposed to the standard 36 pyramids per piece. The length of the pyramids and the thickness of the absorber's base were also varied slightly. The effect of using more cones results in a smaller half-angle cone dimension and in smaller absorber surfaces. However, a larger number of tips and edges are introduced. Additional carbon is also made available in the material by using more cones. The effects of these changes were believed to improve the absorbers overall performance by increasing the random scattering nature of the absorber, especially at normal incidence, and to reduce the specular scattering terms at the low incidence angles. The additional carbon in the material and the higher number of cones was also thought to improve its low frequency performance.

The results of the evaluations conducted on these materials show that slightly improved performance is

achieved at the low frequency band for both normal and near-grazing incidence. At the high frequency band some improvements for normal incidence were also observed. However, the low incidence angle performance was not improved and even less benefit of turning the material 45 degrees was realized. The limitations were believed to be associated with the increased number of edges and tips. The overall performance of the modified materials was not as good as was originally desired and performance levels were not reached which would offer a suitable pyramid replacement for the wedge materials.

Figures 4.20 and 4.21 show the performance comparisons between the standard 36 cone design and the 49 and 64 cone designs for VV polarization and at both frequency bands. All of the results shown are for materials from the same vendor and include fire retarding salts. The results again show the most improvement at the low frequency bands. But only slight improvements of a few dB were realized. Figure 4.22 shows normal reflectivity results for the various materials and that up to 5 dB better normal incidence performance was reached with the new designs. Probably the most benefit of using a higher density pyramidal design is in realizing improved performance at normal incidence, especially for the longer pyramid materials and at lower frequencies.

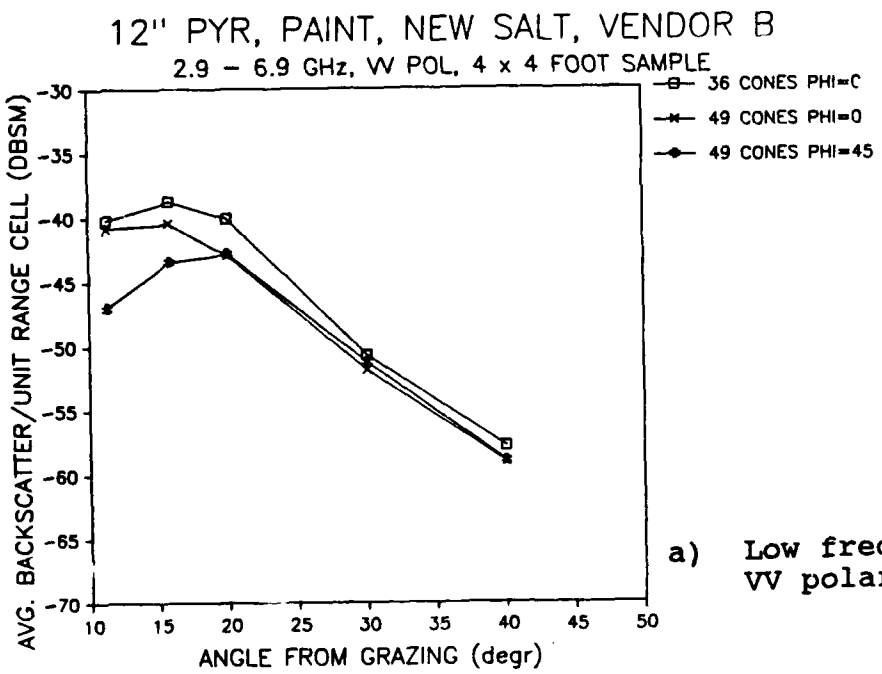

a) Low frequency band VV polarization

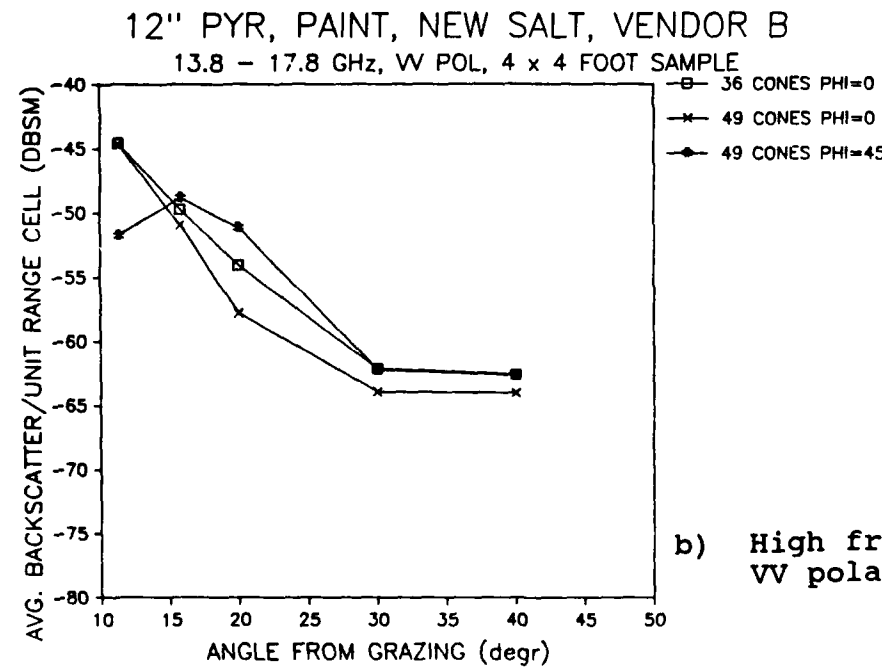

b) High frequency band VV polarization

Fig. 4.20. Measured backscattering performance of various 12 inch absorbers with 36 and 49 shapes per piece.

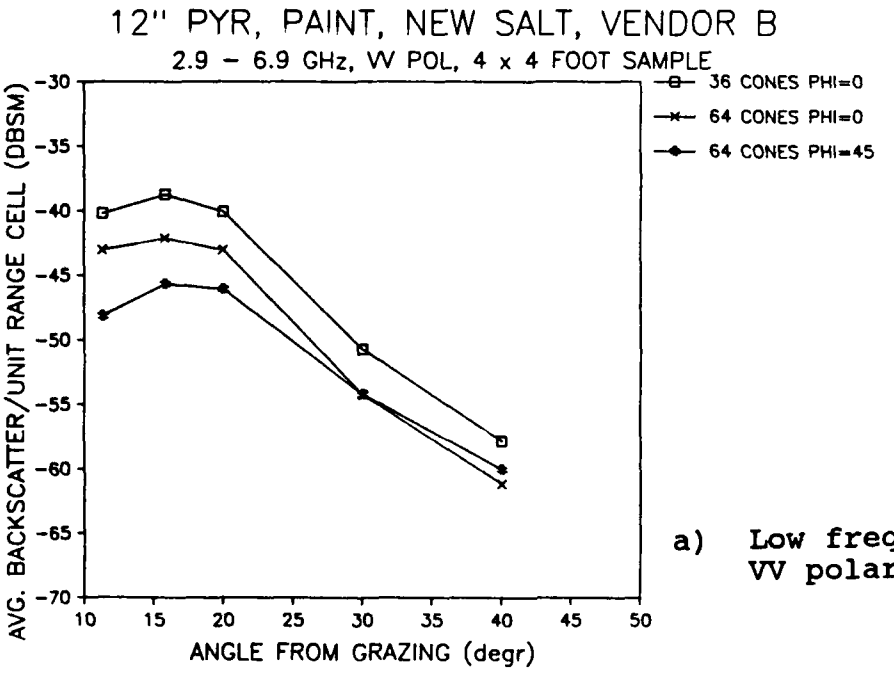

a) Low frequency band VV polarization

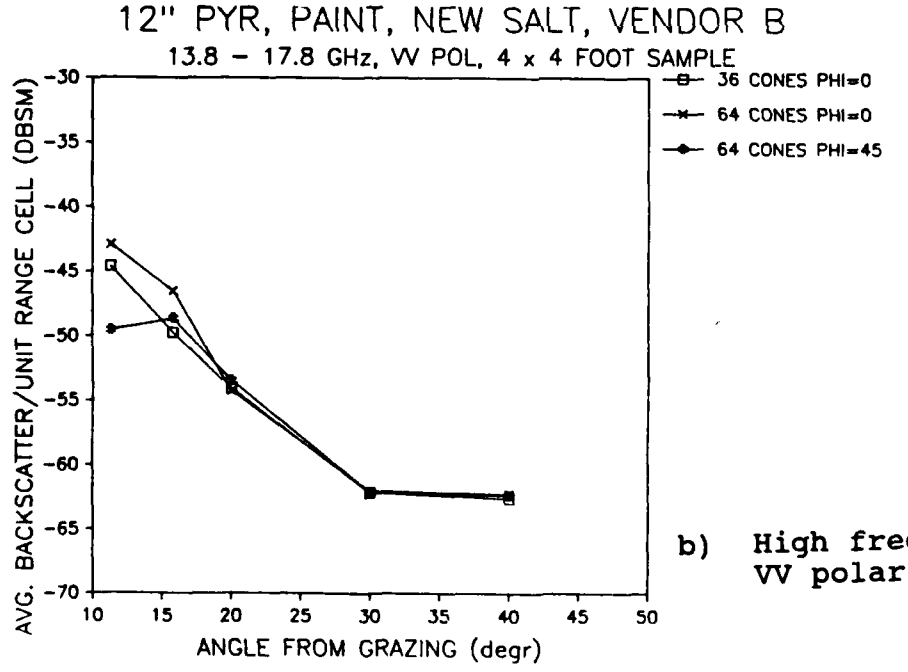

b) High frequency band VV polarization

Fig. 4.21. Measured backscattering performance of various 12 inch absorbers with 36 and 64 shapes per piece.

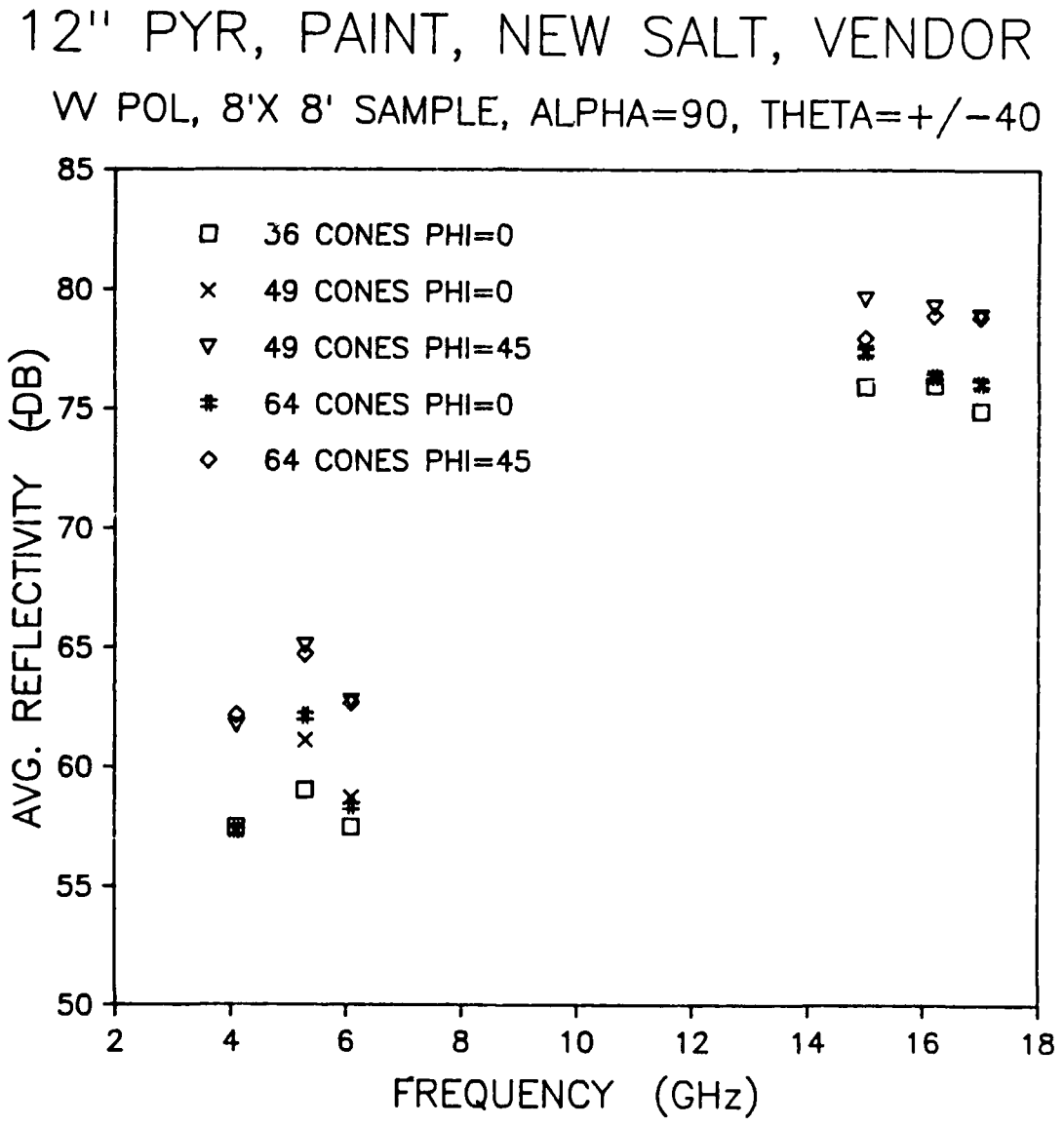

Fig. 4.22. Measured reflectivity of various 12 inch absorbers with 36, 49 and 64 shapes per piece.

4.4 EFFECTS OF METAL BACKING

This absorber study also investigated the effects of using a metal backing on anechoic absorber performance. The goal of this investigation was to determine the need and/or benefit of a metal backing as compared to a less expensive or more convenient backing surface or even an air backing.

The presence of a backup structure potentially influences the absorber's performance in two ways. First, if electromagnetic energy penetrates the absorbing material, without being substantially absorbed, then the backup structure mostly determines where that energy is scattered or directed. This is especially important for low frequency applications where the absorber is much less than a wavelength thick. If a metal backing is used then the penetrating energy is specularly reflected back into the absorber undergoing a second attenuation and is then radiated into the media from which it came. The advantage of using a controlled metal surface, in this case, is that the reflected energy can be intentionally directed in an unimportant area of the chamber.

The second potential effect of the backup structure is its influence in determining the effective impedance match at the dielectric to air interface. However, because of the highly lossy nature of the carbon loaded absorber, only at extremely low frequencies should the backup structure have

a significant effect on the impedance match of the materials.

One way to evaluate the significance of the absorber backing is by determining the electromagnetic skin depth of the material. One skin depth is a measure of the distance that electromagnetic energy can penetrate a media before it is attenuated by 8.68 dB. Thus, for a two-way path through a media, the signal power is attenuated by over 50 dB for a penetration of 3 skin depths.

By using the skin depth and by understanding the penetration mechanisms of the absorber materials, the amount of energy returned from a metal backplane can be determined. The exact formulation involves characterizing the absorber's reflection and transmission properties at the dielectric interfaces (impedance matches) over a wide range of incidence angles [9],[10],[39], and[40]. Modeling this arrangement is rather complicated because of the complex geometry of the shaped absorbers and the non-homogeneities found throughout the materials. However, a rather conservative approximation would be to assume that only 5 percent of the energy which is incident on an absorber is reflected from the absorber's surface. The rest of the energy then is assumed to enter the absorber and is directed normally to the flat backplane of the material.

The skin depth for any non-magnetic material can be calculated at a given frequency if the complex permittivity

is known. The presence of the carbon in the material determines the imaginary part, or the lossy properties of the absorber. Some typical permittivities are given in [9] for anechoic absorber materials. Using these results, permittivities of 1.5-j.69 at 3.75 GHz and 1.44-j.56 at 14.5 GHz were assumed for this study. These provide skin depths of 1.8 and 0.57 inches at these two frequencies respectively. These values suggest that for better than a 50 dB attenuation of the return from a metal backplane, the material should have a carbon loaded thickness of at least 5.4 inches at 3.75 GHz and 1.7 inches at 14.5 GHz. For most commonly used materials, minimum base thicknesses of 2 to 4 inches and pyramidal or wedge lengths of 6 inches and larger are usually used. Thus, at the frequencies investigated during this study it was expected that the effects of the backplane of the absorber would not be significant.

To determine the actual effects on performance, evaluations were conducted on absorber samples both with and without a metal backplane. Some of the tests were conducted by evaluating various single absorber sections mounted on a small styrofoam support structure. The measurement methods used were the time-domain coherent wideband radar techniques illustrated in Section 3.3.3.4. The frequency bands evaluated were 1.5 to 6 and 11 to 18 GHz.

These tests involved measuring the time-domain RCS

response of a section of absorber which was 8 by 8 inches at its base and was placed so that the flat back side of the material was normal to the radar. A flat metal square plate, 5.75 by 5.75 inches, was placed at the center of the absorber's back surface to form a metal backing. The metal target was smaller than the absorber sample to reduce edge effects. The small absorber section was used instead of the 8 by 8 foot test wall to minimize alignment problems. The RCS of the metal plate at normal incidence was -1 dBsm at 3.75 GHz and +11 dBsm at 14.5 GHz.

At the 11 to 18 GHz band, for all of the absorbers tested, no noticeable effects of the metal backplane were found by the evaluations. The absorber samples included 3 inch convoluted, and 8, 12 and 24 inch pyramidal and wedge absorbers. Figure 4.23 illustrates typical results at this frequency band for the 12 inch pyramidal materials with and without a metal backing. The physical backplane of the absorber section is located at approximately 0 meters in range. However, returns from the metal backing plate would occur from 1.1 to 6.8 centimeters behind the absorber's physical backplane since a propagation factor of 1.22 exists in the dielectric absorber. Even down to a -70 dBsm level the metal target response is shown to be undetectable. The slight variations in the two responses show the repeatability of the measurement. This represents at least a 80 dB reduction in the response of the metal backplane.

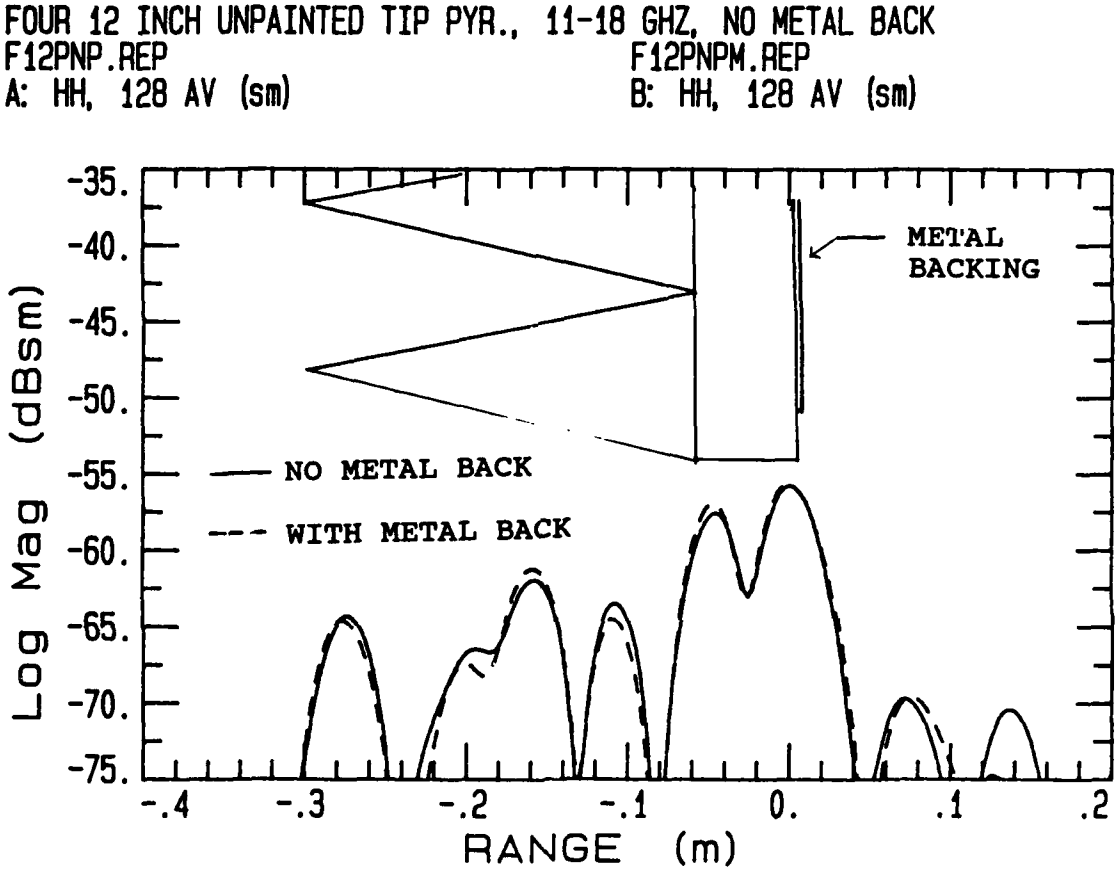

Fig. 4.23. Time-domain results of 12 inch pyramidal section both with and without metal backing for the 11 to 18 GHz band.

The performance of the absorber is shown to be mostly dictated by the scattering from the absorber's surface and not by a limitation in its absorption properties.

Results for the 1.5 to 6 GHz band for the 12 inch pyramidal absorbers are shown in Figure 4.24. Even at this lower frequency band, the effects of the metal backing are not the dominant contributors to the total scattering and better than a 45 dB reduction in the return from the metal plate was obtained. However, the backplane of the absorber does contribute to the scattering and is more significant than the tip diffraction terms. This is explained by the increased skin depth in the material at these frequencies. At the areas of the metal backing, differences of less than 5 dB are shown. The propagation factor in the material at this frequency is 1.25.

For 8 inch pyramidal material the results for the low frequency band are shown in Figure 4.25. Again, the effects of the metal backing appear at a range behind the absorber's returns, but for this case these returns are negligible with respect to the overall return from the absorber. The tip and pyramid shape returns are up to 10 dB larger than the returns from the backing. Part of the reason is because of the increased number of shapes.

The smallest material which was evaluated was a 3 inch convoluted absorber. The results of this material at the low frequency band are shown in Figure 4.26. The effects of

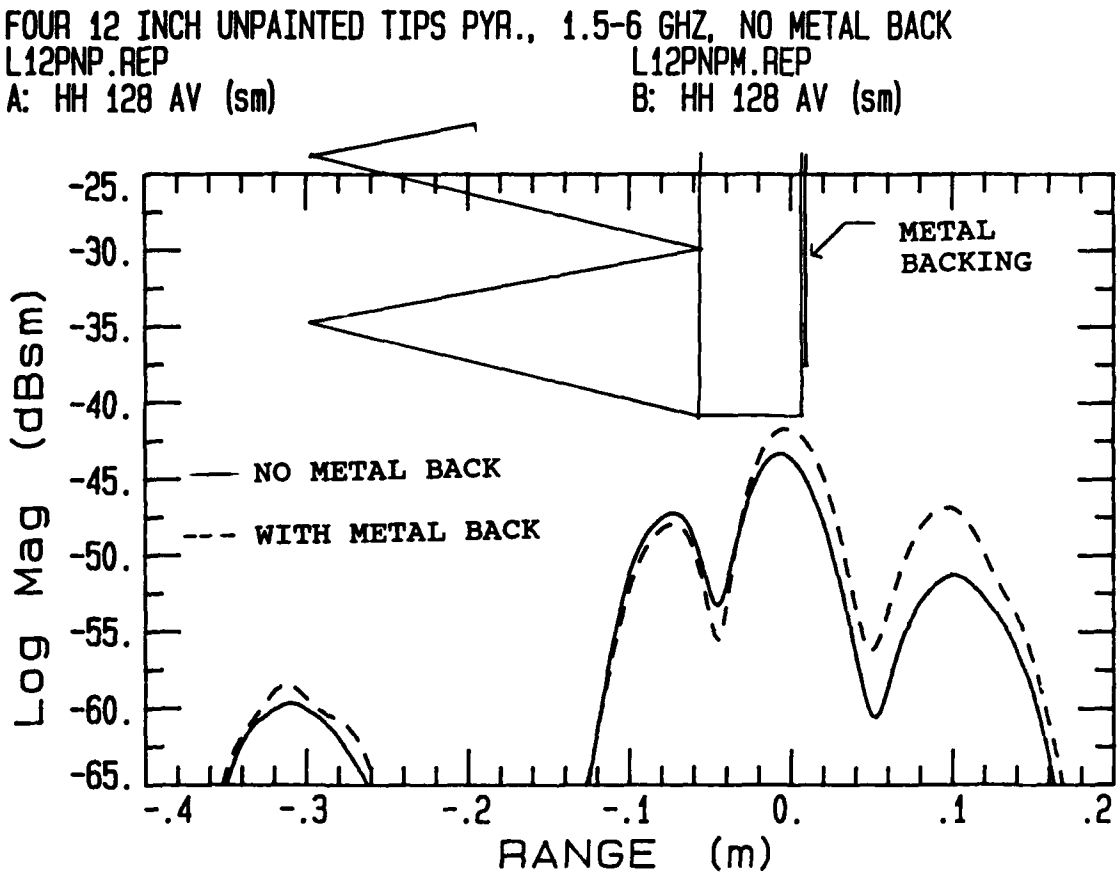

Fig. 4.24. Time-domain results of 12 inch pyramidal section both with and without metal backing for the 1.5 to 6 GHz band.

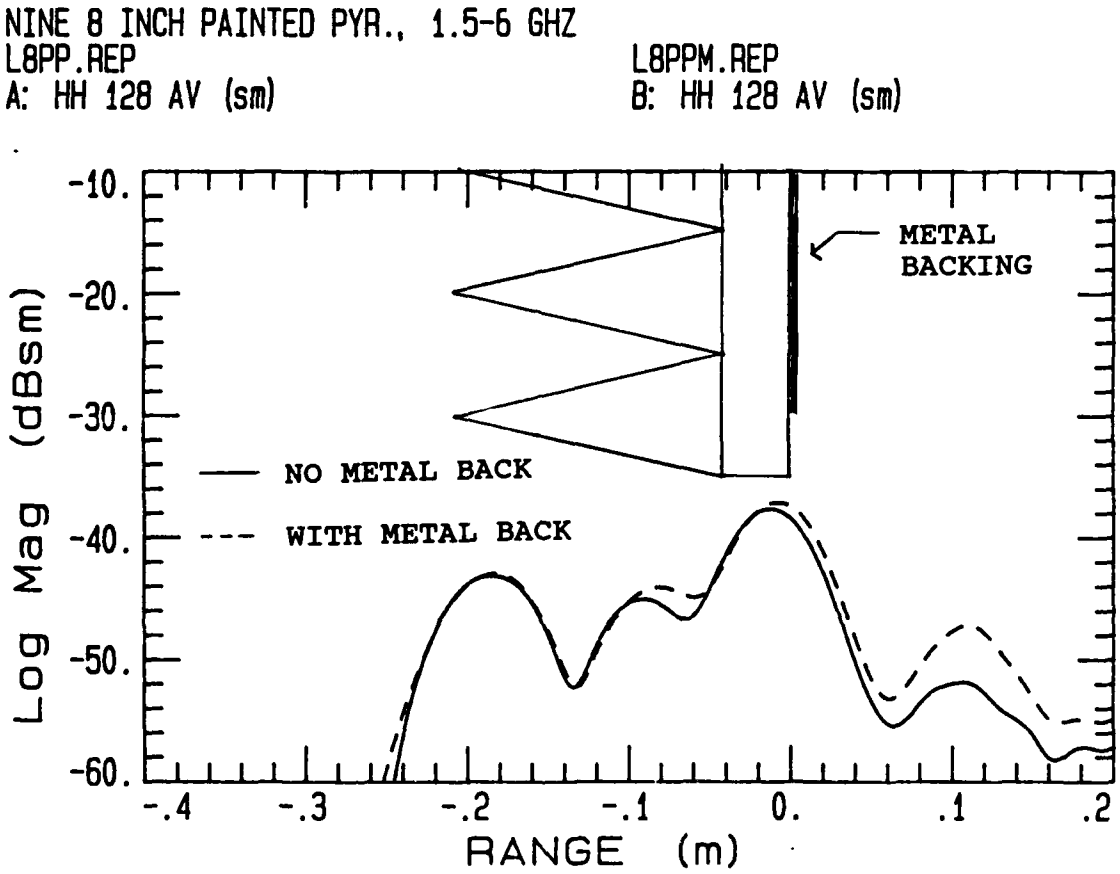

Fig. 4.25. Time-domain results of 8 inch pyramidal section both with and without metal backing for the 1.5 to 6 GHz band.

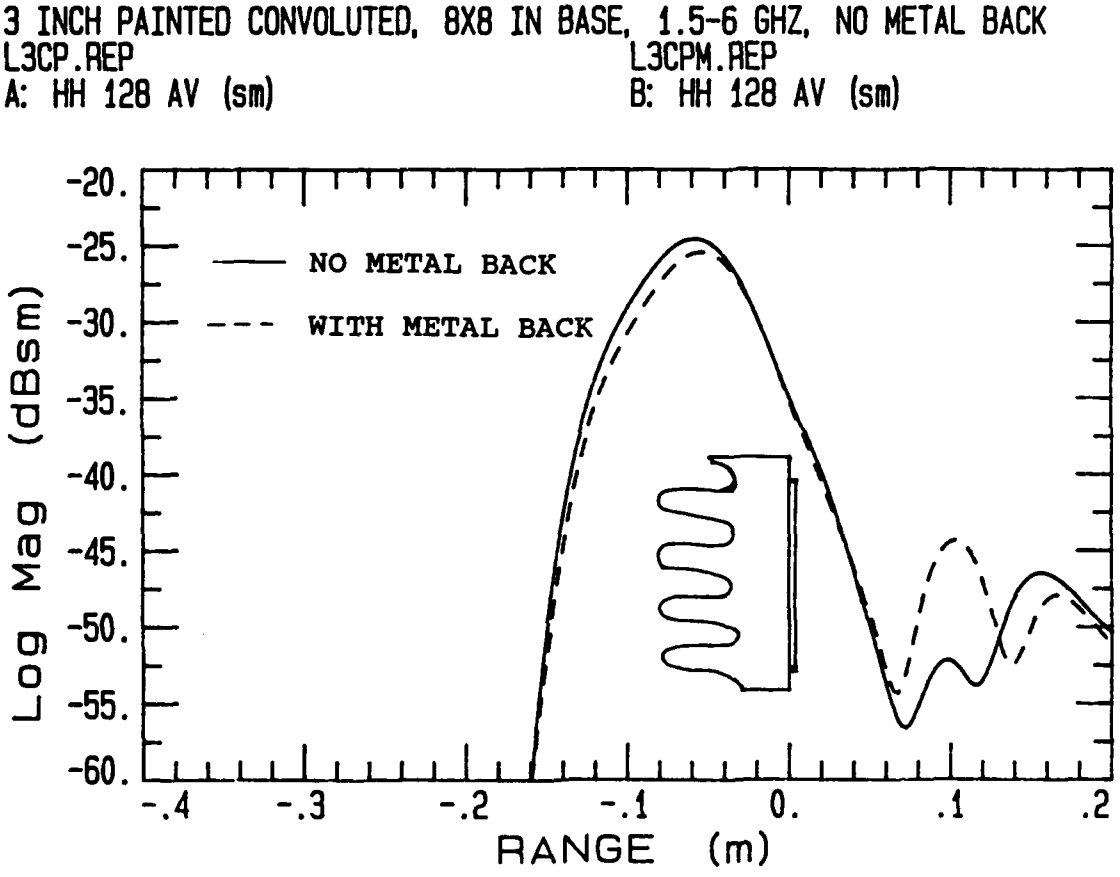

Fig. 4.26. Time-domain results of 3 inch convoluted section both with and without metal backing for the 1.5 to 6 GHz band.

the metal backing are clearly shown in the range of +.1 meters. Even still, the metal backing effects are 20 dB below the scattering returns from the absorbers surfaces and are not significantly important.

4.5 EFFECTS OF FIRE-RETARDING CHEMICALS

One of the significant results of this absorber study was in determining some of the performance degradations which occur when fire retarding chemicals are added to absorbing materials. Such chemicals, which are composed of various salt compounds, are placed in the materials for safety reasons. Most facilities are required to use these salts in their absorbers to meet local fire code requirements.

Measurements were conducted on various 12 inch materials with and without fire retardants. All of these materials were provided by the same absorber vendor and only this vendor's material was evaluated. Section 4.7 illustrates that the different vendor's materials vary slightly in performance as a result of the particular salts used, therefor, the results of these particular tests may not apply to all the materials currently available. Evaluations were conducted at both normal and near-grazing incidence. The overall results show that performance degrada-

tions as high as 10 dB are realized when salts are used in the materials, especially for the off-normal incidence angles toward grazing.

The measured backscattered RCS for the 12 inch pyramidal absorber, both with and without salts, is shown in Figure 4.27 for a phi and theta angle of 0 degrees and at the 13.8 to 17.8 GHz band. These evaluations were conducted using the ISAR imaging techniques discussed in Section 3.3.3.2. For VV polarization, the materials without fire retarding salts is shown to offer from 5 to 10 dB better performance over the entire range from 11.3 to 40 degrees. The HH polarization results show that only slight improvements were obtained at some angles. Similar tests conducted on 12 inch wedge materials show that slight improvements of 2 to 3 dB exist for materials without salts over the same angular region.

The results for near-normal incidence, shown in Figure 4.28, illustrate that the reflectivity values for the materials with and without salts change only slightly for the 12 inch pyramidal materials at the high frequency band. But, at the low band the non-salted materials tend to have better performance. The wedge materials, however, show just the opposite response. The low-band performance of the 12 inch wedges shows only small differences between the materials with and without salts and the high-band results show that the unsalted absorbers are better by 3 to 5 dB.

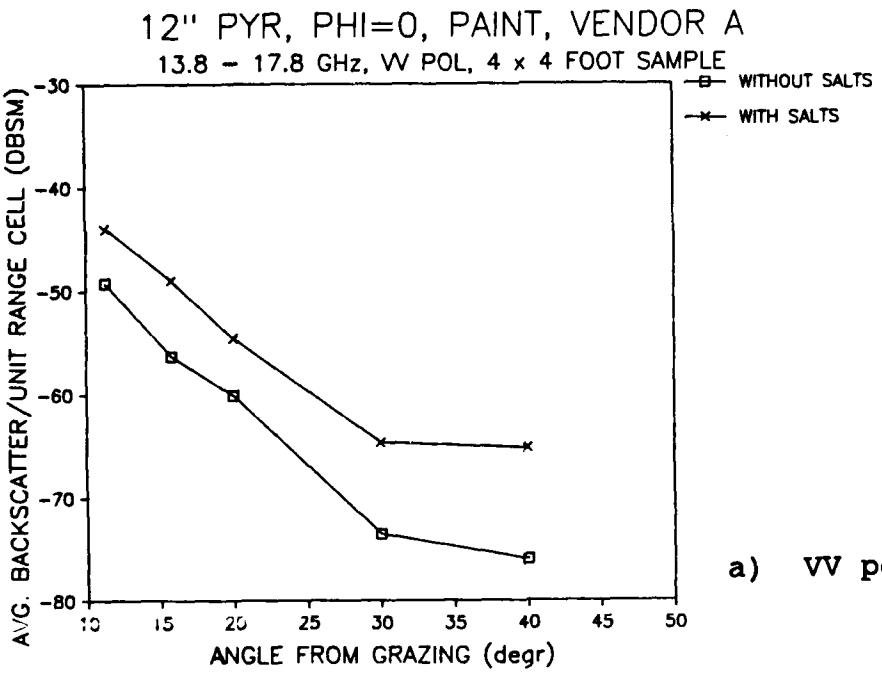

a) VV polarization

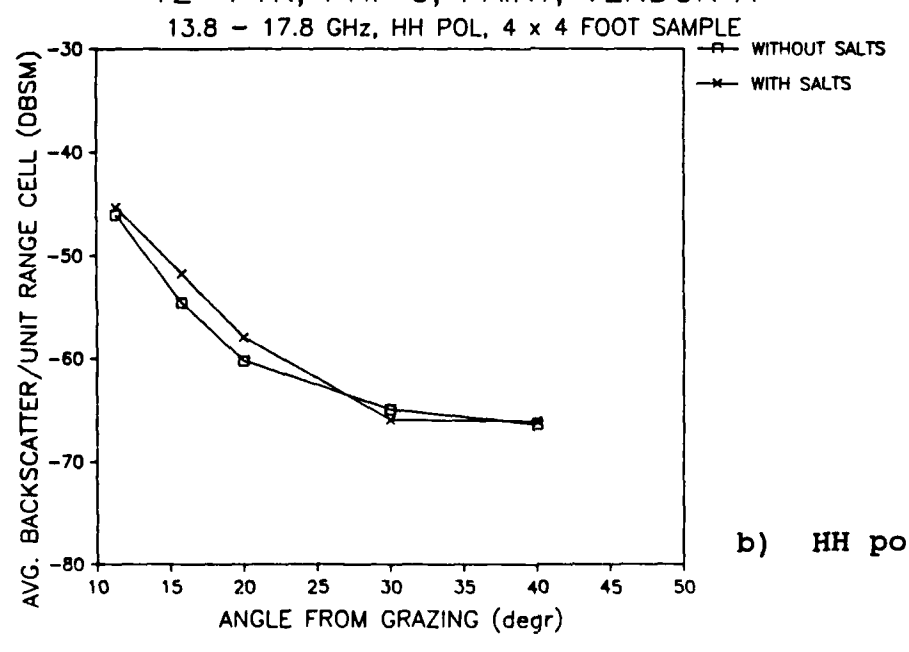

b) HH polarization

Fig. 4.27. Measured backscattering performance of 12 inch pyramidal absorber both with and without fire retarding salts.

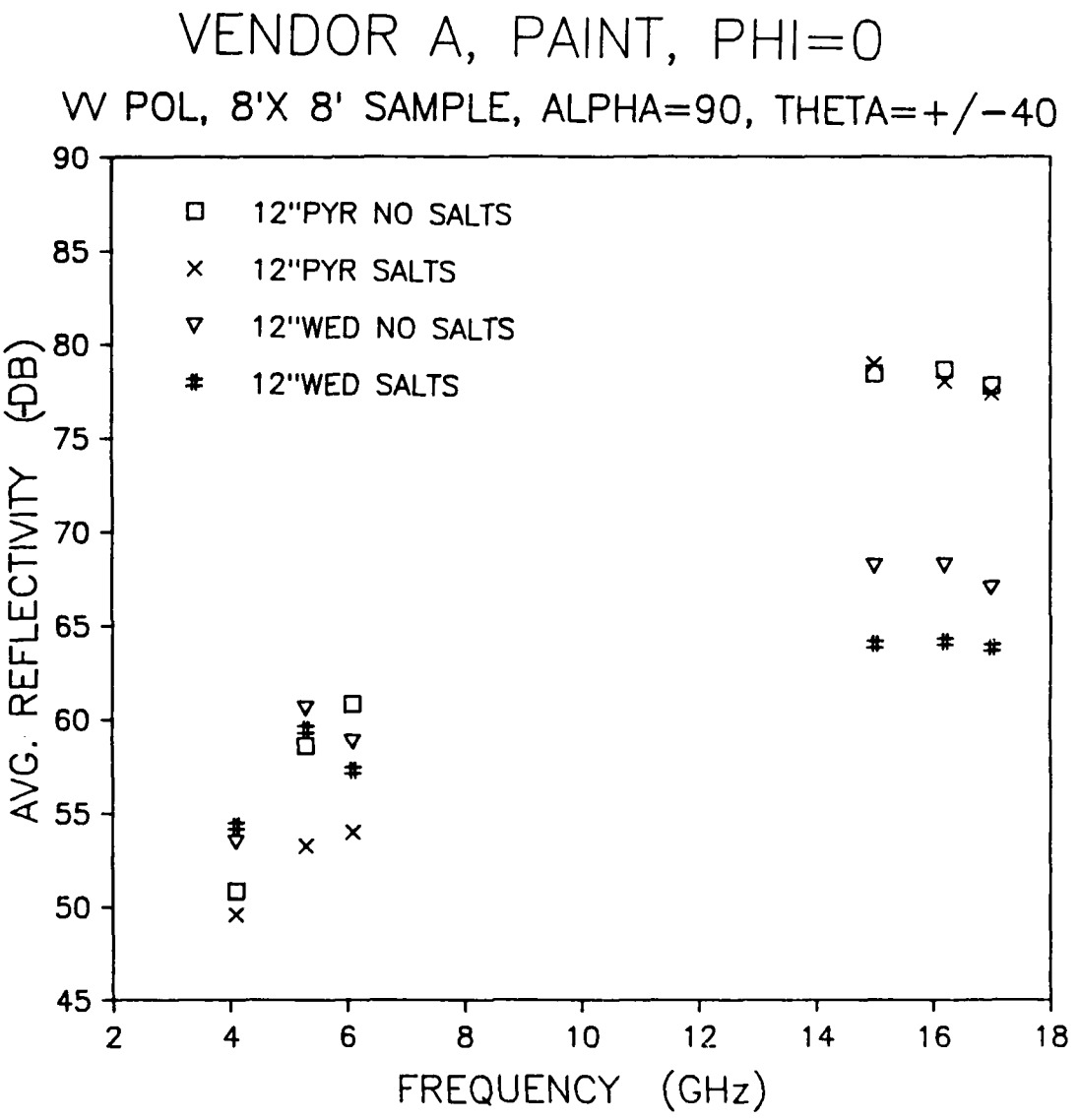

Fig. 4.28. Measured reflectivity of 12 inch pyramidal and wedge absorbers both with and without fire retarding salts.

4.6 EFFECTS OF PAINTING MATERIALS

Absorbers are typically painted both to help protect the materials and to increase the amount of light reflected from the absorber's surface. The effect of paint on the absorber's performance was one of the parameters investigated during this study. The concern about the paint is that it increases the amount of reflected and diffracted energy from the absorber's surfaces and edges, thus, degrading its performance. This is especially a concern for higher frequency operation. Earlier work in this area at 94 GHz [41] reports that painting the materials does degrade the absorber's performance for some cases.

The evaluations conducted during this study involved measuring various painted and unpainted 12 inch pyramidal and wedge absorbers, all from the same vendor. All of the materials tested also contained no fire retarding salts. Of the painted materials tested, no obvious excessive paint layers or clots were found. Measurements were made using the 8 by 8 foot test wall discussed in Section 3.3.2. Results for both normal and near-grazing incidence were obtained in the 2.9 to 6.9 and 13.8 to 17.8 GHz bands. Within these frequency bands no noticeable performance degradations were observed due to the presence of the paints. These results are consistent with those published in [9].

Time-domain measurements were also conducted using materials which were both completely painted and which had unpainted tips. Single pyramidal absorber sections were used. Recent trends in absorber painting is to leave the absorber's tips unpainted while painting the rest of the surfaces. The objective is to reduce tip diffraction components especially above 30 GHz. Figure 4.29 shows the worse case comparisons between materials with and without the tips painted over the 11 to 18 GHz band. The data illustrates that the tip components are changed only slightly between the two cases. In fact, much larger performance variations are shown at other areas of the absorber than for the tips. This is caused by other parameters of the materials which are not consistent between the two pieces, such as the carbon density.

4.7 VENDOR PERFORMANCE COMPARISONS

Comparisons between similar pyramidal and wedge materials from the three vendors were also conducted during this study to evaluate the various fabrication techniques used. Each of the three vendors, who supplied materials for this study, fabricate the absorbers in a slightly different manner. Small variations in the carbon loading and fire retarding salts also exist.

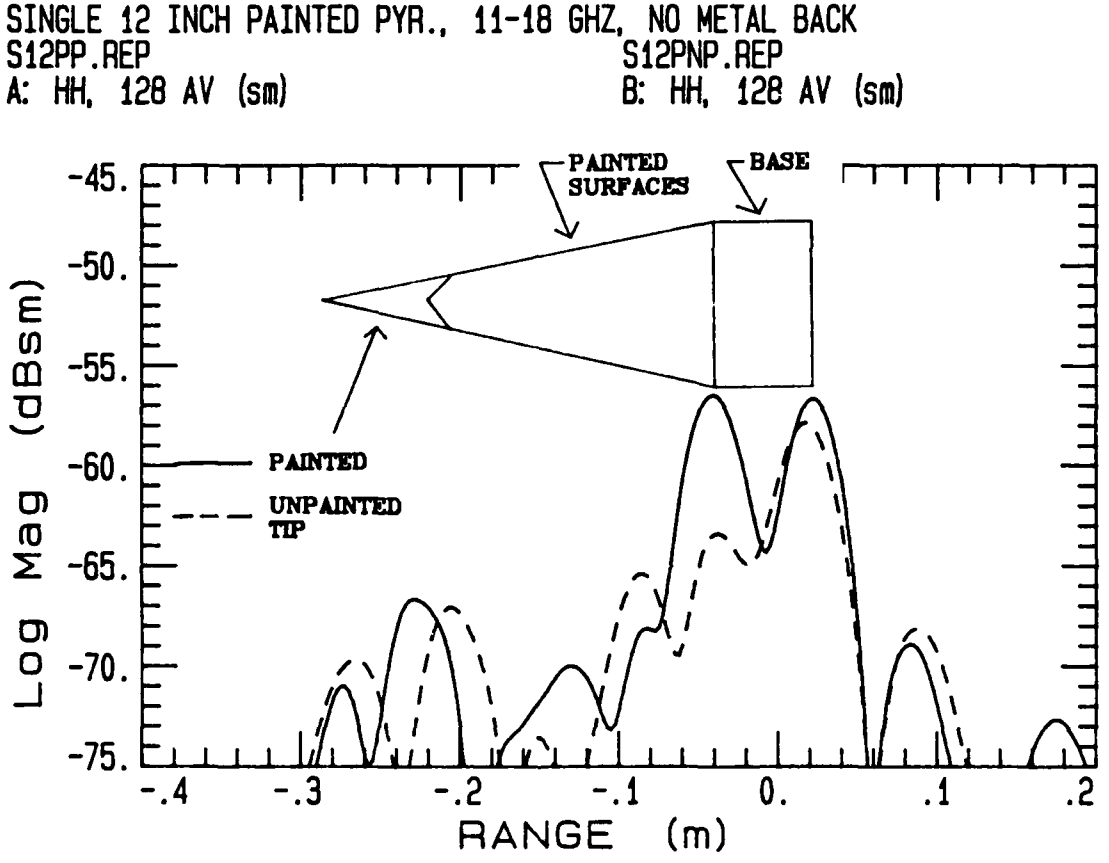

Fig. 4.29. Time-domain results of single 12 inch pyramid both with and without a painted tip.

Figures 4.30 and 4.31 illustrate some of the differences in performance for the various 12 inch pyramidal materials evaluated. All of the materials were painted and had fire retarding salts. At the upper frequency band, vendor B's material had up to a 10 dB higher backscatter level at 30 to 40 degrees from grazing and a 5 dB lower reflectivity at normal incidence. The other two materials performed about the same with vendor A's material being slightly better. At the lower frequency band, vendor A's material had the best off-normal performance but the worse normal incidence reflectivity.

A very noticeable physical difference also existed between the materials. Vendor B's material was much heavier and had a hard crusty surface due to the fire retarding chemicals used. The other vendor's materials were nearly the same in weight and stiffness. The amount and color of the paint used on the materials also varied between the vendors.

4.7.1 New Fire Retardant Material Design

During the same period of time over which this study was being conducted, vendor B was also working on a new fire retarding design for their materials. Samples of 12 inch pyramidal absorbers with the new fire retarding salts were supplied by vendor B for comparison to their old

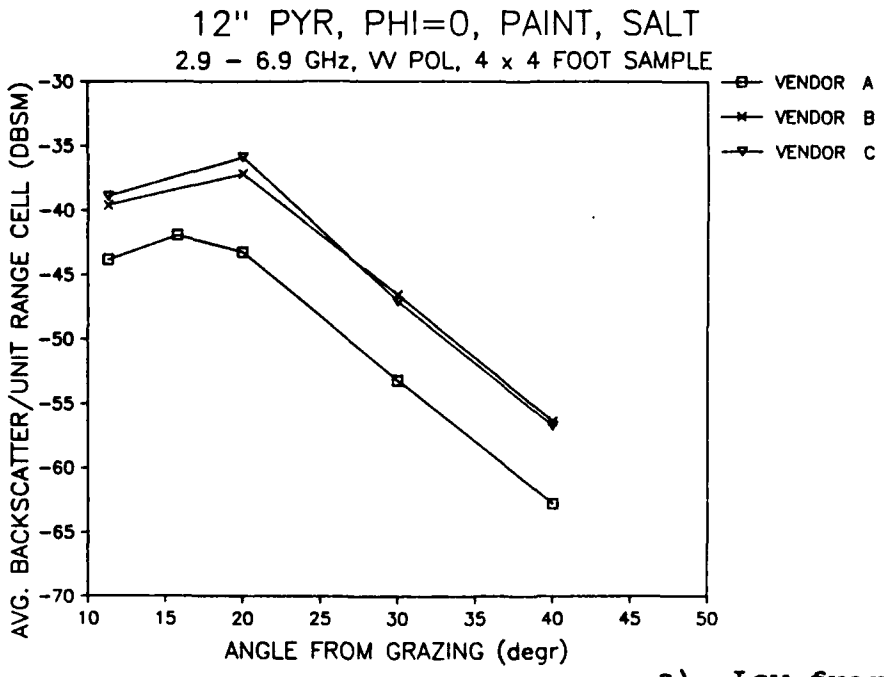

a) Low frequency band VV polarization

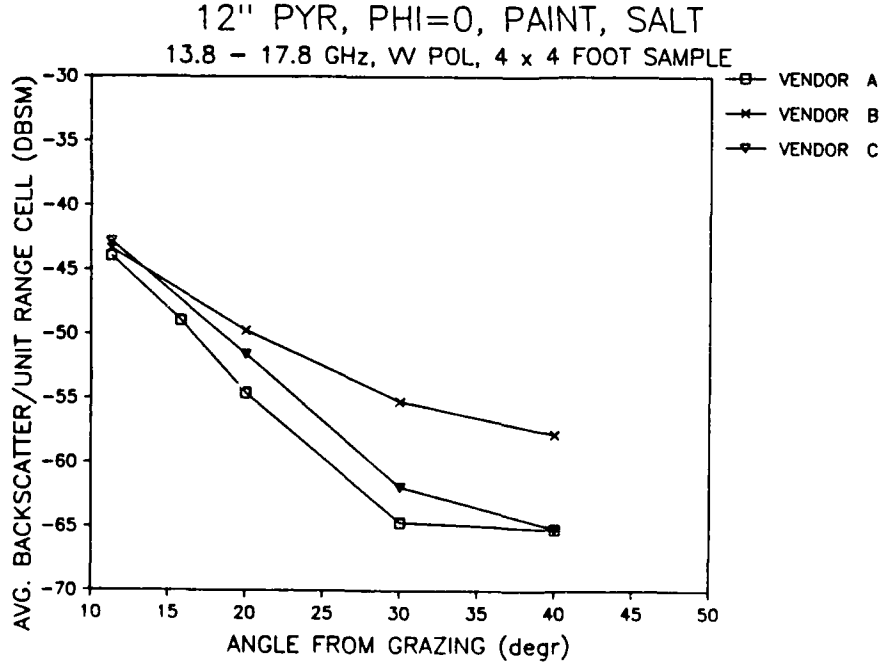

b) High frequency band VV polarization

Fig. 4.30. Measured backscattering performance of similar 12 inch pyramidal absorbers from the three vendors.

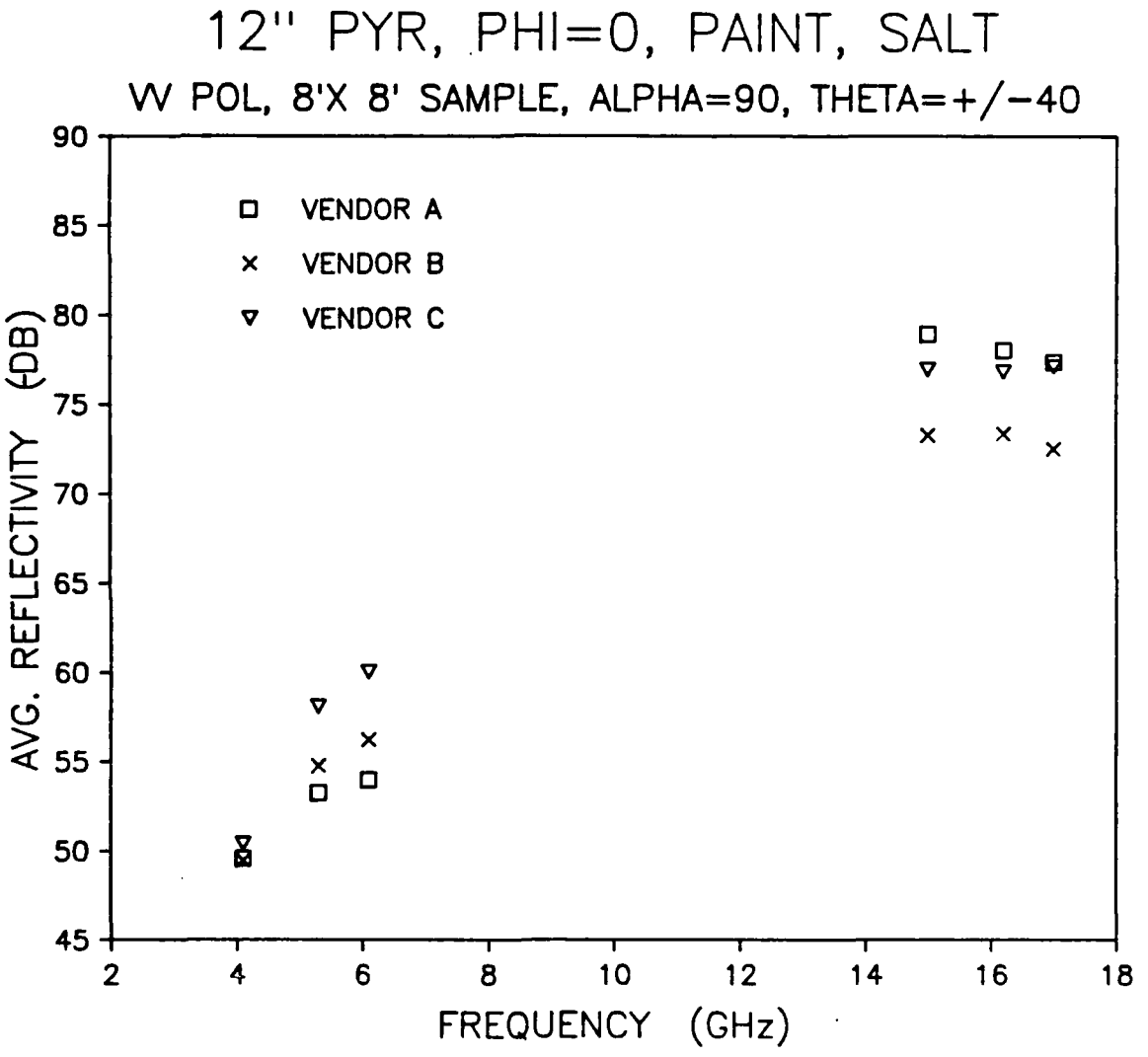

Fig. 4.31. Measured reflectivity of similar 12 inch pyramidal absorbers from the three vendors.

design. The new design reduced the weight and stiffness of their material significantly. Figures 4.32 and 4.33 show the performance of vendor B's new and old designs. Vendor A's results are shown as a reference for comparison. The new fire retardant design is shown to improve the absorber's performance at both the upper and lower frequency bands and for both normal and near-grazing incidence.

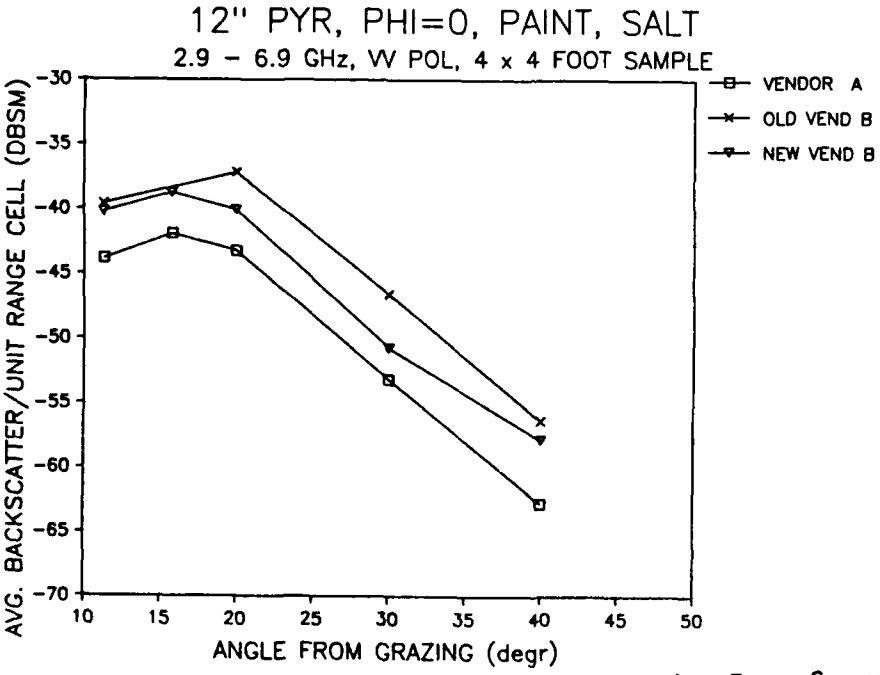

a) Low frequency band VV polarization

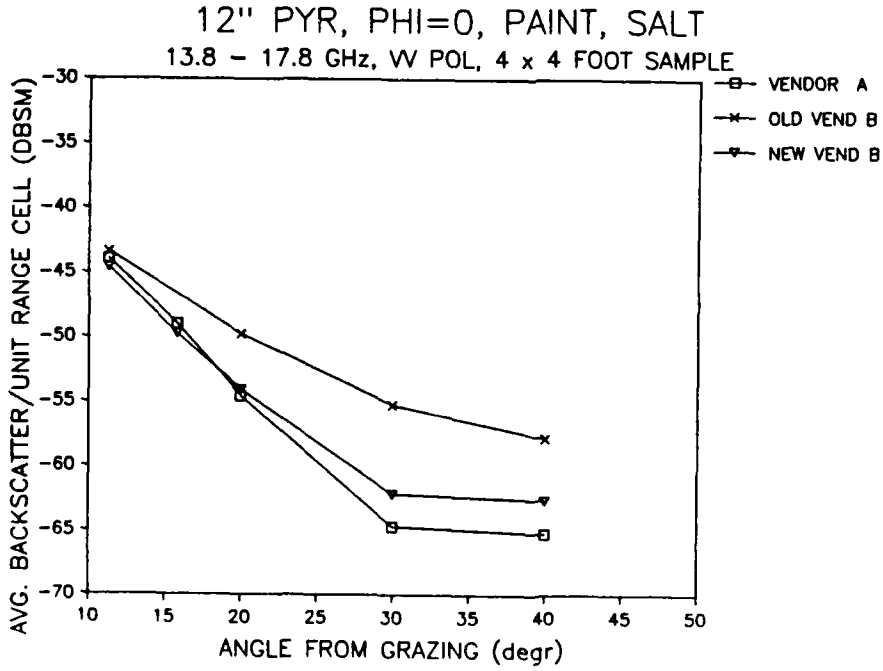

b) High frequency band VV polarization

Fig. 4.32. Measured backscattering performance of vendor B's new and old fire retardant absorber designs.

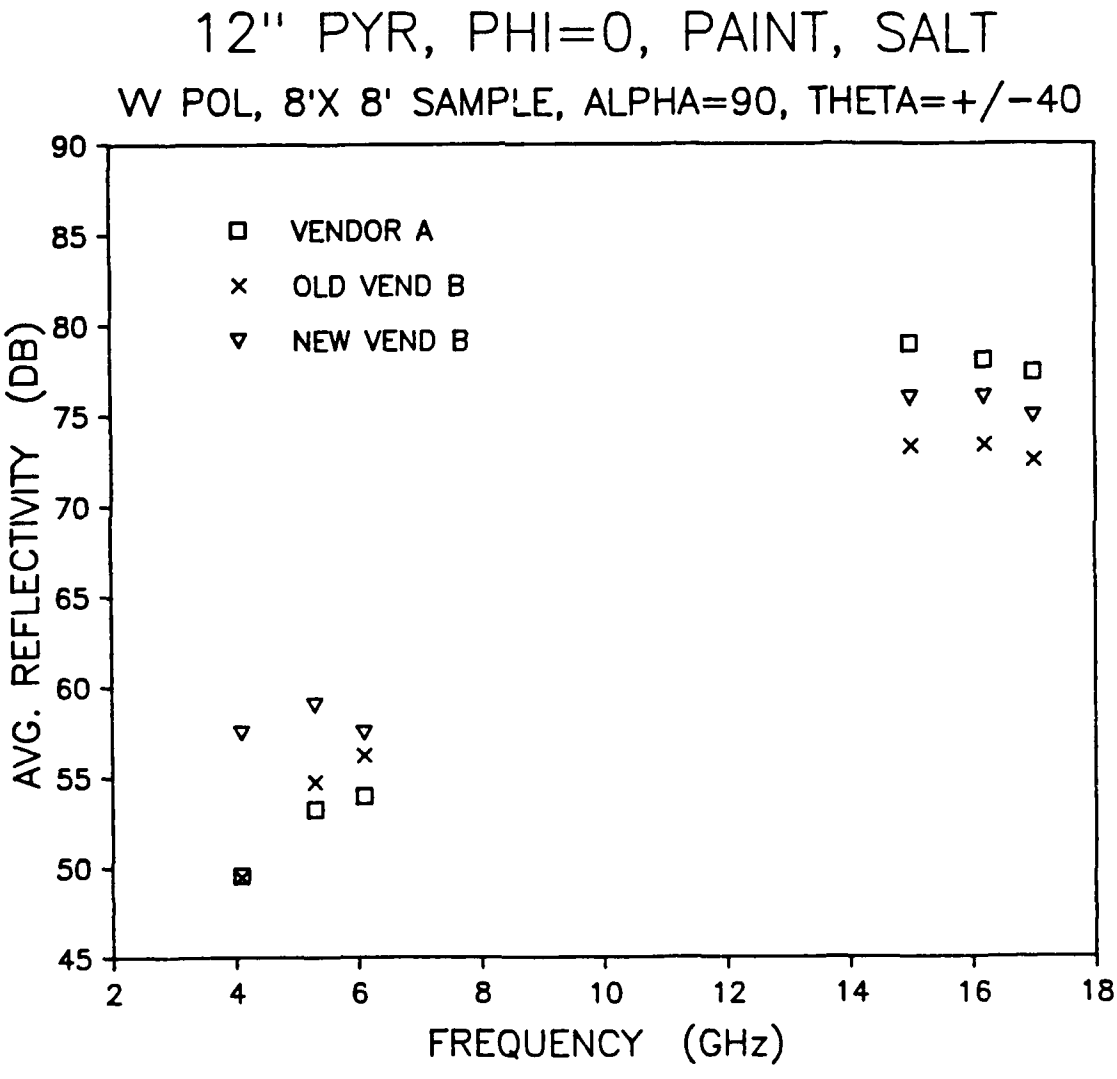

Fig. 4.33. Measured reflectivity of vendor B's new and old fire retardant absorber designs.

5.0 APPLICATIONS OF ABSORBER EVALUATION RESULTS

5.1 INTRODUCTION

There are many applications for a better characterization and understanding of the performance level of microwave anechoic absorbing materials. The number of applications is almost as many as the number of current facilities which make use of such materials. Each chamber is uniquely designed to meet a specified goal for conducting measurements on at least one specific hardware or system type. Each different measurement requirement usually places its own specific requirements on the performance level of the anechoic room in which the measurements are conducted. And, many anechoic chambers are used to conduct various types of tests on more than one hardware type or system. The size and design of such chambers also vary from facility to facility. By applying a better understanding of the quality of the chamber, and thus the absorbing material, many of these measurements could be performed with improved accuracies. Anechoic chamber designs could also be implemented which allow for more demanding measurement requirements to be satisfied. This chapter addresses only a few of the more general applications of the absorber performance results which were obtained during this study. Specifically, only applications relating to improved absorber and RCS chamber performance levels are discussed.

5.2 IMPROVED ABSORBER PERFORMANCE

The results of this absorber study can be directly applied to improved absorber performance in at least two ways. First, by the continued application of the modern diagnostic absorber measurement techniques, developed during this study, to better evaluate the actual performance of present and future materials. And secondly, by using the results of the evaluations already conducted to better define the limitations and problem areas with the current materials.

The diagnostic measurement techniques, making use of coherent wideband radar and imaging instrumentation, have been shown to be extremely useful in determining and characterizing the scattering mechanisms associated with the various types and sizes of material. Using these evaluation techniques, the exact reasons or causes of degraded absorber performance can be found, and, as a result, modified fabrication methods or absorber design solutions can be determined which should lead to improved performance. Once the performance limitations of current absorbers are fully understood, then the development of the next generation of newly designed materials with improved capabilities can begin. The use of these modern measurement techniques should be of great significance in this development.

During this study the use of these techniques led to the discovery of several absorber performance limitations. A summary of these discoveries is presented.

In general, the absorbers were found to be non-homogeneous in their carbon densities and fire retarding salts and also in their physical size. Use of this non-homogeneous nature in obtaining noncoherent and random scattering conditions can actually improve the performance level of the absorbers. However, it was determined that a controlled and predictable method of designing for these nonhomogeneities, instead of letting them occur by chance during the fabrication process, should lead to even further performance improvements.

In most cases, the use of the fire retarding salts in the absorbers were found to reduce their performance at some aspect angles. It was found that the amount and type of salts vary between the different vendors and that performance levels also vary. One vendor changed the design of their fire retarding salts with the new design showing improved performance results. These results were shown in Section 4.7.

A newly designed wedge material was also made available by one vendor during this study which offered a six-foot long absorber section as opposed to the standard two-foot length. The technique used to fabricate this design made use of a numerical controlled cutting machine and

computer controlled impregnator and holding tank. The carbon was placed in the raw foam prior to cutting. These advances in fabrication technique led to much improved consistencies between absorber pieces in both carbon density and physical size. For the first time, a continuous length of wedge materials can be installed in a chamber which forms a straight continuous wedge between pieces without having to modify or glue the ends of each piece. Further application of such fabrication techniques should also lead to controlled methods of introducing noncoherent scattering effects in the absorbers as well.

New pyramidal absorber designs were also developed during this study which had a higher number or density of pyramids per absorber piece. This was done in an effort to improve the random nature of the absorbers over all aspect angles and to also improve the low frequency operation of the material since more carbon would also exist. The results showed a slightly improved performance at near-normal incidence but not a major improvement at other angles. The specular reflections from the flat absorber sides were shown to be reduced; however, the diffraction scattering components were increased because of the increased number of shapes. Results for these materials were shown in Section 4.3.4.

The effects of painting the absorber materials were also evaluated. The concern about the paint is its effect

on the impedance match at the air to dielectric interface and also its degradation of performance if it clots or is applied too heavily, especially at the absorber tip or base. At the frequencies observed during this study, no noticeable degradation in performance was obtained due to the materials being painted. However, at millimeter-wave frequencies, as shown by other investigators [41], the paint is expected to become more of a problem.

The performance level of the absorber materials evaluated during this study were found to be dependent on the absorber's shape, orientation and size. Improvements in performance can be obtained by simply selecting the proper absorber type or installation orientation for the specific intended purpose. Having a better understanding and knowledge about the absorbers, enables the anechoic chamber designer or user to obtain improved performance even from currently available materials. Probably the most useful immediate result of this study for achieving improved absorber performance is in the application of the absorber performance curves, many of which are found in Chapter 4.

5.3 IMPROVED CHAMBER PERFORMANCE

In many ways, the performance of the absorbing materials used in an anechoic chamber directly determines

the performance of the chamber. For this reason improved chamber performance should be obtained with improved absorber performance and characterization. This can best be realized through utilization of the absorber data to aid in proper absorber selection and installation to reduce unwanted chamber responses such as target or antenna coupling interactions with the chamber surfaces. The most direct application of the absorber data is in generation and development of accurate and useful chamber prediction models to aid in chamber design and performance optimization.

Models, based on an accurate absorber characterization, would be extremely useful in obtaining improved chamber designs since the expected performance of the chamber could be predicted and optimized prior to chamber construction. Currently, most chamber designs are based on the experience and knowledge of the chamber designer. The only chamber performance models which generally exist are based on ray-tracing techniques which only approximate the absorber covered surfaces of the chamber [36],[42]. The results and accuracies of such models have been somewhat inconclusive.

The other components and required information for constructing adequate models involve the source illumination and instrumentation and are generally well understood and defined. The missing part has been the accurate

scattering/absorption characteristics of the absorber covered surfaces. Such models could be used for both compact range and conventional chamber designs. This is important since compact range techniques typically place different requirements on the absorber's performance throughout the chamber than for conventional chamber designs.

The large costs involved with construction and design of a modern anechoic test facility, especially with increasing RCS target and compact range sizes, also warrant the need for such prediction models. Large cost savings can be obtained by the wise selection of the proper absorber (or lack thereof) prior to range construction. The increased requirements on accuracy and low-level measurements also necessitate the need for accurate models to aid in achieving these more demanding chamber performance levels.

Computer models, based on the monostatic absorber results of this study, have been constructed which are useful in the design of low-level RCS chambers or compact ranges [4],[37]. These models have been found to adequately predict a chamber's RCS background level and have been used to design at least two compact range chambers. Superior performance levels have been achieved in these chambers as a result of using these prediction models.

Figure 5.1 shows the predicted and measured empty

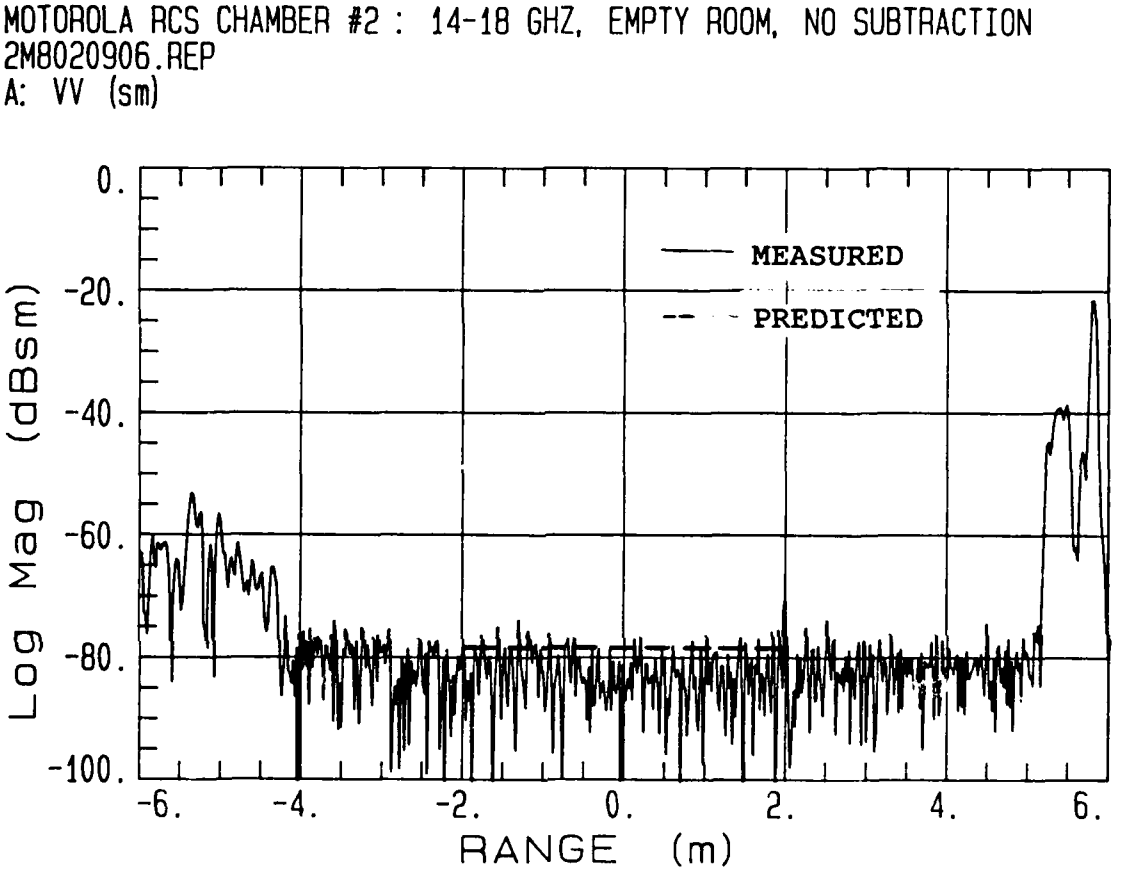

Fig. 5.1. Measured and calculated empty room RCS background levels for a compact range chamber designed using absorber evaluation results.

chamber RCS background, in the time-domain, of one of these chambers which was designed and constructed at Motorola. This particular chamber uses a compact range located in an anechoic room which is 26 by 26 by 52 feet in size. Up to an 8 foot diameter target can be measured in this facility. The results in Figure 5.1 not only show good agreement between measured and predicted performance, but, also show that extremely low background levels were actually obtained. The data shows that the down-range test zone (or quiet zone) area of the chamber, which exists between the ranges of +/- 2 meters, exhibits less than a -75 dBsm unsubtracted background level. The zero range value represents the center of the test zone. The performance of the chamber may even be lower than these levels since it is expected that the measurements were limited by the thermal noise level of the receiver. Only a few such chambers are currently known to exist which demonstrate such low background levels, especially without the use of subtraction techniques. The application of the improved absorber characterization data is partially responsible for achieving this superior performance.

6.0 SUMMARY AND RECOMMENDATIONS

The purpose for conducting this thesis, and studying anechoic chamber absorber materials, was to better the current understanding and characterization of the performance level of such materials. As a result, a better absorber knowledge should lead to improved absorber and chamber performance. The need for an improved understanding of absorbing materials has been demonstrated through a review of past work in this area and a discussion of some of the recent performance requirements being placed on anechoic chambers, especially for low-level RCS measurements. These modern measurement requirements, in many ways, dictate the need for improved absorber performance which can only be achieved by first obtaining a better characterization of the current materials. Significant developments in anechoic absorber technology have not occurred in over 25 years.

In general, the results of this study have led to a significant increase in the knowledge and understanding of absorber materials, especially for their monostatic normal and off-normal performance. The performance curves provided in Chapters 3 and 4 illustrate only some of the absorber characterizations and performance data which were obtained during this study.

The results of this study have also been used to assist in the formulation of badly needed accurate chamber performance models which can be used to aid in chamber

performance optimizations and studies. In the past, the limitations of such models have been with the lack of adequate absorber characterization and performance data. An example of the RCS background performance obtained in one chamber designed using an improved chamber model based on the absorber results of this study is illustrated in Chapter 5. Superior RCS performance levels were achieved in this compact range chamber as a result of the application of the improved chamber model.

The approach taken during this absorber study was to obtain and experimentally evaluate numerous absorber samples of various material shapes and sizes. Materials from three different vendors were provided for these evaluations. Analytical methods were not used because of the complexities and inadequacies of these techniques. Past researchers have formulated such analytical approaches and have found that because of the complex scattering nature of the shaped absorbers, and because of the lack of data on the material's electrical properties, analytical formulations can be somewhat inconclusive. Nonhomogeneities and inconsistencies are also found with the materials which add to the complexity of the analytical models.

Evaluations were conducted on the absorber samples at microwave frequencies from 1.5 to 6.9 and from 11 to 18 GHz for both principal polarizations. It was discovered during this study that the conventional free-space absorber

testing technique, namely the NRL arch, had some limiting abilities in adequately evaluating the true performance nature of the absorbing materials. New and non-conventional absorber evaluation methods were developed making use of compact range technology, modern coherent wideband radar instrumentation, and synthetic aperture imaging techniques. Chapter 3 of this thesis presented the details of the evaluation techniques used during this study.

These modern techniques allowed the true scattering nature and performance levels of the absorbers to be evaluated. A diagnostic measurement capability was also added since the coherent wideband radar techniques offer time-domain, range-resolved absorber scattering results. These techniques were used to determine which part or component of an absorber sample actually limited or dictated the performance of the absorber. Using these techniques, the nonhomogeneities associated with the absorber materials were clearly displayed and evaluated.

The measured reflectivity results obtained during this study for the various absorbing materials were also conducted using these non-conventional RCS measurement techniques. These results showed that consistently better absorber performance than that quoted by the vendors was also obtained. This was partially caused by the increased accuracy and sensitivity of the improved evaluation techniques. The reflectivity of the absorbers were also found

to be dependent on the evaluation sample size since the absorbers are generally random, non-coherent scatterers.

These absorber evaluations have led to many discoveries which have been used to explain the scattering mechanisms associated with the operation of the absorber materials and have also demonstrated the diffuse scattering nature of the material. Results have also shown that the fire retarding salts, used in the absorbers, degrade the performance of the materials for some applications. One vendor modified the design of their fire retarding salts during this study and the new design was shown to offer better than 5 dB improvements in performance. The effects of a metal backing was also shown to be minimal for typical absorber types and sizes used at microwave frequencies down to 3 GHz, even for 3 inch convoluted materials. Painting the materials was also shown to not degrade the performance of the materials at the frequencies evaluated. The orientation and selection of the absorber's shape was also shown to have a large effect on the overall backscattering nature of the absorber as well. Chapter 4 and parts of Chapter 5 discuss the exact results of this study in more detail.

Recommendations for future work in the areas of anechoic absorber materials and chamber performance improvements include the following. 1) The modern evaluation techniques used during this study, which provide diagnostic and more accurate results, should be given consideration

when absorber evaluations are to be conducted. 2) Techniques which simplify the testing of the bistatic response of the absorbers should also be determined and additional bistatic studies of the absorber should be conducted. This study only briefly considered the bistatic response of the absorbers. 3) A more precise positioning system used to support the absorber sample, for the case of the 8 by 8 foot absorber sample, should also be considered to reduce the problems associated with finding the narrow angular specular reflections from the sample wall during rotation measurements. 4) Evaluations over additional frequency bands would also be of interest. Absorber results for the materials evaluated during this study and for larger materials at frequencies below 2 GHz and above 18 GHz would be beneficial for many applications. 5) In the area of improved absorber performance, development activities should include techniques of improving the impedance match at the air to dielectric interfaces of the materials and in new absorber shapes to better control the scattering from the materials. The lossy absorptive properties of the carbon loaded materials are believed to be adequate. 6) And finally, chamber performance models, which accurately predict the performance of various chambers for different applications, and which are based on the results of an accurate absorber characterization, should be extended and more commonly used in the design of such chambers to

achieve improved chamber performance.

REFERENCES

[1] W.H. Emerson, "Electromagnetic wave absorbers and anechoic chambers through the years," IEEE Trans. Antennas Propagat., vol. AP-21, no. 4, pp. 484-489, July 1973.

[2] J. Pustai, "Compact ranges get radar cross-section data abundance," Microwave & RF, vol. 26, no. 5, pp. 118-130, May 1987.

[3] S. A. Brumley, "Use of modern imaging techniques for evaluating anechoic chamber absorbing materials," Presented to the AMTA/APS Workshop on anechoic chamber design technology, Blacksburg, Va., June 19, 1987.

[4] S. A. Brumley, "Better RCS data with anechoic absorber characterization," Microwave & RF, vol. 26, no.5, pp. 143-152, May 1987.

[5] S. A. Brumley, "Evaluation of anechoic chamber absorbers for improved chamber designs and RCS performance," AMTA Proceedings, Seattle, Wa., Sept. 29-Oct. 1, 1987.

[6] R. C. Johnson, "Radar-absorbing material: A passive role in an active scenario," International Countermeasures Handbook, pp. 375-381, 1986.

[7] D. L. Mensa, "Microwave absorber test results," unpublished, July 1983.

[8] W. D. Burnside, and L. Peters Jr., "New compact range reflector design and their novel application," Proc. of the Compact Range Workshop, Philadelphia, June 1986.

[9] B. T. DeWitt, "Analysis and measurement of electromagnetic scattering by pyramidal and wedge absorber," Ph.D. dissertation, Ohio State Univ., 1986.

[10] O. M. Bucci, and G. Franceschetti, "Scattering from wedge-tapered absorbers," IEEE Trans. Antennas Propagat., vol. AP-19, no. 1, pp. 9[illegible]-104, Jan. 1971.

[11] P. Baldwin, "Some analytical solutions for a simple model of a microwave absorber," Wave Motion, vol. 1, no. 3, Univ. of Newcastle-upon-tyne, Engl., pp. 215-223, July 1979.

[12] H. L. Bassett, "Ram evaluation techniques," Presentation given at Georgia Institute of Technology, Radar cross-section reduction short course, 1984.

[13] Montgomery, **Techniques of Microwave Measurement.** MIT Rad. Labs: Mcgraw-Hill, vol. 11, pp. 612-616, 1947.

[14] B. F. Lawrence, "RF anechoic chamber test facilities," Second ESTEC spacecraft EMC seminar, Noordwijk, Netherlands, 1982.

[15] E. B. McMillan, and H. J. Schmitt, "Doppler method for absorber testing," Microwave Journal, vol. 3, pp. 64-68, nov. 1960.

[16] A. R. Howland, and T. J. Loyn, "Broadband reflectivity and scatter evaluation of RF absorbers," AMTA Proceedings, Ottawa, Canada, Sept. 1986.

[17] E. F. Buckley, "Microwave reflectivity measurements - theory and practice," Electronic Design, March 15, 1962.

[18] R. E. Hiatt, E. F. Knott, and T. B. A. Senior, "A study of VHF absorbers and anechoic rooms," Univ. of Mich. rep #5391-1-F, Feb. 1963.

[19] E. F. Buckley, "Design, evaluation and performance of modern microwave anechoic chambers for antenna measurements," Electronic Components, Dec. 1965.

[20] V. H. Weston, "Theory of absorbers in scattering," IEEE Trans. Antennas Propagat., pp. 578-584, Sept. 1963.

[21] S. Galagen, "Understanding microwave absorbing materials and anechoic chambers - parts 1-3," Microwaves, Dec. 1969, Jan. 1970, May 1970.

[22] G. Thiele, RCS fundamentals short course notes, section XI on absorbers, PP. XI-1 to XI-6, Sept. 1983.

[23] E. F. Knott, J. F. Shaeffer, and M. T. Tuley, **Radar Cross Section.** Dedham, Ma: Artech House, Inc., 1985.

[24] Rantec Absorber Products Catalog, Rantec Division, Emerson Electric Co., Canoga Park, Ca.

[25] Emerson & Cuming Microwave Products Catalog, W. R. Grace and Comp., Canton, Ma.

[26] Advanced Absorber Products Catalog, Keene Corp., Amesburg, Ma.

[27] Advanced Electromagnetic Inc. Products Catalog, Santee, Ca.

[30] D. L. Mensa, **High Resolution Radar Imaging.** Dedham, Ma: Artech House, 1982.

[31] A. W. Rihaczek, **Principles of High Resolution Radar.** Los Altos, Ca: Peninsula Publishing, 1985.

[32] D. R. Wehner, **High Resolution Radar.** Norwood, Ma: Artech House, 1987.

[33] J. Boyles, "Recruit an ANA for RCS tests," Microwaves & RF, pp. 87-92, Mar. 1985.

[34] HP Product note 8510-2, "Radar cross section measurements with the HP8510 network analyzer," Hewlett-Packard, Santa Rosa, CA.

[35] **ARCS Program User's Guide.** version 1.1, March Microwave Inc., Mesa, Az., 1987.

[36] S. R. Mishra, "Computer aided design of anechoic chambers," AMTA Proceedings, Melbourne, Fl., Oct. 29-31, 1985.

[37] S. A. Brumley, "A modeling technique for predicting anechoic chamber RCS background levels," AMTA Proceedings, Seattle, Wa., 1987.

[38] Y. Naito, and K. Suetake, "Application of ferrite to electromagnetic wave absorber and its characteristics," IEEE Trans. Microwave Theory and Techniques, vol. MTT-19, no. 1, Jan. 1971.

[39] R. Redheffer, "The dependence of reflection on incidence angle," IRE Trans. Microwave Theory and Techniques, pp. 423-429, oct. 1959.

[40] K. Walther, "Reflection factor of gradual-transition absorbers for electromagnetic and acoustic waves," IRE Trans. Antennas Propagat., pp. 608-621, Nov. 1960.

[41] H. E. King, F. F. Shimabukuro, and J. L. Wong, "94-GHz measurements of microwave absorbing material," Aerospace Rep. # TR-669(6230-46)-5, Mar. 1966.

[42] L. A. Robinson, "Design of anechoic chambers for antenna and radar-cross-section measurements," SRI Project 2495 Rep. #2 under contract N00014-81-K-0182, Nov. 1982.

[43] **ARCS ISAR imaging Manual,** version 1.1, March Microwave Inc., Mesa, Az., 1987.

[44] R. N. Bracewell, **The Fourier Transform and its Applications.** New York: McGraw-Hill, 1986.

APPENDIX A

THEORY OF ISAR IMAGING

A1.0 INTRODUCTION

Radar techniques currently exist for gathering and displaying information about complex targets as to their unique shape, size or appearance. One technique generally used is radar imaging. A radar image is a display of the target's isolated scattering sources showing the position and strength of each individual scatterer as a function of at least two spatial or time-domain coordinates. These coordinates are usually referred to the target's down-range and cross-range position relative to the radar which constructs the image. Example images of the absorber covered wall target are shown in Section 3.3.3.2. Using this image data, much can be learned about absorber scattering characteristics, and diagnostic evaluation techniques can be implemented. The wide availability of such imaging radars also makes their use for absorber evaluations a practical choice since many radar cross-section measurement facilities employ imaging techniques to obtain diagnostic results for development of measured hardware.

Images can be constructed in two ways. One method is to use a large aperture, or antenna, to scan over a target

area and record the measured signal returns as a function of the scan direction. This technique requires a directional, high gain antenna beam to achieve any amount of image resolution. The resolution available is directly proportional to the aperture size. Very large antennas may be required to obtain the necessary resolution for a given image and often limit this method's capabilities. The second, and more commonly used, method for image construction involves a synthetic aperture as opposed to a real aperture. If data can be collected from a target at different and known view angles, then this data can be processed to form the same image results as with the real aperture. The image resolution for the synthetic aperture is related to the range and extent of the target's observation. For this reason, much better image resolution can usually be obtained with synthetic aperture approaches.

Synthetic aperture images can be generated from measured target data by either moving the radar relative to a fixed position target, or by observing a moving target with a fixed radar. The first approach is called SAR (Synthetic Aperture Radar) and the second method is called ISAR (Inverse Synthetic Aperture Radar). The general theory of these imaging techniques are very similar and are well discussed in the open literature [30],[32], and [43]. ISAR techniques are more suitable for use in most RCS measurement facilities since normal measurement techniques already

require target motion relative to a fixed radar. This appendix reviews the basic theory of ISAR since many of the absorber evaluations conducted during this absorber study made use of ISAR imaging.

Both SAR and ISAR imaging radars use standard wideband radar techniques to obtain down range profiles of the target area as a function of the target's view angle prior to image construction. Many different types of radars can be used to perform this function, although the theory and application of imaging is nearly the same in all cases. The analysis presented here will address an imaging system which employs a stepped frequency or synthetic short pulse wideband radar.

A2.0 ISAR MEASUREMENT PROCEDURE

The procedure used to construct an ISAR image is relatively simple and straightforward. The purpose is to obtain and display the spatial distribution of the individual scatterers which make up a complex target. Figure A.1 illustrates a complex target composed of several isolated scatters. A good example would be a wall of anechoic absorber material. The image constructed displays the location, magnitude and phase of each of these scatterers as also shown in Figure A.1. The resolution of the image is

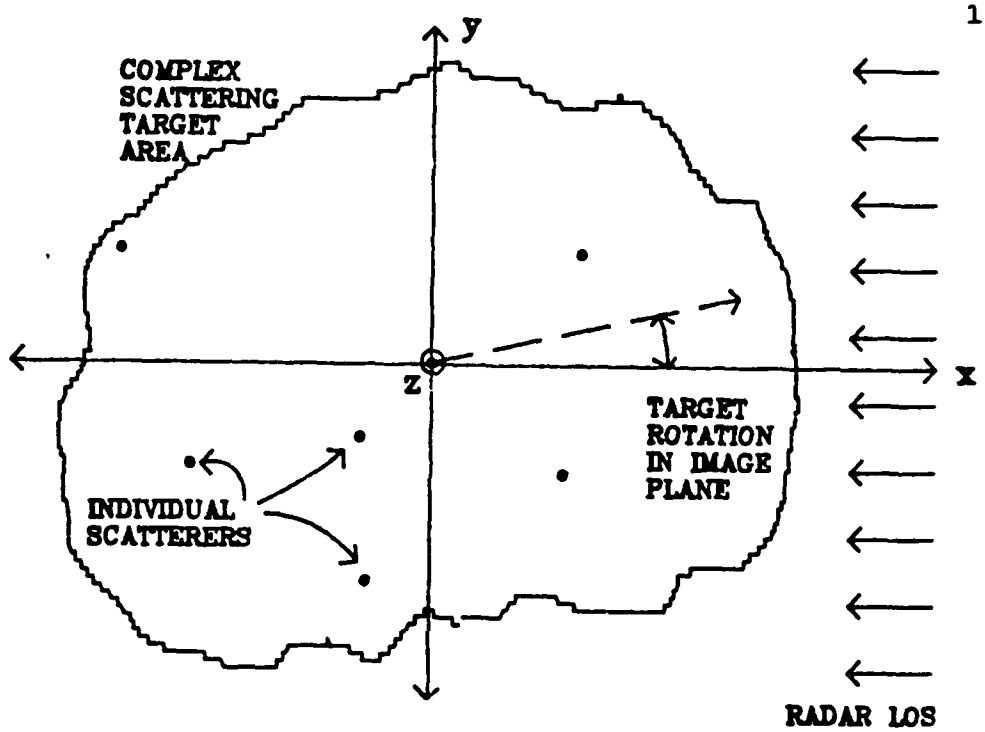

a) Complex target geometry

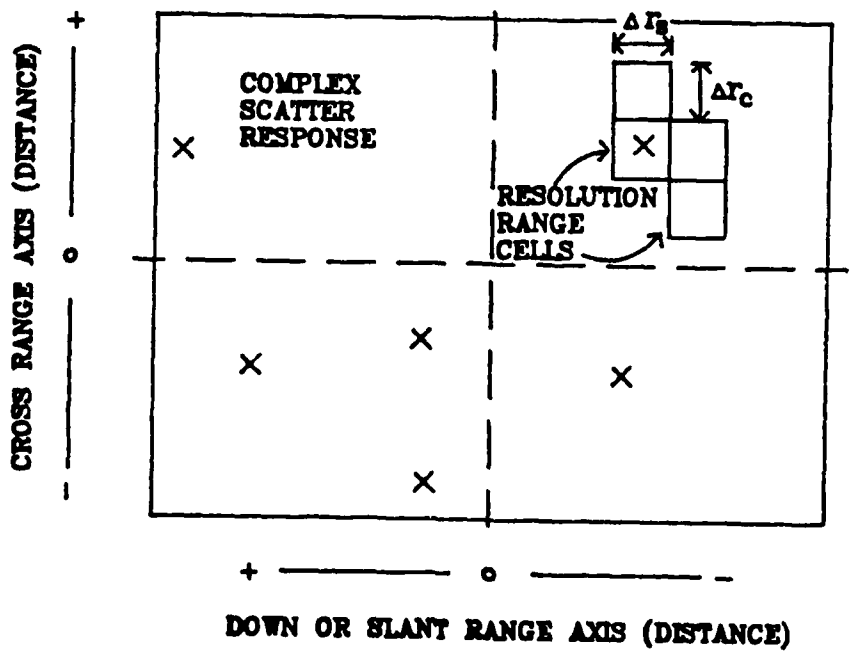

b) Radar image of complex target in a)

Fig. A.1. Comparison between an actual complex target geometry and the constructed radar image showing the spatial distribution of the individual scatters.

defined by the distance which two scatterers can be separated and still be uniquely detected (usually the 3 dB point of their time-domain response). The image cell size is determined by both the down-range and cross-range resolutions (Δr_c and Δr_s). For the case in this figure, a monostatic radar is assumed to be located in the +x direction and plane wave incidence or far-field conditions are also assumed. For illumination on the target area other than plane wave illumination, the image is distorted because of phase curvature and phase corrections must be included in the processing. Only plane wave illumination will be addressed in this appendix.

The procedure used to construct an ISAR image is as follows. A wideband radar is used to collect a series of down-range profiles of the target area as the target rotates about a fixed point. For the synthetic stepped frequency radar, this requires collecting data over a frequency band and performing an inverse Fourier transform to obtain these time-domain down-range profiles. From this series of range profiles, a time history of the scattering from each cell is obtained over the entire angular rotation. Each down-range cell's time history is then Fourier transformed to obtain the doppler frequency shifts of that cell during the rotation of the target. Since the doppler frequency of each scatterer is related to its distance from the center of rotation, different scatterers have different

doppler shifts and their location in cross range can be determined. Thus, the image is constructed using both the down-range and cross-range information. Using the stepped frequency radar, then requires a 2 dimensional Fourier transform for image construction. The down-range resolution of the image is determined by the total frequency bandwidth used and the cross-range resolution by the total angular rotation extent. The plane of the image is established by the direction of incidence from the radar and the plane of rotation. The center of rotation is used to define the zero values of both the down-range and cross-range dimensions.

A3.0 FOURIER TRANSFORM RELATIONSHIP

In equation form, the construction of an ISAR image, using the stepped frequency approach, is represented by a 2 dimensional Fourier transform [43] as

$$G(x,y) \sim \int_{-\infty}^{\infty} \int_{-\infty}^{\infty} G(f_x, f_y)\, e^{j2\pi(f_x x + f_y y)}\, df_x\, df_y \qquad (1)$$

where $G(x,y)$ is the desired complex function defining the response of the individual scatterers of the target as a function of their position (the image), $G(f_x,f_y)$ is the complex measured target function in the spatial frequency

domain and f_x and f_y are the standard spatial frequency variables and are related to the actual measured real frequency variable (f) and angular position (θ) by

$$f_x = \frac{2f}{c} \text{ SIN } \theta$$
$$f_y = \frac{2f}{c} \text{ COS } \theta \qquad (2)$$

where c is the velocity of propagation. A two-way radar path distance is also assumed for these expressions. Figure A.2 illustrates the transformation of f and θ into the f_x and f_y coordinates.

A4.0 IMAGE FOCUSING

Since actual measured data is used to construct the image, the signal processing is performed using discrete Fourier transforms (DFTs) or fast Fourier transforms (FFTs). The application of such transforms requires that they be performed on uniformly spaced (equidistant) data points in either the spatial frequency or time domain [44]. For this case, they require that $G(f_x, f_y)$ be sampled uniformly in f_x and f_y. But, because of the relationship

shown in Figure A.2, data actually measured with uniformly spaced samples in f and θ forms a polar grid in f_x and f_y coordinates. This polar grid is shown in Figure A.3. Before the signal processing can be performed, the polar-grid data must be represented by a rectangular grid of samples. Various methods exist for making this representation.

One method commonly implemented is to approximate a rectangular grid with the actual polar data. This is done using the assumptions that the total angle of rotation (θ_t) is small and that the frequency bandwidth used (B) is also small compared to the center frequency (f_o). Thus if

$$\sin (\theta) \approx \theta \quad , \text{for small } \theta$$

$$\cos (\theta) \approx 1$$

and

$$\frac{B}{f_o} << 1$$

then the spatial frequencies become

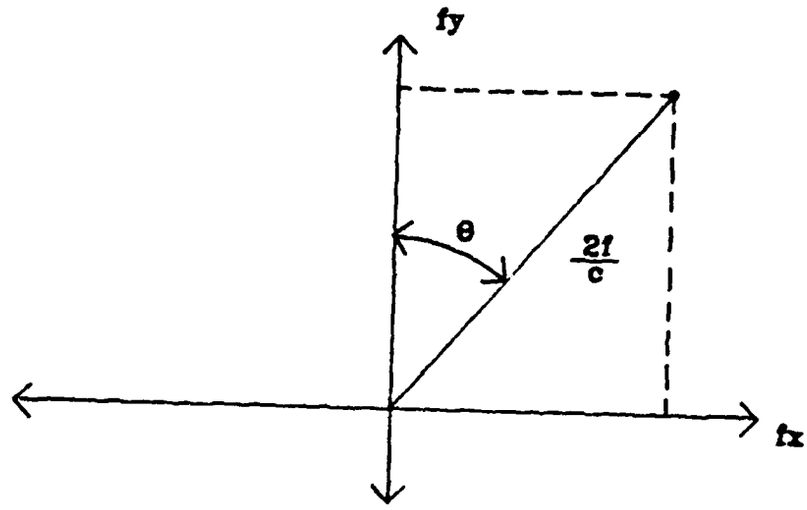

Fig. A.2. Relationship of the spatial frequency variables, f_x and f_y, to the actual measured variables f & θ .

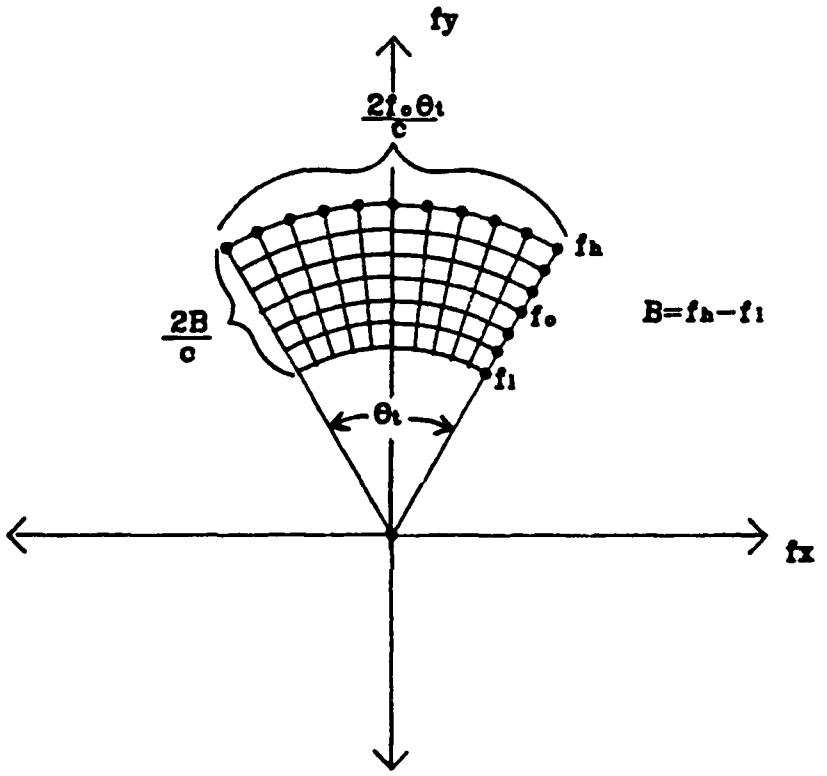

Fig. A.3. The polar grid in f_x and f_y coordinates formed from uniformly spaced samples in f and θ .

$$f_x \approx \frac{2 f_o \theta}{c}$$

$$f_y \approx \frac{2 f}{c} \qquad (3)$$

and the measured samples in f and θ are shown to form a rectangular grid in f_x and f_y. This approximation is shown to be adequate for images where high range resolution is not required and for higher radar center frequencies. But, for other cases, the errors associated with this approximation results in noticeable image distortion (blurring) and amplitude variations. Thus, imaging techniques which use these approximations are usually referred to as nonfocused imaging techniques. Because of this limitation, methods to characterize the level of these errors must be implemented.

Several methods exist to evaluate the limits of nonfocused imaging [32],[43]. One technique most used is that of defining a radius of target sizes where a resolved scatterer migrates through one complete range cell as the target rotates through θ_t. This radius is called the blur radius. The blur radius is a function of the image resolution and radar operating center frequency. For targets smaller than the blur radius, the errors of the approximation are small and their images are essentially focused. Targets larger than this radius will start to have some

defocusing at the edges of their images. All images are focused at or near their center of rotation within the defined blur radius. The blur radius technique is not exact, however, and does have some limitations. It does not allow for determining how severe the errors are for targets which exceed this radius and it also does not account for the fact that the image degrades faster along the cross-range extent than it does along its down-range. Another technique is that of calculating the phase contours within an image for a given range resolution and frequency. This technique is well described in the references and does account for some of the deficiencies of the blur radius approach but is more difficult to apply.

The preferred method to evaluate image errors makes use of computer simulations of theoretical or known targets, using the actual image parameters to quantify the effects of image nonfocusing errors. This technique is demonstrated in Section 3.3.3.2.2.

Exact focusing techniques do exist for constructing focused images from measured data for any size target and resolution requirement. These techniques usually require additional processing or a more complicated data collection scheme. The use of these techniques are referred to as focused imaging. One technique is to collect the measured data using nonuniformly spaced samples and actually map this data into a rectangular f_x and f_y grid. This requires

a very complicated measurement system and is seldom used. Another method is to make use of a transform other than the DFT, which does not require the uniformly spaced sample data. Such transforms as the chirp-z transform have been proposed for such a system.

The method which is most common for constructing focused images is that of polar-to-rectangular reformatting [32]. This technique makes use of an interpolation method to construct a rectangular grid from the polar grid as shown in Figure A.4. Many different interpolation routines can be used. Using this technique allows for fully focused image construction for most practical target sizes and configurations and is not generally limited to the range resolution or operating frequency used. The disadvantages of the technique are that additional signal processing is required and effective range resolution is usually reduced, depending on the interpolation used. This is shown in Figure A.4, where the actual angular range (θ_t) and bandwidth (B) are reduced to the limits of θ_{tf} and B_f. The focused images shown in Section 3.3.3.2.2 make use of this focusing technique.

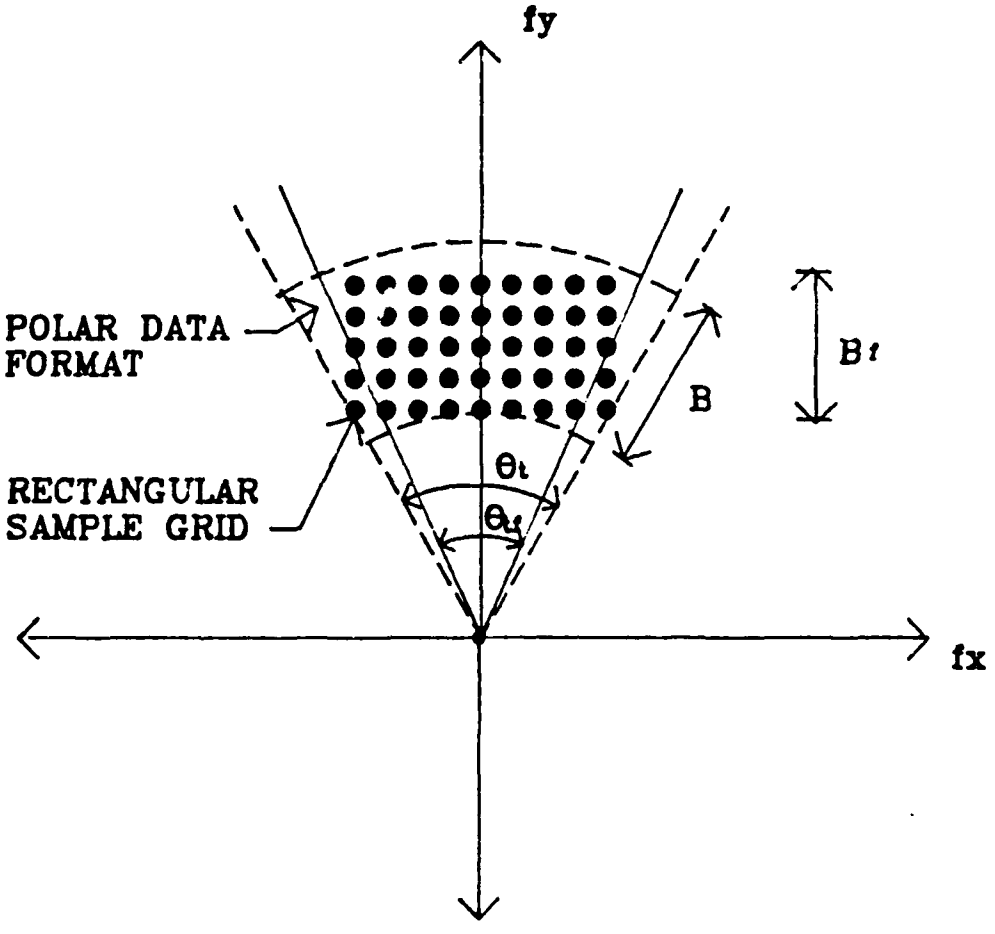

Fig. A.4. Polar-to-rectangular sample reformatting used to create fully focused images.

A5.0 DEFINITION OF RANGE RESOLUTION AND IMAGE SIZE EXTENTS

The resolution cell size of an image is determined by both the down (slant)-range and the cross-range resolutions. The amount of resolution available is determined as follows. Using the small angle approximations and the results of eq.(3), the overall extent of the sampled spatial frequency data is shown to be $2B/c$ in the f_y direction and $2f_o\,\theta_t/c$ in the f_x direction as shown in Figure A.3. Applying the standard Nyquist sampling theory to these extents results in the minimum sampling spacings or resolutions achievable. As a result, the range resolutions are

$$\Delta r_s = c/2B = \text{down (slant) range resolution}$$
$$\Delta r_c = \lambda_o/2\,\theta_t = \text{cross range resolution} \qquad (4)$$

where $\lambda_o = c/f_o$. The down-range resolution is shown to be identical to that normally defined with any wideband radar approach for range resolution and not specific to imaging. The cross-range resolution is determined by the maximum spatial frequency component available and is directly related to the radar's operating frequency and the target's

total angular extent. These are the conventional values for range resolution usually used to define the image's range resolution cell size. It must be noted, however, that they only apply to the case of the small angle approximation using Fourier transforms. The use of other transforms or focusing techniques may modify the amount of range resolution achievable.

Another aspect of the signal processing is the presence of processing sidelobes caused by the finite extent or range of the measured data. These effects are usually reduced by the application of weighting functions convolved with the data. The use of weighting functions also reduces the effective resolution of the system. The resolutions defined in eq.(4), assume a rectangular weight (no weighting). To account for the use of a weighting function, an appropriate multiplication factor must be used with the resolution calculation to obtain the correct result. As an example, if a Hanning weighting function is used, then the results of eq.(4) must be multiplied by 1.64 to obtain the true resolution achievable.

Since DFTs are used, another result of the signal processing is that aliasing will limit the maximum size of the image achievable. The effect of aliasing results in image foldover and false or incorrect image indications. These effects are reduced by proper sampling rate selection. Windows on the maximum image size extents are related

to the discrete number of sampling steps and are given by

$$W_s = n_f \Delta r_s = c/2 \Delta f = \text{down range image window}$$

$$W_c = n_a \Delta r_c = \text{cross range image window} \quad (5)$$

where n_f and n_a are the number of frequency and angular samples taken and Δf is the frequency step size for the stepped frequency synthetic radar and is equal to B/n_f. As an example, for an image size of 8 by 8 feet with a square resolution of 1.5 inches, a minimum of 64 frequency samples (steps) and 64 angular samples must be taken.

BIOGRAPHICAL SKETCH

Stephen Brumley is currently a Senior Staff Engineer at Motorola's Government Electronics Group in Scottsdale, Arizona. He has been with Motorola since 1982. His research interests are in applied electromagnetics, antennas, radar cross-section, and radar systems. His studies in radar cross-section has involved development of reduced RCS antennas and structures, scattering prediction and modeling, and measurement and evaluation of scattering or radiating objects. He has most recently been involved in the design and implementation of new RCS measurement facilities at Motorola and in anechoic chamber and compact range modeling and evaluation. Before joining Motorola, Brumley received the Bachelor of Science in Electrical Engineering degree from West Virginia University in 1982 where he was a Magna Cum Laude graduate. He is currently completing graduate studies for Master of Science degree in Electrical Engineering at Arizona State University. He is a member of the Institute of Electrical and Electronics Engineers, Eta Kappa Nu, and Tau Beta Pi. He has authored nine journal articles and scientific papers on various topics.